



UNIVERSITÀ
degli STUDI
di CATANIA

DIPARTIMENTO di INGEGNERIA ELETTRICA,
ELETTRONICA e INFORMATICA

PH.D. COURSE IN SYSTEMS ENGINEERING
XXVIII CYCLE

Ph.D. Thesis

**A MICROFLUIDIC COMMUNICATION NETWORK
FOR PROGRAMMABLE PASSIVE DROPLET-BASED
DEVICES:
DESIGN, MODELING AND ANALYSIS**

ING. LIDIA DONVITO

Coordinator

Chiar.mo Prof. L. FORTUNA

Tutor

Chiar.mo Prof. A. LOMBARDO

To the loving memory of my father

SOMMARIO

I dispositivi microfluidici costituiscono una rivoluzione nella manipolazione di piccole quantità di fluidi, anche inferiori al picolitro. Le gocce in questi dispositivi fungono da microreattori, poiché sono utilizzate per incapsulare campioni e reagenti. Esse vengono manipolate all'interno del dispositivo per eseguire, su un chip con area nell'ordine dei centimetri, esperimenti normalmente realizzabili solo in laboratorio.

L'obiettivo di questa tesi è estendere le funzionalità attuali dei dispositivi microfluidici passivi che manipolano gocce. Questi dispositivi non richiedono l'integrazione di componenti elettronici sul chip microfluidico né strumentazione di controllo per manipolare le gocce in maniera attiva. Essi, piuttosto, sfruttano soltanto effetti idrodinamici e, quindi, non richiedono un processo di fabbricazione complesso e costoso essendo totalmente passivi.

I dispositivi microfluidici passivi che manipolano gocce sono usati principalmente per esperimenti e analisi chimiche e biologiche ma non sono in grado di eseguire protocolli di analisi complessi. Infatti, ogni dispositivo è progettato unicamente per una specifica applicazione ed

è in grado di compiere solo operazioni semplici sulle gocce. Queste limitazioni possono essere superate introducendo una tecnologia di networking flessibile e modulare, che doti questi sistemi di una rete di comunicazione in modo da consentire sia lo scambio di informazione che di specie chimiche, trasportate entrambe dalle gocce. La rete microfluidica risultante sarà in grado di combinare le funzionalità specifiche di ciascun dispositivo microfluidico connesso ad essa, formando una potente e versatile piattaforma microfluidica in grado di implementare protocolli biochimici diversi su un unico chip.

ABSTRACT

Microfluidic devices represent a revolution in handling small volumes of fluids down to less than pico-liters. Droplets in these devices are used as microreactors to encapsulate samples and reagents. They are manipulated to perform laboratory functions on a single chip of only a few square centimeters in size.

The aim of this thesis is the extension of the current capabilities of microfluidic passive droplet-based devices. These devices do not rely on in-chip electronics and macro-scale control supplies to actively manipulate droplets. They exploit, instead, hydrodynamic effects without requiring complex and costly production processes.

Microfluidic passive droplet-based devices are mainly used for chemical and biological experiments and analyses, but lack of capabilities to perform complex and programmable laboratory workflows (i.e. they are single-purpose). These limitations can be overcome by introducing a flexible and modular microfluidic networking technology to provide to such systems a communication network for the exchange of both information and chemical/biological samples carried by droplets. The resulting microfluidic communication network will

combine the specific functionalities of each connected microfluidic device, in a programmable and versatile microfluidic platform for diverse assay protocols on a single chip.

CONTENTS

1	Introduction	1
1.1	Background and motivations	1
1.2	Thesis outline	5
1.3	Acknowledgements	7
2	Basic Principles of Microfluidics	9
2.1	Scaling law	9
2.2	Navier-Stokes equations	10
2.3	Hagen-Poiseuille law: hydrodynamic resistance	13
2.4	The Reynolds number	16
2.5	Analogy with electric circuits: Kirchhoff's laws	18
2.6	Surface phenomena	20
2.6.1	Surface tension	20
2.6.2	The Young-Laplace equation	20
2.6.3	Contact angle	21
2.6.4	Capillary phenomena	21
2.7	Boundary conditions: the <i>no-slip</i> condition	22

3	Droplets microfluidics	27
3.1	Fabrication methods and materials	28
3.2	Effect of surfactants on droplets	33
3.3	Droplet generation	35
3.4	Droplets manipulation methods	40
3.4.1	Passive methods	41
3.4.2	Active methods	43
3.4.3	Splitting	47
3.4.4	Merging	50
3.4.5	Mixing	54
3.4.6	Other operations	58
3.5	Bubble Logic	58
3.6	Droplet resistance	63
4	Simulation tools for microfluidics	67
4.1	Computational Fluid Dynamics	67
4.1.1	Overview of numerical methods	68
4.2	Interface capturing methods	70
4.2.1	Phase field	71
4.2.2	Lattice-Boltzmann	72
4.2.3	Level set	72
4.3	VOF: Volume Of Fluid method	73
4.3.1	Interface Compression	76
4.3.2	Calculation of surface tension	77
4.4	OpenFOAM settings	78
4.4.1	Code and solvers	79
4.4.2	Solution domain discretization: Mesh	80
4.4.3	Time discretization	83

4.4.4	Equations discretization schemes	84
4.4.5	Boundary conditions	88
5	Hydrodynamic Controlled microfluidic Networking	93
5.1	Challenges and motivations	94
5.2	Overview and architecture	99
5.3	Information Encoding	104
5.4	Signaling	105
5.4.1	Common channel signaling	106
5.4.2	Channel associated signaling	110
5.5	Distance encoding scheme	113
6	Droplets switching	117
6.1	Background	117
6.2	Switch design	119
6.3	Methods and materials	125
6.3.1	Computational Fluid Dynamic analysis	125
6.3.2	Switch layout	126
6.3.3	Device fabrication	126
6.3.4	Experimental setup	127
6.4	Results and discussion	128
6.4.1	Simulation results	128
6.4.2	Experimental testing	129
7	Medium Access Control in microfluidic channels	137
7.1	Rationale and overview of the device	138
7.2	Design of the device	140
7.3	MAC functionalities validation	143

8	μ-NET: a microfluidic communication network	147
8.1	μ -NET Overview and architecture	148
8.1.1	μ -NET interaction model	149
8.2	Microfluidic Networking Interface	152
8.2.1	Notation and electrical analogy	153
8.2.2	Design	154
8.3	μ -NET Analysis: design tips	160
8.3.1	Circuit analysis	162
8.3.2	Addressing	167
8.3.3	Throughput analysis	173
8.3.4	Simulation results	180
9	Conclusions and suggestions for further works	185
9.1	Results of the research activity: publications	189

LIST OF FIGURES

2.1	Flow regimes.	18
2.2	Contact angle.	24
2.3	Interpretation of the <i>slip</i> length λ_s [1].	25
3.1	Some Lab-on-Chips from "Micronit Microfluidics": (a)- (b) micromixers; (c) microreactor; (d)-(e) droplets gen- erators.	29
3.2	Scheme of the soft lithography process to fabricate mi- crofluidic devices [2].	31
3.3	Microfluidic chips for droplets generation: (a) PDMS chip fabricated through rapid prototyping; (b) trans- parent photopolymer chip fabricated through 3D- printing [3].	32
3.4	Surface tension of a surfactant solution with increasing concentration and formation of micelles.	34
3.5	Configuration of passive microfluidic droplets genera- tors: co-flowing, flow focusing and cross-flowing.	37

- 3.6 Schematic overview of the droplet manipulation techniques. (a) A squeezed droplet can decrease its interfacial energy by expanding in a hole; (b) Increasing the air pressure above the local water pressure expands the membrane into the crossing microchannel, effectively blocking it; (c) A polarizable medium will move towards the region with highest electric field intensity; (d) The electrostatic energy will be minimal when a droplet covers the activated electrode; (e) A droplet passing two electrodes finds a minimum energy when centered above the electrodes; (f) By taking charges from the open electrode, a droplet can be precharged. A precharged droplet will move towards the oppositely charged electrode; (g) Paramagnetic particles move towards the highest magnetic field strength and can drag a droplet along with them; (h) The interdigital transducer creates a surface acoustic wave that is attenuated at the PDMS pillar, creating an upward pressure wave that can move droplets; (i) At specific frequencies the piezo can create resonating pressure waves in a channel, forcing a droplet towards the antinodes; (j) A medium with better polarizability at optical frequencies than the surrounding medium will move towards the region of high intensity laser light. Reprinted from [4]. 42
- 3.7 EWOD (*electrowetting-on-dielectric*): (a) configuration; (b) mechanism; (c) example of contact angle change. Reprinted from [5] ©2003 IEEE. 46

3.8	Droplet splitting by EWOD (<i>electrowetting-on-dielectric</i>). Reprinted from [5] ©2003 IEEE.	48
3.9	Geometry mediated droplets fission: (a) symmetrical configuration; (b) asymmetrical configuration. The parameters l_0 and w_0 are the length and with of the droplet before it arrives at the junction. These parameters are used in eq. (3.8) to calculate the critical capillary number at which the droplet break-up occurs.	49
3.10	Droplet merging through EWOD. Reprinted from [5] ©2003 IEEE.	51
3.11	Electrocoalescence, diagram of the device: the water droplets of two different sizes are generated independently using a T-junction and are merged together in a single channel, when the smaller droplet reaches the larger one coalescence is performed by the application of an electric field by means of two electrodes. Reprinted with permission from [6]. Copyright 2006, AIP Publishing LLC.	52
3.12	Geometry mediated droplets fusion can be achieved by: (a) stopping the droplet at a narrowed channel; (b) slowing down the droplet movement in a widening channel.	54

-
- 3.13 Effects of initial conditions on the mixing due to recirculating flow inside droplets that move in a straight channel. (a) The flow recirculation (represented by black arrows) effectively mix the solution of reagents which are initially localized in the front and rear halves of droplet. (b) The flow recirculation does not mix effectively the solution of the reactants initially localized in the left and right halves of droplet. Reprinted with permission from [7]. Copyright 2003 American Chemical Society. 55
- 3.14 A symmetric system for droplets generation that transfers the concentration gradient of the continuous flow to the droplets. Adapted with permission from [7]. Copyright 2003 American Chemical Society. 56
- 3.15 " *Twirling* " effect: facilitates the mixing but only occurs for small droplets. Reprinted with permission from [7]. Copyright 2003 American Chemical Society. 56
- 3.16 Diagram of mixing in droplets through a serpentine showing that the droplets are stretched, reoriented and folded, this allows a fast and effective mixing. Reprinted with permission from [8]. Copyright 2003, AIP Publishing LLC. 57

- 3.17 Microfluidic bubble Logic. A bubble in a channel represents one bit. **A** and **B** indicate the two inputs of the device. The top row shows a two-input AND-OR gate with two symmetrical input channels **A** and **B** and two asymmetrical output channels ($\mathbf{A} + \mathbf{B}$ and $\mathbf{A} \cdot \mathbf{B}$ computing the two outputs simultaneously). The bottom row depicts a universal $\overline{\mathbf{A}} \cdot \mathbf{B}$ gate with gain that can be used to switch a larger bubble by a smaller one. The device has two asymmetries, a T-junction at the bottom and a thin channel that provides a variable flow from the top contro channel [9]. The scale bar in the figure is 100μ m. Reprinted from [10] with permission from AAAS. 60
- 3.18 The T or "toggle" flip-flop: a) electronic circuit symbol
e b) truth table 60
- 3.19 Microfluidic one-bit memory implemented as a toggle flip-flop. The gate stores its state indefinitely (zero for the blue bubble) until a toggle signal arrives (orange bubble, left to right). This switches the state of the flip-flop from zero to one, until another toggle bubble arrives. Adapted from [10]. Reprinted with permission from AAAS. 61
- 3.20 Encoding and decoding a signal. (A and B) Schematic diagrams of the encoder/decoder devices. Droplets arrived at the first loop separated by varying, aperiodic time intervals, which form a signal, and emerge from the first loop encoded in a period-2 fashion. From [11]. Reprinted with permission from AAAS. 63

4.1	Interface representation methods.	71
4.2	Volume fraction $\alpha = \frac{V_1}{V_1+V_2}$, where V_1 and V_2 are the volumes occupied by phase 1 and 2, respectively. . . .	75
4.3	OpenFOAM software structure.	79
4.4	Example of structured mesh for a T-junction geometry.	82
4.5	Example of unstructured mesh for a T-junction geom- etry.	82
4.6	Interpolation from values of cell center to face center: f is the face, P and N are the centers of two cells in which the solution is known. Examples of interpolation schemes available in OpenFOAM are: upwind, linear, vanLeer.	87
4.7	Example of a simulated geometry: <i>inletWater</i> is the inlet of the dispersed phase; <i>inletOil</i> is the inlet of the continuous phase; <i>outlet</i> is the outlet of the de- vice; <i>bottom</i> is the back of the device; <i>wall</i> are the remaining boundaries.	89

5.1	A toolbox of unit operations for droplet microfluidics. This overview shows one selected example of each module for the manipulation of microfluidic droplets. These modules can be integrated like jigsaw pieces to suit the requirements of specific biological experiments. It should be noted that this display is far from comprehensive: alternatives exist for many of these modules and more will certainly arise in the future. Criteria for their future evaluation will be fidelity, ease of use and interoperability. The modules are: (a) droplet generation; (b) mixing and generation; (c) fusion ; (d) short-term incubation; (e) stationary storage; (f) detection; (g) sorting; (h) re-injection; (i) splitting ; and (j) off-chip incubation. Adapted from [12] Copyright 2010, with permission from Elsevier.	95
5.2	A summary of integrated microfluidic workflows. Recently published workflows for biological experimentation are represented as combinations of jigsaw pieces from 5.1. (a) Directed evolution of yeast cells; (b) in vitro enzyme expression of DNA; (c) sensitive detection of cell-surface biomarkers on compartmentalized single cells using enzyme amplification (ELISA assay); (d) toxicity screening. Reprinted from [12] Copyright 2010, with permission from Elsevier.	96
5.3	Bus Topology of HCN.	100
5.4	Ring topology of HCN. The left part of the picture shows microfluidic chips commercially available from http://www.dolomite-microfluidics.com	100

5.5	Example of a re-injection system: (a) an emulsion is produced by a flow focusing device and delivered into storage chambers connected to reservoirs. The collecting, storing, and re-injecting of droplets is controlled by applying gravity-driven hydrostatic pressure to reservoirs; (b) apparatus for droplet re-injection and its optical micrograph. Reprinted from [13] with permission of The Royal Society of Chemistry.	103
5.6	Proposed system architecture for HCN when using channel associated or common channel signaling. The dotted line represents a distinct channel in which the signaling information, e.g. control droplets, is carried out when the common channel signaling architecture is adopted.	107
5.7	Possible MNI designs for a microfluidic communication network with common channel signaling: MNI implementing DPAE scheme (left); MNI implementing CE scheme (right).	109
5.8	Possible MNI designs for a microfluidic communication network with channel associated signaling based on droplet size encoding scheme.	112
5.9	T-shaped droplets generator [3].	116
5.10	Variance of droplet size and droplet inter-distance vs. the total flow rate.	116
6.1	Distance-based switch [14].	121
6.2	Electrical equivalent circuit of the distance-based switch [15, 14].	122

6.3	Switch simulated geometry [14].	125
6.4	Prototype of the switching device [14].	128
6.5	Simulation results for the case in which the payload droplet is addressed to the <i>out</i> ₁ [14].	130
6.6	Simulation results for the case in which the payload droplet is addressed to the <i>out</i> ₂ [14].	131
6.7	Simulation results of streamline pattern in the bypass channel at different droplet positions [14].	132
6.8	Experimental results for the case when the payload droplet enters branch 2 [14].	133
6.9	Experimental results for the case when the payload droplet enters branch 1 [14].	134
6.10	Theoretical vs. experimental results for inter-droplet distances in the alternating regime [14].	136
6.11	Probability of switching success versus the inter-droplet distance [14].	136
7.1	Device implementing Medium Access Control for droplets [16].	139
7.2	Electrical equivalent circuit of the device for MAC [16].	141
7.3	Simulation results that assess the correct MAC func- tioning [16].	145
8.1	μ -NET architecture.	151
8.2	Distance-based switching [17, 15].	152
8.3	Device implementing medium access control of droplets [16].	153

8.4	Representations of the equalized MAC proposed for μ -NET [18].	158
8.5	Simulation results of streamline pattern in the flow equalizer channel.	159
8.6	μ -NET network scheme [18].	161
8.7	Electrical equivalent circuit of μ NET reduced by using delta-star transformations [18].	163
8.8	Cell i of the μ -NET electrical equivalent circuit [18]. . .	163
8.9	Droplets positions at different times [18].	169
8.10	Distance between header and payload droplets when the i -th LoC is addressed [18].	171
8.11	Variation of δ_{margin} , as percentage of $D_{HP}^{*(i)}$, for seven μ -NET configurations connecting up to eight LoCs. . .	174
8.12	Distances between droplets [18].	176
8.13	Throughput of μ -NET vs. the number of MNIs, N , obtained in two different settings [18].	177
8.14	Throughput of a μ -NET with $N = 8$ vs. (a) the input flow velocity; (b) the sum of the length of the Pipe 1, $L_1^{(S)}$, and the Pipe 2, $L_2^{(S)}$, of the switch [18].	179
8.15	Values of the distances $D_{HP}^{(i)}$ and $D_{HH}^{(i)}$ for different values of i [18].	181
8.16	Simulation results that demonstrate the μ -NET functioning [18].	184

LIST OF TABLES

2.1	Volumetric flow rate for different shapes of microchan- nel cross-section.	15
2.2	Hydrodynamic resistance for straight channels of differ- ent cross-section shape.	17
4.1	Example of boundary conditions used to perform 3D simulations of the T-junction generator in Fig. 4.7; α is the volume fraction, U the velocity field and p_{rgh} is the pressure in eq.(4.10).	90
7.1	Parameters characterizing the geometry illustrated in Figure 7.1 [16].	143
8.1	Resistances of the electrical equivalent circuit of the device for MAC (see Figure 5(c)) reduced by using star- delta transformations, required in eq. (8.4).	156
8.2	Equivalent resistances illustrated in Figure 8.7(b). . . .	164

8.3	Example of a valid addressing (that is, $D_{HP}^{*(i)}$ values) for seven μ -NETs connecting up to eight LoCs (the distances are expressed in millimeters).	173
8.4	Parameters characterizing the MNIs geometry integrated in the μ -NET illustrated in Figure 8.16.	182

INTRODUCTION

1.1 Background and motivations

Microfluidics is a research field of huge interest and in full development. There are many theoretical and empirical studies on this topic motivated by multiple applications of microfluidic devices in various scientific fields such as chemistry, biology, medicine, and physics. Microfluidics deals with the study of the behavior, control and manipulation of fluids at the sub-millimeter scale. One of its most promising applications is the *Lab-on-Chip* (LoC) technology. LoC devices allow to shrink complex laboratory workflows into a small chip format. Indeed, they are employed to perform typical laboratory operations, with low consumption of reagents and short reaction times, enabling all the advantages of miniaturization for different problems in analytical and synthetical chemistry, in molecular biology, and for screening purposes [19, 20].

One subcategory of microfluidics is droplet-based microfluidics. Unlike continuous flow systems that manipulates a single phase flow, droplet-based systems focus on creating discrete volumes with the use of immiscible fluids. A droplet in a microfluidic system can be seen as an isolated reactor encapsulating cells, DNA, and other particles or molecules, with minimal dispersion and flexible control. Several *unit operations* can be performed on droplets, for example, controlled generation (needed to obtain droplets that are regular in size and shape), fission, fusion, sorting, and mixing [12]. Each of these unit operations corresponds to an experimental step of a biochemical protocol. A droplet-based LoC consists of a series of microchannels integrating one or more unit operations to meet the requirements of a specific laboratory workflow.

Currently, such systems are usually realized through monolithic devices. Samples, encapsulated into droplets, are processed by passing them through a preset sequence of fixed microfluidic channels. Therefore, these systems are single-purpose and perform only a limited set of fixed processing operations and this means that any custom process protocol requires the design from scratch of a specific LoC device. The current challenge of microfluidics is the improvement of LoC technology by the development of a small number of multi-purpose microfluidic processors. In this envisioned platform, modular individual elements are connected to perform more complex and programmable laboratory operations.

In the recent past, a large number of attempts have been made to define a framework, including both hardware and software technologies, for realizing programmable microfluidic systems [21, 22, 23, 24] able to execute a large number of different elementary analyses within

a single device [25].

This goal has been almost achieved for continuous flow microfluidic devices. However, they suffer of many drawbacks that limit their application. In facts, continuous flow devices often use microvalves and micropumps [26, 27, 28, 29] requiring a complicated fabrication process and macro-scale off-chip controllers, or they are modular but not reconfigurable [30] in real-time. Moreover, these devices exhibit other limitations related to their intrinsic characteristics, such as cross-contamination of samples and difficult mixing due to the laminar properties of the flow. Some of these limitations can be overcome using droplets as vessel for samples [31], instead of a continuous phase.

Also current programmable droplets microfluidic chips rely on active droplets manipulation methods, such as the electrowetting on dielectric method, requiring a complex multilayer microfabrication process for the chip and may not be suitable for some biological settings due to problems of biocompatibility of electrical signals on some cells or biomolecules [32, 33].

The purpose of this thesis is the design of a droplet-based programmable microfluidic device exploiting only hydrodynamic droplets manipulation that does not require the control of in-chip electrodes or valves but, only relies on channel geometry and external actuators (pumps and reservoirs) to control droplets motion. Devices employing this passive manipulation can be cheaply fabricated and easily employed.

However, the fulfillment of this purpose will require the design of a complex network of microchannels and a method to guide droplets through them. The dynamics of droplets traveling through a network of microchannels is a topic of great interest in the current literature

because it involves a complex set of phenomena [34, 35, 36, 37]. They occur because each droplet, traveling in a microchannel, affects the pressure field in the whole system, which in turn affects the trajectories of the subsequent droplets.

Despite this complexity, the introduction of the innovative concept of Bubble Logic [10] has shown that the design of microfluidic passive platforms, performing non trivial operations (e.g. merging and mixing) on droplets, is technologically feasible. In particular, logic operations performed by droplets traveling in appropriately designed microfluidic networks paves the way to both communication and networking facilities in passive droplet-based microfluidic devices. A first step in this direction has been proposed in [11] where ciphering and deciphering of signals encoded in the distance between consecutive droplets has been introduced.

A programmable microfluidic droplet processing platform should provide the ability to control samples processing through a convenient modular assembly of LoCs. This goal can be achieved by introducing interconnectivity among the LoCs, in such a way that several specialized functions can be coordinated into a network of LoCs to dynamically address the sequence of elements involved in the workflow. Thus, a *microfluidic communication network* provides the support to complex, programmable, multi-step liquid-handling protocols implementing the advocated vision for flexibility, scalability, and reduced costs of such devices.

To this purpose, this thesis shows how to exploit networking and communication techniques typical of the telecommunications engineering transposing them in the microfluidic domain through a novel paradigm, called Hydrodynamic Controlled Network (HCN). This

transposition is accomplished by designing microfluidic devices and protocols that realize the following basic networking functionalities: information encoding, switching, and medium access control. Each of these devices will be detailed and then assessed through numerical simulations. Then, the integration of these devices in a complete communication network infrastructure, called μ -NET, will be addressed. Finally, a model for this communication network will be derived to analyze the μ -NET network performance.

1.2 Thesis outline

This thesis presents the modeling and analysis of elements that implement networking functionalities and their integration in a microfluidic communication network, which overcomes the limitations of traditional passive droplet-based devices by supporting dynamic addressing of various microfluidic elements aimed at executing different laboratory workflows into a common chip format.

This dissertation is organized in nine chapters (including this introduction) as follows:

Chapter 2 provides basic definitions of microfluidics as science, emphasizing all those physical phenomena that are important and critical when treating problems on a microscopic scale.

Chapter 3 presents an overview of droplet microfluidics providing a short review of the manipulation methods used to generate, split, combine, sort, and transport droplets through microfluidic devices.

Chapter 4 examines the Computational Fluid Dynamics (CFD) and describes the simulation software (OpenFOAM) used to carry out

the numerical simulations presented throughout this thesis. Moreover, this chapter provides the settings of the performed simulations.

Chapter 5 proposes information encoding techniques for droplet-based microfluidic devices and presents a model of communication network architecture, called HCN, for them. Existing sorting devices are then proposed as possible solutions for switching droplets in each identified encoding scheme. In particular, the chapter focuses on distance based encoding, the approach employed to implement the microfluidic communication network presented in the following chapters.

Chapter 6 explores the feasibility of a microfluidic switch able to selectively direct a packet of droplets to the desired end-user. The results of numerical simulations and experimental testing of the designed device will be reported in this chapter.

Chapter 7 presents the design of a network element that provides a channel access control mechanism to avoid the coalescence, due to undesired collisions, between droplets that come from different microfluidic elements and flow into a common shared channel.

Chapter 8 provides the integration of the networking elements proposed in the previous chapters, in a microfluidic communication network, called μ -NET. A model for the analysis of network performance will be derived in this chapter and simulations results validating μ -NET operations will be presented.

Chapter 9 draws the conclusions and suggests further studies related to the presented subject.

1.3 Acknowledgements

I would like to thank my supervisor Prof. Alfio Lombardo for giving me the opportunity to work on very interesting and challenging topics such as microfluidics, for his support in my work but especially for his patience. I would thank Eng. Laura Galluccio and Prof. Giacomo Morabito, two extraordinary researchers, for their collaboration and guidance. I would like to acknowledge Dr. Laura Maria Zanolì, Eng. Alfio Nicolosi and Eng. Marco Reno for their fundamental collaboration in the experimental activities and for the long inspiring discussions on microfluidics.

I am deeply grateful to Salvo, his love is the greatest source of strength for me. I estimate him as researcher, man and for being so funny, I am lucky to have him in my life. I am very grateful to my beloved sister Laura, without her I would be lost, she is the unique reference point in my life since my birth (fortunately she is a good reference point).

BASIC PRINCIPLES OF MICROFLUIDICS

Microfluidics deals with the phenomenological study and implementation of devices for handling and transporting small quantities of fluids ($10^{-18} - 10^{-9}$ liters) through the use of channels of dimensions of the order of tens or hundreds of microns. A strong impetus to the interest to this scientific discipline was given by the spread of Lab-on-Chip technology. It is a miniaturized system that integrates on a single chip, in silicon or in polymeric material, all the components to perform the functions of a cumbersome laboratory of analysis. Before discussing in detail the microfluidic devices it is important to understand their theoretical basis and practical consequences.

2.1 Scaling law

To analyze the physical properties of microsystems it is necessary to introduce the concept of *scaling law*, namely the law of variation of

physical quantities with the size l of the system or the object in question, while keeping constant other quantities such as time, pressure, and temperature.

The implications of this law in miniaturized systems leads to important considerations: in fact, by considering the volume forces (such as the force of gravity or inertia) and surface forces (such as surface tension or viscosity), the *scaling law* for the ratio of these two kinds of forces will be expressed by:

$$\frac{\text{surface forces}}{\text{volume forces}} \propto \frac{l^2}{l^3} = l^{-1} \xrightarrow{l \rightarrow 0} \infty \quad (2.1)$$

This implies, for example, that for miniaturized systems the volume forces are negligible compared to the surface forces.

Throughout this dissertation, the validity of the continuum hypothesis of fluids on the microscopic scale is assumed. This hypothesis states that it is possible to neglect the interactions between the molecules forming a fluid considering it structurally continuous, for the physical parameters of interest.

Moreover, this dissertation will cover only incompressible Newtonian fluids. A fluid is incompressible if its density is constant and occupies the same volume, even if the fluid is in motion. A fluid is Newtonian if its viscosity is constant also when a force is applied to it.

2.2 Navier-Stokes equations

This section addresses the major equations that govern the hydrodynamics in general and microfluidics in particular: the Navier-Stokes

equations that describe the dynamic behavior of fluids. These are a set of coupled differential equations describing how the velocity, pressure, temperature, and density of a moving fluid are related. The Navier-Stokes equations cannot be solved analytically, except for some particular cases when simplifying assumptions can be made. In fact, Computational Fluid Dynamics (CFD) techniques are often used to solve approximations to them. The equations may be derived from the conservation principles of mass, momentum, and energy, respectively.

The first equation analyzed is the continuity equation which expresses the conservation of mass. In order to derive it, consider first the general case of a compressible fluid, i.e., a fluid which density ρ varies as a function of space and time.

Consider a region Ω of a fixed arbitrary shape in the fluid. The mass M of fluid that at the time t occupies this volume is equal to

$$M(\Omega, t) = \int_{\Omega} d\mathbf{r} \rho(\mathbf{r}, t) \quad (2.2)$$

where $\rho(\mathbf{r}, t)$ is the density of a compressible fluid and \mathbf{r} is the position vector.

The mass in non-relativistic mechanics is a conserved quantity, therefore, its variation in time must only be caused by a flow through the surface $\partial\Omega$. Define now the mass current density \mathbf{J} as:

$$\mathbf{J}(\mathbf{r}, t) = \rho(\mathbf{r}, t) \mathbf{v}(\mathbf{r}, t) \quad (2.3)$$

where \mathbf{v} is the velocity field. The derivative of $M(\Omega, t)$ with respect to time can be calculated either by differentiating the eq. (2.2) or integrating over $\partial\Omega$ eq.(2.3). Then, imposing their equality, the continuity equation for compressible fluids is obtained as:

$$\partial_t \rho = -\nabla \cdot (\rho \mathbf{v}) \text{ or equivalently } \partial_t \rho = -\nabla \cdot \mathbf{J}. \quad (2.4)$$

This law of mass conservation is identical to the formulation of the electric charge conservation law.

For an incompressible fluid, ρ is constant in space and time so, the eq. (2.4) becomes:

$$\nabla \cdot \mathbf{v} = 0 \quad (2.5)$$

The most elemental form of the Navier-Stokes equations is obtained [38] considering the i th component of the total momentum density $\rho \mathbf{v}$ of the fluid $P_i(\Omega, t)$, within a finite volume of an arbitrary form Ω . By applying the principle of conservation of momentum, taking into account the contributions of the forces that can act to change the momentum $P_i(\Omega, t)$, the rate of change of the i th component of the momentum can be expressed as

$$\partial_t P_i(\Omega, t) = \partial_t P_i^{conv}(\Omega, t) + \partial_t P_i^{press}(\Omega, t) + \partial_t P_i^{visc}(\Omega, t) + \partial_t P_i^{body}(\Omega, t) \quad (2.6)$$

where the terms in the second member respectively represent: the contributions to the change due to the forces of convection, the contact forces that act on the surface $\partial\Omega$ of Ω (e.g. the pressure forces and viscous forces), and the body forces which act inside of Ω , (e.g. the force of gravity, capillarity, and electrical force). The equation (2.6) in vector notation for incompressible fluids becomes:

$$\rho[\partial_t \mathbf{v} + (\mathbf{v} \cdot \nabla) \mathbf{v}] = -\nabla p + \mu \nabla^2 \mathbf{v} + \rho \mathbf{g} + \rho_{el} \mathbf{E} \quad (2.7)$$

where μ is the dynamic viscosity of the fluid expressed in $[Pa \cdot s]$. The third governing equation is the heat-transfer equation of the fluid

relating the rate of change of the energy density to the energy density flux. This equation is obtained from the energy conservation law and takes into account the enthalpy, the temperature, and the dissipation of energy due to viscous effects. The rate of change of the energy inside the volume Ω due to convection, pressure and friction forces on the bounding surface $\partial\Omega$, and by heat conduction, can be written as:

$$\partial_t E_i(\Omega, t) = \partial_t E_i^{conv}(\Omega, t) + \partial_t E_i^{press}(\Omega, t) + \partial_t E_i^{visc}(\Omega, t) + \partial_t E_i^{cond}(\Omega, t) \quad (2.8)$$

This equation properly model the dynamics of all known gases and most of liquids.

2.3 Hagen-Poiseuille law: hydrodynamic resistance

As already discussed, the Navier-Stokes equations are non-linear differential equations too difficult to solve analytically. However, there are cases where it is possible to solve the problem analytically as it happens for the pressure-driven, steady state flows called Poiseuille flows. The solution of the Navier-Stokes equations for these fluids is important to understand the behavior of liquids in Lab-on-Chip systems.

In a Poiseuille flow, the fluid is guided by imposing a pressure difference between the two ends of a long, rigid, and straight channel. For this type of flow the resolution of the Poiseuille problem provides the value of the volumetric flow rate Q , i.e. the fluid volume that passes through the section of microchannel per unit time:

$$Q = \int_{\mathcal{C}} dydzv_x(y, z) = \frac{\Delta p}{2\mu L} \frac{\mathcal{A}^3}{\mathcal{P}^2} \quad (2.9)$$

where \mathcal{A} and \mathcal{P} are respectively the area and perimeter of channel's section.

This formula is obtained by solving:

$$Q \equiv \int_{\mathcal{C}} dydzv_x(y, z) \quad (2.10)$$

where \mathcal{C} is an arbitrarily shaped cross-section in the yz-plan translationally invariant in the x direction. The table 2.1 reports the values of Q for some typical shapes of microchannel's cross-section.

Therefore, the pressure drop and the flow rate are proportional as states the Hagen-Poiseuille's law:

$$\Delta p = R_{hyd}Q = \frac{1}{G_{hyd}}Q \quad (2.11)$$

where the proportionality factors R_{hyd} and G_{hyd} are the hydrodynamic resistance and the hydrodynamic conductance, respectively. The Hagen-Poiseuille's law, eq. (2.11), is formally equivalent to Ohm's law, $\Delta V = RI$. The hydrodynamic resistance, in analogy with the electrical equivalent, allows to estimate the resistance of the channel to the fluid flow.

While the concept of electrical resistance is linked to the energy dissipation by the Joule effect, the concept of the hydrodynamic resistance is representative of the viscous dissipation of mechanical energy into heat, due to the internal frictions of the fluid.

By using the results for the Poiseuille flow in table 2.1 the values of hydrodynamic resistance for different shapes of the channel


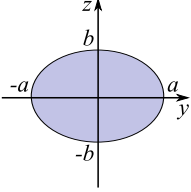
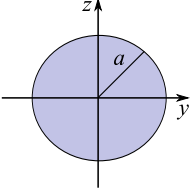
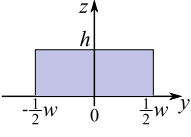
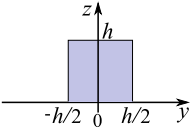
Cross-section	Q
parallel plates 	$\frac{h^3 w}{12\mu L} \Delta p$
elliptic 	$\frac{\pi}{4} \frac{1}{\mu L} \frac{a^3 b^3}{a^2 + b^2} \Delta p$
circular 	$\frac{\pi}{8} \frac{a^4}{\mu L} \Delta p$
rectangular 	$\frac{h^3 w \Delta p}{12\mu L} [1 - 0.630 \frac{h}{w}]$ for $h < w$
squared 	$\frac{h^4 \Delta p}{12\mu L} [1 - 0.630 \times 0.917]$

Table 2.1: Volumetric flow rate for different shapes of microchannel cross-section.

cross-section are reported in Table 2.2. These resistances are valid for straight channels (i.e. translationally invariant), because only in such cases the symmetry of nonlinear term $(\mathbf{v} \cdot \nabla)\mathbf{v}$ in the Navier-Stokes equation vanishes. For example, the hydrodynamic resistance, R , of a rectangular channel with length L , height h , and width w , traversed by a monophasic flow is given by

$$R = \frac{\Delta p}{Q} \approx \frac{12\mu L}{h^3 w (1 - 0.63h/w)} = \alpha \frac{L}{w} \quad \text{with } h < w \quad (2.12)$$

where μ denotes the fluid viscosity and α is a constant defined as follows:

$$\alpha = \frac{12\mu}{h^3 (1 - 0.63h/w)} \quad (2.13)$$

2.4 The Reynolds number

The nonlinear term $\rho(\mathbf{v} \cdot \nabla)\mathbf{v}$ in the Navier-Stokes eq.(2.7) complicates its solution, but can be neglected if the rate of flow is low as in many microfluidic systems. This consideration arises from the the Navier-Stokes equation written in its dimensionless form [38]

$$Re[\tilde{\partial}_t \tilde{\mathbf{v}} + (\tilde{\mathbf{v}} \cdot \tilde{\nabla})\tilde{\mathbf{v}}] = -\tilde{\nabla}p + \tilde{\nabla}^2 \tilde{\mathbf{v}} \quad (2.14)$$

Re is a dimensionless number called Reynolds number:

$$Re \equiv \frac{\rho V D_h}{\mu} \quad (2.15)$$

where D_h is the characteristic length, V is the fluid velocity, μ its the viscosity, and ρ its density. The characteristic length D_h for a

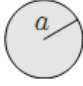
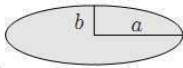
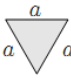
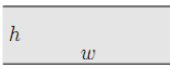
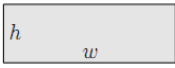
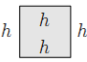
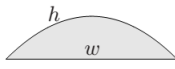

Cross-section		R_{hyd}
circular		$\frac{8}{\pi} \mu L \frac{1}{a^4}$
elliptic		$\frac{4}{\pi} \mu L \frac{1+(b/a)^2}{(b/a)^3} \frac{1}{a^4}$
triangular		$\frac{320}{\sqrt{3}} \mu L \frac{1}{a^4}$
parallel plates		$12 \mu L \frac{1}{h^3 w}$
rectangular		$\frac{12 \mu L}{1-0.63(h/w)} \frac{1}{h^3 w}$
squared		$28.4 \mu L \frac{1}{h^4}$
parabolic		$\frac{105}{4} \mu L \frac{1}{h^3 w}$
arbitrary		$\approx 2 \mu L \frac{P^2}{A^3}$

Table 2.2: Hydrodynamic resistance for straight channels of different cross-section shape.

microchannel of circular cross-section is its diameter, instead for a rectangular cross section $D_h = (2ab)/(a + b)$ where a and b , are the two sides of the rectangle.

Therefore, the Reynolds number is a dimensionless quantity that represents the ratio between the inertial forces and the viscous forces. From (2.14) it can be noted that for $Re \ll 1$ the viscous term $\tilde{\nabla}^2 \tilde{\mathbf{v}}$ prevails (this is the case of laminar flow), while in steady state for $Re \gg 1$ the inertia term $(\tilde{\mathbf{v}} \cdot \tilde{\nabla}) \tilde{\mathbf{v}}$ prevails (this is the turbulent flow case). These two regimes are depicted in Fig.2.1. From the above discussion results that the solution obtained for the Poiseuille flow remains approximately valid if the Reynolds number is small, i.e. $Re \ll 1$ [38].

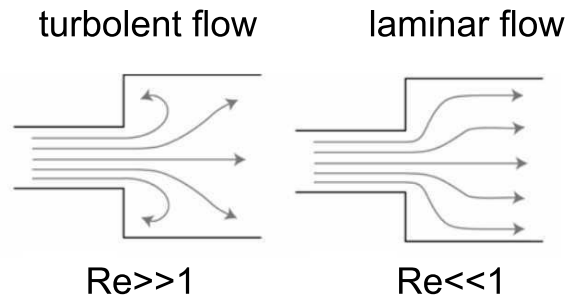


Figure 2.1: Flow regimes.

2.5 Analogy with electric circuits: Kirchhoff's laws

In general, when two straight channels of different dimension are connected the resulting problem is no longer translationally invariant,

thus is no longer possible to apply the expressions found for the ideal Poiseuille flow because the non-linear term in the Navier-Stokes equation is not strictly zero. However, if the Reynolds number is sufficiently low (see section 2.4), the non-linear term can be neglected and the Hagen-Poiseuille law holds with a good approximation.

If two channels are connected in series, their equivalent hydrodynamic resistance can be found by using the additivity of the pressure drop:

$$R = R_1 + R_2 \quad (2.16)$$

To find the expression of the hydrodynamic resistance for two channels connected in parallel the conservation of flow rate Q is exploited, obtaining:

$$R = \left(\frac{1}{R_1} + \frac{1}{R_2} \right)^{-1} = \frac{R_1 R_2}{R_1 + R_2} \quad (2.17)$$

The analogy between the Hagen-Poiseuille's law and the Ohm's law leads a correspondence between the pressure difference Δp and the potential difference ΔV and between the volumetric flow Q and the electric current I .

Therefore, it is possible to apply the principles of circuits theory to microfluidic systems and state the Kirchhoff's laws for a microfluidic network as follows:

1. at any node in the circuit the sum of the flow rates flowing into a node is equal to the sum of the flow rates flowing out of that node;

2. the sum of pressure difference in any closed loop of the circuit is zero.

2.6 Surface phenomena

As already pointed out, one of the characteristics of the microfluidics is the predominance of the surface effects on the volume effects. This section discusses the main features of the surface phenomena and in particular the capillarity.

2.6.1 Surface tension

The concept of surface tension can be explained by considering the intermolecular interactions in liquids. A molecule in the bulk of a fluid forms bonds with the other molecules that surround it gaining cohesive energy, and for the symmetry conditions the resultant force is zero. For a molecule at the free surface does not exist this symmetry then it is affected by a force directed towards the interior of the liquid. To bring a molecule from the inside of the liquid to the surface a work against the force mentioned above is needed, namely:

$$dW = \gamma dS \quad (2.18)$$

where γ is the surface tension of the liquid which depends on: the liquid, the gas above the free surface, the temperature.

2.6.2 The Young-Laplace equation

The Young-Laplace equation establishes that the surface tension causes a pressure drop across an interface in thermodynamic equi-

librium, which depends on the shape of that interface. In particular, considering the case of a curved interface, the pressure drop across this interface is given by:

$$\Delta p_{surf} = \left(\frac{1}{R_1} + \frac{1}{R_2} \right) \gamma \quad (2.19)$$

2.6.3 Contact angle

The contact angle θ_c is the angle between the interfaces solid/liquid and liquid/gas at the line of contact between the three phases. At equilibrium it is determined by the three surface tensions γ_{sl} , γ_{lg} , γ_{sg} (Fig. 2.2(a)).

The expression for θ_c is obtained by balancing the energy (or, equivalently, the forces of adhesion and cohesion) to the contact line:

$$\cos \theta_c = \frac{\gamma_{sg} - \gamma_{sl}}{\gamma_{lg}} \quad (2.20)$$

A surface is hydrophobic (cohesion predominates adhesion, i.e. high wettability) if $\theta_c > 90$, whereas it is hydrophilic (adhesion predominates cohesion, i.e. low wettability) if $\theta_c < 90$, as shown in Fig.2.2(b).

2.6.4 Capillary phenomena

Another class of phenomena related to the surface tension are the capillary phenomena. They occur when a liquid is in a narrow tubes. If a capillary tube is dipped into a liquid, the level of the liquid inside the tube is different from that of the container: is greater if the liquid wets the tube walls while it is lower on the contrary. The phenomenon can be explained by observing that the free surface in the capillary is

approximately spherical and concave or convex depending on the fluid. The height h of the liquid inside the capillary can be calculated from the Young-Laplace equation:

$$h = \frac{2\gamma \cos\theta_c}{\rho g a} \quad (2.21)$$

where a is the capillary radius.

A dimensionless quantity often used to characterize the microfluidic phenomena is the capillary number defined as:

$$Ca \equiv \frac{\text{viscous force}}{\text{surface of tension force}} = \frac{\mu V_0}{\gamma}. \quad (2.22)$$

2.7 Boundary conditions: the *no-slip* condition

Throughout this dissertation the (*no-slip*) boundary condition is implicitly imposed for liquid flow at solid walls of the domain (i.e. the microchannel). This condition postulates that all the components of the fluid velocity on a solid surface are equal to the components of the velocity of the surface itself, so if the solid wall is moving at a speed v_{wall} on that boundary $\partial\Omega$ (that is the edge of the domain) is imposed that:

$$\mathbf{v}(\mathbf{r}) = \mathbf{v}_{wall}, \text{ for } \mathbf{r} \in \partial\Omega \quad (2.23)$$

It was experimentally proven that this condition does not affect the macroscopic behavior of a fluid flow, but can lead to significant effects on a microfluidic flow. In the literature, various experimental [39] and

analytical [40, 41, 42, 42, 43] studies can be found on this topic, in order to find when this condition holds and the measurements methods of the *slip* length.

The *slip* boundary condition was introduced by Navier [44]:

$$\mathbf{v}_n = \mathbf{0}, \quad (2.24)$$

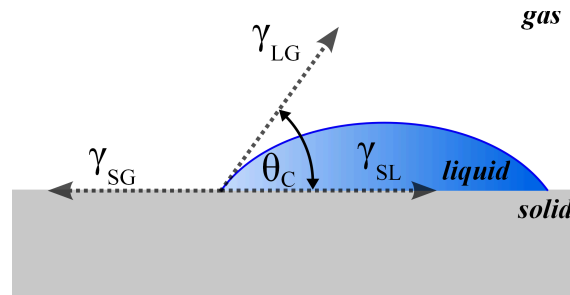
$$\mathbf{v}_t = -\lambda_s(\mathbf{n} \cdot \nabla)\mathbf{v}_t \quad (2.25)$$

where \mathbf{v}_n is the velocity normal component, \mathbf{v}_t is the velocity tangential component, \mathbf{n} is the normal vector at the surface and λ_s is the *slip* length defined as the distance from the surface where the tangential velocity vanishes, i.e. the point inside the wall where the conditions of *no-slip* is satisfied (see Fig. 2.3). Note that the velocity normal component is zero, since the wall is impenetrable.

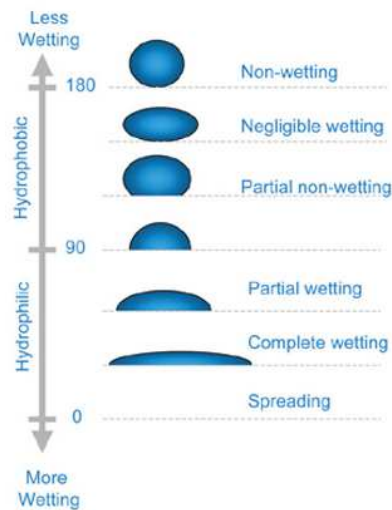
Therefore, for a flow between two infinite parallel plates with stationary walls and a flow velocity parallel to the x axis, the Navier's hypothesis states that the fluid velocity at a surface is proportional to the shear rate at this surface [44]:

$$v_x(z=0) = \lambda_s \frac{\partial v_x(0)}{\partial z} \Big|_{z=0} \quad (2.26)$$

Therefore, the value $\lambda_s = 0$ corresponds to the *no-slip* boundary condition.



(a) A droplet of liquid placed on a solid surface assumes a contact angle θ_c determined by the balance of forces at the point of interface



(b) Wetting and non-wetting liquid at a solid surface

Figure 2.2: Contact angle.

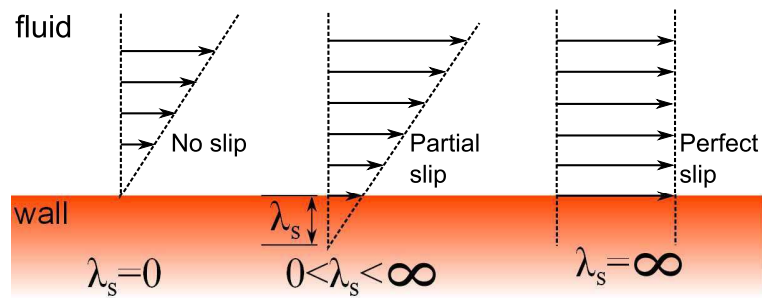


Figure 2.3: Interpretation of the *slip* length λ_s [1].

CHAPTER
THREE

DROPLETS MICROFLUIDICS

The most promising application of microfluidics is the Lab-on-Chip (LoC) technology. As already mentioned, a LoC is a microfluidic device that integrates on a small chip, one or several laboratory operations, such as transportation, processing, analysis, detection of samples. These devices are used for the detection and manipulation of cells, microorganisms, viruses, DNA, proteins, etc [45, 19]. The miniaturization of operation normally handled in a laboratory offers many advantages, including low consumption of reagents, short reaction times, compactness and cheap fabrication and disposal. Such systems are characterized by low Reynolds number, then the flow is essentially laminar. Microfluidic devices can be classified into two categories:

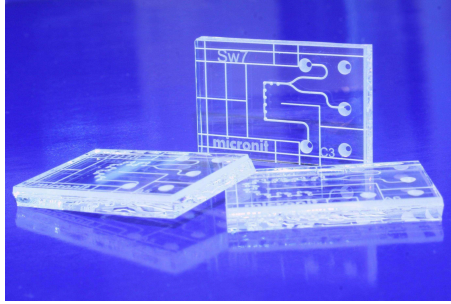
continuous flow systems based on the manipulation of a single-phase flow usually performed by means of integrated pressure valves and micropumps;

droplet based systems focus on the formation and manipulation of discrete volumes - denoted as *dispersed phase* - dispersed into another immiscible fluid - denoted as *continuous phase*.

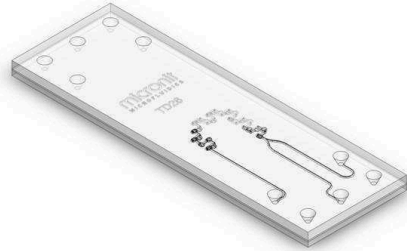
The droplets in microfluidic devices are used as vessels for samples and reagents and each droplet can be seen as a confined microreactor to perform reaction and assay independently. Thus, droplet-based microfluidic systems enhance the features offered by conventional continuous flow microfluidic systems offering many advantages over them, such as ultra-low consumption of reagents and samples, fast mixing, flexible control, minimization of absorption of sample on channel surface, high-throughput and avoid cross-contamination between the processed samples [20, 31]. Several manipulation can be performed on droplets from their generation: mixing, merging, spitting, sorting, trapping (incubation), detection. Each of these unit operations corresponds to a step of a biochemical protocol. A droplet based LoC integrates one or more of these functional modules to create a pre-programmed platform for a specific application. Applications include: encapsulation of cells and DNA for analysis and diagnostics, protein crystallization, drug delivery and formulation, etc [19]. In Fig.3.1 are shown some commercially available droplet-based LoCs. The following discussion addresses the current methods developed to manipulate droplets in microfluidic devices (e.g. LoCs) and their fabrication.

3.1 Fabrication methods and materials

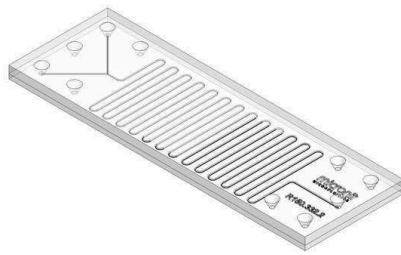
A Lab-on-Chip consists of several integrated components such as mixers, detectors, valves, pumps connected by a network of microchan-



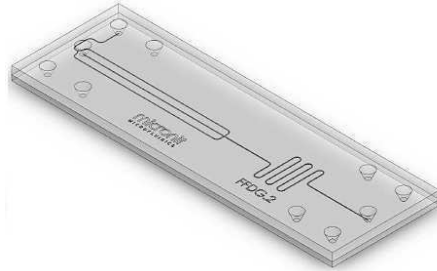
(a)



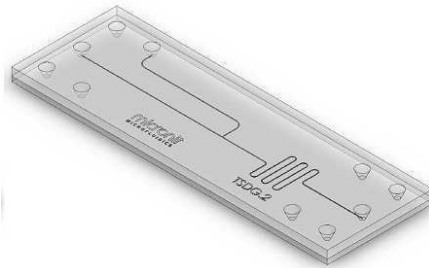
(b)



(c)



(d)



(e)

Figure 3.1: Some Lab-on-Chips from "Micronit Microfluidics": (a)-(b) micromixers; (c) microreactor; (d)-(e) droplets generators.

nels. Usually microfluidic chips are fabricating by using two polymers: PDMS (polydimethylsiloxane) and PMMA (polymethyl methacrylate or Plexiglas) which exhibits respectively, hydrophobic and hydrophilic properties[46]. The PDMS is an elastomeric polymer, flexible, cheap, transparent, biocompatible, that withstands large temperature ranges. These attractive features makes the PDMS the most widely used material for microfluidic chips. However, PDMS suffers of several drawbacks: due to its elasticity it is prone to deformations when subject to pressure higher than 10^5 Pa [47, 48], absorbs hydrophobic drugs and swells in many organic solvents such as decane [49, 50, 51]. The deformations consequently can lead to an inaccurate calculation of the flow rates and also affect the droplet trajectories in microchannels [47].

The common fabrication method for microfluidic devices is called *soft lithography* (SL), with the variations *single* and *multilayers* (used to produce devices with a more complex design); the adjective "soft" derives from the use of elastomeric materials. The common SL technique consists of several steps, the first is the creation of a device design by using CAD software and the validation of this design through CFD simulators. The second step is the *master* fabrication: the device pattern from the CAD file is printed on transparent films with high resolution and glued on a borosilicate slide obtaining the photo mask. Then, a silicon wafer coated with a layer of photoresist is covered with the photo mask and exposed to ultraviolet rays; a bath will remove the unexposed region to obtain the negative master.

The third step is the mold fabrication: a pre-polymer consisting of elastomer and curing agent (to accord it structural rigidity) is mixed at a 10 parts to 1 part ratio and degassed to remove bubbles created when mixing. Liquid PDMS pre-polymer is poured over the master

and cured for a certain period of time at an appropriate temperature. The mold is then peeled from the master, and this replica is bonded to a flat surface (glass, PDMS, silicon) to enclose the channels (usually by oxygen plasma treatment). The overall fabrication process takes about 24 h [46]. A schematization of the soft lithography process is shown in Fig. 3.2; often this technique is also called rapid prototyping. A PDMS device fabricated according to this technique is depicted in Fig.3.3(a).

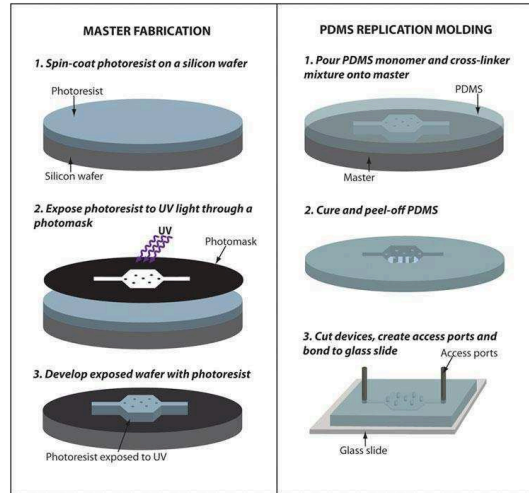


Figure 3.2: Scheme of the soft lithography process to fabricate microfluidic devices [2].

As above discussed the soft-lithography techniques [52] are time consuming and require high cost clean room equipment and facilities as well as skilled personnel. 3D printing as a new tool for low-cost and rapid prototyping of microfluidic devices is attractive because speeds

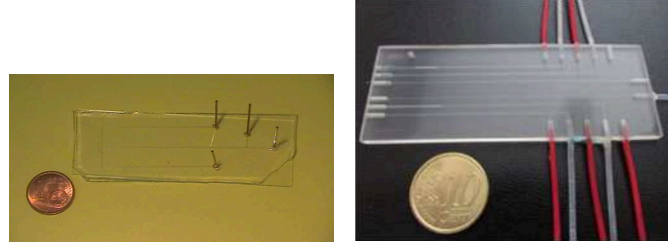


Figure 3.3: Microfluidic chips for droplets generation: (a) PDMS chip fabricated through rapid prototyping; (b) transparent photopolymer chip fabricated through 3D-printing [3].

up the fabrication process and reduces it to the creation of a computer model of the device to be printed [53, 54, 55, 56]. This oversimplification of the fabrication process is particularly important during the design validation phase, when it is necessary to test and optimize quickly the device functioning. This is possible thanks to the enhancement of the 3D printing resolution and the availability of new transparent robust and biocompatible materials. Observe that the convenience of this innovative production process is also to be searched in the low cost as compared to the price of a manufactured photolithography mask. The thermoplastic polymers (e.g. polystyrene and polycarbonate) and photopolymers commonly used for 3D printing, have been already proposed as alternative materials for the production of microfluidic devices [49, 57, 58, 59, 60, 61]. Indeed, these materials are generally transparent, therefore suitable for optical detection and resolve the critical issues of the material usually employed for fabrication of microfluidic chips, i.e. the Polydimethylsiloxane (PDMS). The 3D printing technique for the fabrication of microfluidic devices was re-

cently demonstrated also for droplet based microfluidics. In [3] the feasibility of this new approach is assessed through the characterization of a 3D printed T-junction generator, carrying out an experimental study on the droplet size providing a statistical characterization of the generation process and measurements of polydispersity index of the prepared emulsion. The findings demonstrate the feasibility of this new approach.

3.2 Effect of surfactants on droplets

Surfactants (surface active agent, SAA) are molecules characterized by a polar hydrophilic head and a nonpolar lipophilic tail. The classical distinction of these compounds refers to the nature of the hydrophilic part: anionic, cationic, etc. A surfactant, placed in water in small quantities, tends to arrange itself to the water surface with the non-polar part of the molecule in contact with the air, therefore the surface tension of water results greatly decreased. There is a threshold value of the surfactant concentration (i.e. the critical micelle concentration or CMC) above which the surfactant molecules are aggregated, giving place to a particular polymeric structure called *micelle*, in this situation the surface tension of the liquid remains almost constant as shown in Fig.3.4. Specifically, the degree of hydrophilicity or lipophilicity of a surfactant is determined by its HLB (*hydrophilic-lipophilic balance*), this value determines whether the surfactant is soluble in water, $HLB > 10$, or in oil, $HLB < 10$.

The role of surfactants in microfluidics is relevant and widely studied [62, 63, 64, 65], indeed also small amounts of surfactant can

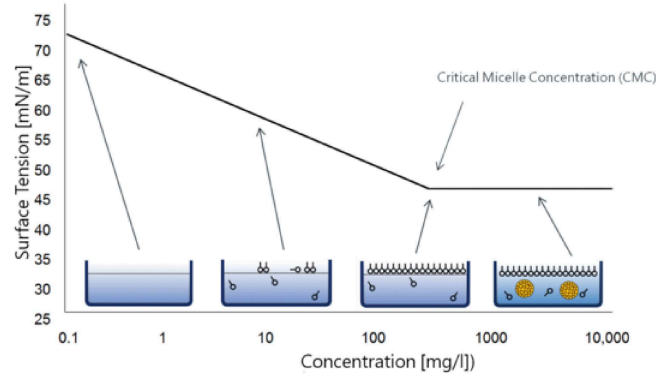


Figure 3.4: Surface tension of a surfactant solution with increasing concentration and formation of micelles.

dramatically impact on the behavior of bubbles and droplets in microchannels. For example, a bubble in an aqueous solution with addition of surfactant rises more slowly than in pure water. This phenomenon is explained by the Marangoni effect due to the non-uniform distribution of the surfactant concentration along the bubble surface[66]. Surfactants are often added to facilitate the creation and transport of droplets, but can also exist as impurities in fluids or as product of chemical reactions. The wettability of the microchannel surface and, in turn, the flow behavior can be changed by varying the employed surfactant and its concentration. For example, in [67] it is proved that the addition of Span80 agent to oleic continuous phase, can change the surface of the PMMA from partially hydrophilic to completely hydrophobic, whereas the addition of Tween 20 to the aqueous continuous phase converts the surface of the PMMA in a oleophobic surface. These contact angle modifications are due to the

absorption of the surfactant molecules at the interface between the two phases.

In the devices for droplets generation surfactants are added to emulsions both to decrease the surface tension facilitating the droplets formation, and to prevent unwanted coalescence. In fact, emulsions are thermodynamically metastable and the addition of the appropriate surfactant makes them stable avoiding coalescence phenomena. For example, w/o emulsions (i.e. water used as dispersed phase and oil as continuous phase) may be made stable by the addition of a lipophilic surfactant (e.g. Span80) to the continuous phase, whereas o/w emulsions by the addition of a hydrophilic surfactant (e.g. Tween 20) to the aqueous continuous phase. In particular, the effect of surfactants on the droplet formation by a T-junction generator has been studied in [68, 69, 70, 71]. These studies demonstrate that the addition of surfactant also increases the rate of droplet generation.

3.3 Droplet generation

The first step in the life cycle of a droplet is its generation. The passive methods to generate a continuous stream of droplets, monodisperse (i.e. having the same shape and the same size) and evenly spaced, exploit the flow field to deform the interface between two immiscible phases promoting an increase in the instability at that interface. Generally, these mechanisms allow the production of droplets with polydispersity index, defined as the percentage ratio between the standard deviation and the average droplets size, between 1 – 3%. Water-in-oil emulsions (W/O) are best formed in hydrophobic channels (PDMS),

whereas oil-in-water (O/W) emulsions can be generated in hydrophilic channels (PMMA), this to prevent droplets from sticking to the microchannel walls.

Passive

The fluid used to be dispersed into droplets (or bubbles) is called dispersed phase and the fluid that transports the droplets is the continuous phase. Depending on the type of flow field in the region where the two phases meet, these structures can be classified into three configurations:

co-flowing a thin glass capillary or a metal needle carrying the disperse phase is inserted as a center channel inside an outer channel carrying the continuous phase (Fig. 3.5(a));

flow-focusing the dispersed phase is located in a center channel while the continuous phase enters from two parallel side channels. In this way, the dispersed phase is squeezed between the two continuous phase flows [4] (Fig. 3.5(b));

cross-flowing (also called T-junction) the dispersed and continuous phases flow through two orthogonal channels and the dispersed phase is sheared by the continuous phase at the junction (Fig. 3.5(c)).

In general droplets formation is due to the competition between viscous shear stresses, which tends to deform the interface between the

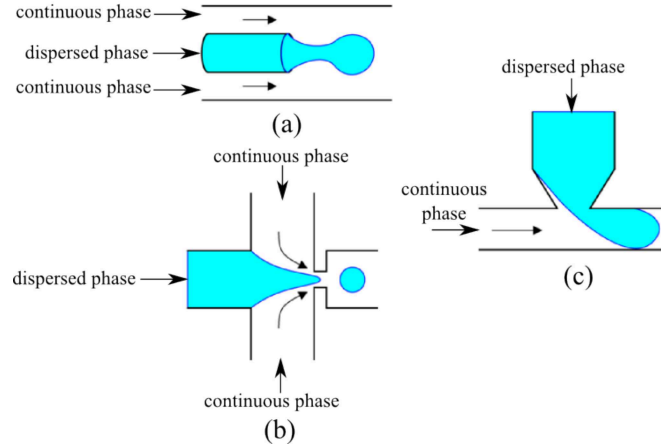


Figure 3.5: Configuration of passive microfluidic droplets generators: co-flowing, flow focusing and cross-flowing.

two phases, and the capillary pressure ¹, acting to resist deformation, this competition is expressed by the capillary number Ca [72].

There are many parameters which can affect size and rate of the generated droplets, such as channel dimensions and geometry, flow rates, channel wetting properties, use of surfactants, physical properties of the two phases. Several theoretical and numerical studies can be found in literature on the characterization of droplets formation process, these focuses on the study of relationships to control and predict droplets size and rate in co-flowing geometry[73, 74, 75], flow focusing geometry [76, 77, 64],and cross-flowing geometry [78, 79, 80, 81].

¹The capillary pressure is defined as the pressure difference across the interface between two immiscible fluids: $p_c = \frac{2\gamma \cos \vartheta}{r}$ (see section 2.6.4)

The T-junction geometry is the most used and studied because the parameters on which to act to control the droplets production are less than the flow-focusing geometry, and because the droplet generated are highly monodisperse and evenly spaced with respect to the co-flowing method. Droplets through a T-junction can be generated in three different regimes: jetting, dripping and squeezing, depending on the value of the capillary number Ca . The three formation regimes differ in where the droplet break-up (pinch-off) occurs.

In the squeezing regime droplets pinch off at the junction, in the dripping regime in a region near the junction, whereas the jetting regime is characterized from a break-up process at the end of an extended thread formed by the dispersed phase away from the nozzle. In the squeezing regime the stream of the dispersed phase in the first stage of droplet formation, obstructs the main channel causing a spike in the upstream pressure which squeezes the neck of the emerging droplet determining its break-up [78]. In the dripping regime the formation mechanism is determined by the viscous shear stress. In the jetting regime the droplet neck is broken by the Plateau-Rayleigh instability. The droplets generated by instabilities are less uniform in size and spacing because the break-up process is more erratic. Moreover, the instabilities can produce small satellite droplets in addition to the main droplets. Therefore, as demonstrated in many experimental works, the more stable regime is the squeezing regime which produces a regular and monodisperse droplets stream for small values of the capillary number ($Ca < 0.002$) [81, 3]. Several works support the idea of a two-stage growth and necking stage for the droplet detachment process to find a relationship that predicts the droplet size

from the flow rates of the two phases [78, 82, 83, 84, 85]:

$$V_d^* = \chi + \beta Q_d/Q_c \quad (3.1)$$

where $V_d^* = V_d/w_c^2$ is the dimensionless droplet volume and χ and β are parameters corresponding to the two stages of the droplet detachment process. Generally, these two parameters can be considered constant for a specific generator geometry and capillary number [86, 87]. Droplets spacing is also a function of these two parameters[87]:

$$\lambda^* c = 1 + Q_d/Q_c (\chi Q_c/Q_d) \beta \quad (3.2)$$

where λ is the dimensionless droplets spacing. The eqs. (3.2) and (2.1) are proven valid in squeezing and dripping regime. In particular for the squeezing regime the following relationship for the droplet size holds [78]:

$$L/w_c = 1 + \chi Q_d/Q_c \quad (3.3)$$

where L is the droplet's length, w_c is the microchannel's width and the constant χ is of order unity. Therefore, a control over the droplet generation and spacing (i.e. the frequency) can be achieved by changing the flow rates ratio between the dispersed and the continuous phase.

Active generation [4]

The above discussed techniques generate continuous streams of droplets. To generate single droplets on-demand active control is required. Firstly, the dispersed phase has to be static for this application. This can be achieved by stopping the flow, but in case of syringe pumps, control can be hindered by elastic effects from the tubing and is therefore not very fast or stable. A simpler approach is

to use a pressure controller for the dispersed liquid phase. Stopping the soon-to-be-dispersed liquid phase can be facilitated by using a tapered channel: as the liquid traverses through the tapering channel, its curvature increases. Ultimately the increasing Laplace pressure will match the applied pressure on the liquid phase, causing the flow to stop. By applying a short pressure pulse a droplet can be generated on demand. Other active methods for on demand drop generation include electrowetting [5, 88, 89], SAWs [90], pneumatic valves [91, 92, 93] and laser-induced cavitation [94]. A nice feature of the pneumatic valves is that consecutive pneumatically controlled droplet generators can directly combine different solutions into one droplet at controllable ratios [95].

Also industrial solutions (*Mitos Dropix by Dolomite*) are available to generate droplets off-chip with accurate user-defined control of droplet size, frequency and isolation of contents [96].

3.4 Droplets manipulation methods

As interests grow in the field of droplet-based microfluidics, more technologies are being developed to control and manipulate droplets. Methods to generate and manipulate droplets can be classified into [31, 20]:

- *passive methods*, related to the use of pure hydrodynamic or surface forces to control the droplets through an appropriate design of microchannels.
- *active methods*, related to the use of electrical control, pneumatic valves, acoustic waves, temperature gradient to control

the droplets motion.

These methods are used to force droplets to perform unit operation, i.e. to execute the desired biochemical protocol such as reagents mixing, sample incubation, detection of species, etc. A schematic overview of the droplet manipulation techniques is provided in Fig.3.6.

3.4.1 Passive methods

The physics underlying microfluidic devices involves complex phenomena occurring at the microscale [38]. In the following are summarized only some basic principles that are usually exploited to design a passive device for droplets motion control by exploiting the microchannels geometries.

The analogy between the Ohm's law and the Hagen-Poiseuille's law discussed in section 2.3 allows to design a microfluidic network using an equivalent electrical circuit model exploiting the Kirchhoff's laws, where the electrical resistance will be replaced by the hydrodynamic resistance of each microchannel segment. Taking into account this analogy, it is possible to model the flow fields and, therefore, predict how a bubble or a droplet moves in a microfluidic network; in particular, a droplet always moves along the path with minimum instantaneous hydrodynamic resistance or equivalently the path with the highest instantaneous flow rate.

Another important aspect to be taken into account to design a passive microfluidic device is the minimization of the *surface energy*. A droplet will naturally tends to minimize this energy by reducing its surface area. Considering that the sphere is the geometrical form with the smallest surface/volume ratio, an isolated droplet will tend

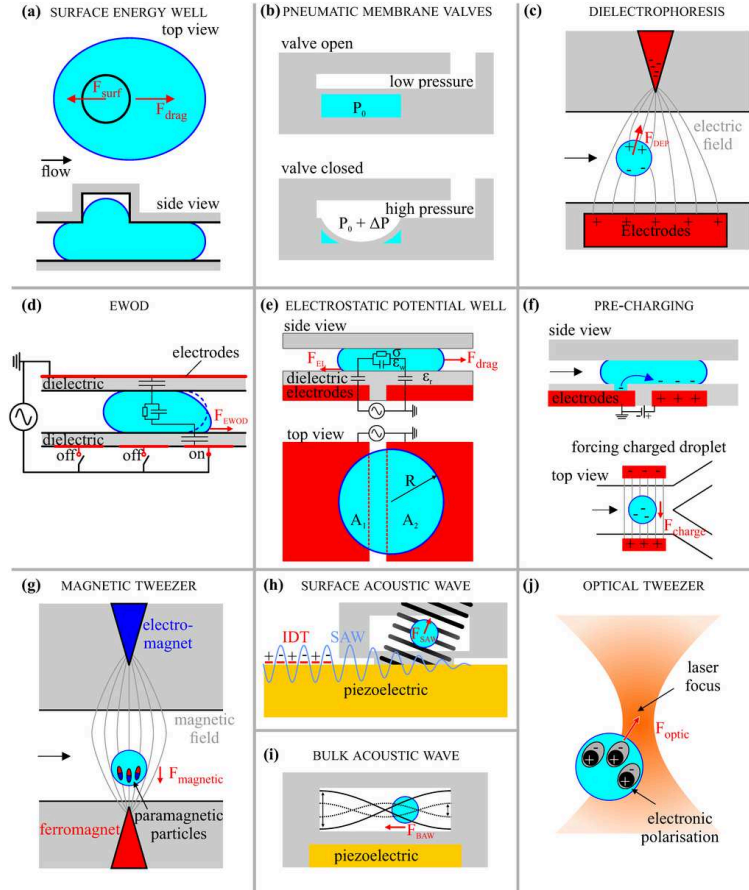


Figure 3.6: Schematic overview of the droplet manipulation techniques.

(a) A squeezed droplet can decrease its interfacial energy by expanding in a hole; (b) Increasing the air pressure above the local water pressure expands the membrane into the crossing microchannel, effectively blocking it; (c) A polarizable medium will move towards the region with highest electric field intensity; (d) The electrostatic energy will be minimal when a droplet covers the activated electrode; (e) A droplet passing two electrodes finds a minimum energy when centered above the electrodes; (f) By taking charges from the open electrode, a droplet can be precharged. A precharged droplet will move towards the oppositely charged electrode; (g) Paramagnetic particles move towards the highest magnetic field strength and can drag a droplet along with them; (h) The interdigital transducer creates a surface acoustic wave that is attenuated at the PDMS pillar, creating an upward pressure wave that can move droplets; (i) At specific frequencies the piezo can create resonating pressure waves in a channel, forcing a droplet towards the antinodes; (j) A medium with better polarizability at optical frequencies than the surrounding medium will move towards the region of high intensity laser light. Reprinted from [4].

to assume this shape. When the droplet is confined in a channel is flattened and so has a greater surface energy. A direct result of surface tension is the Young-Laplace equation, discussed in section 2.6, that relates the pressure drop across the curved droplet interface to the curvature of this interface. The curvature can be imposed by an appropriate design of channel geometries; in this way it is possible to affect the droplet behavior, exploiting the counteracting effects associated to the hydrostatic pressure, given by the Hagen-Poiseuille law, and the confinement induced Laplace pressure drop. These hydrodynamic interactions are often used to trap a droplet for incubation operation.

3.4.2 Active methods

Active manipulations change the behavior of a droplet (in flow) by an external, user-controlled mechanism. To this purpose, several techniques have been developed. Some of them are listed in the following.

Pneumatic valves

A bilayer PDMS chip is used as the basis for pneumatic membrane valves. The bottom layer contains microchannels for flowing liquids (flow layer). The upper layer integrates a network of air filled channels (control layer). At the points where the channels cross, the two layers are separated by a thin PDMS membrane. By increasing the pressure of air, the control layer can selectively compress and clog channels of the fluidic layer deflecting the membrane into the flow channel. This mechanism enables the fluids and then the droplets motion control. This technique has been applied for creating a peristaltic pump [97],

for the sorting of droplets, and for droplets generation [4].

Dielectrophoresis

Droplets can be handled using electric fields applied locally in the microchannel. The energy of an electric field is altered by the introduction of a dielectric body as a water droplet. If the electric field is non-uniform, the alteration of the energy will be greater when the dielectric body is located in the region of higher field force. The dielectrophoretic force is the rate of change of electrical energy with the displacement of the dielectric body. By exciting appropriately the electrodes, the electric field distribution can be reconfigured under electronic control to direct the droplets motion. The manipulation of droplets through dielectrophoresis is possible due to the polarization of the droplets which occurs when they are subjected to an non-uniform electric field. The dielectrophoretic force F_{DEP} for a drop of volume V suspended in a medium of dielectric constant ε_s and under the effect of an non-uniform electric-field E , can be mathematically described as:

$$F_{DEP} = \frac{3}{2} V \varepsilon_s f_{CM} \nabla E^2 \quad (3.4)$$

where f_{CM} is the real part of the Clausius-Mossotti factor that is equal to

$$f_{CM} = Re \left\{ \frac{\varepsilon_d - \varepsilon_s}{\varepsilon_d + 2\varepsilon_s} \right\} \quad (3.5)$$

where ε_d and ε_s are respectively the complex dielectric constant (frequency-dependent) of the dispersed phase and the continuous phase.

When $\varepsilon_d > \varepsilon_s$ a positive dielectrophoresis moves the droplet toward the region with highest electric field while for $\varepsilon_d < \varepsilon_s$ the droplet is repelled and trapped in a "cage" of energy. The DEP does not require contact between the droplet and the substrate (this is not valid for EWOD), then this manipulation method can be used with polar, non-polar, aqueous and organic droplets.

EWOD

Electrowetting-On-Dielectric (EWOD) (also known as digital microfluidics, DMF) generally uses arrays of control electrodes insulated by a thin dielectric layer to control conductive droplets [4] as shown in Fig. 3.7(a). In particular, EWOD mechanism allows to control the contact angle (the wettability of liquids) between a liquid and a solid dielectric surface by using an electric voltage (see Fig. 3.7(b)). The EWOD is based on the Lippmann principle:

$$\gamma_{SL} = \gamma_{SL}^0 - \frac{\varepsilon V^2}{2d} \quad (3.6)$$

where γ_{SL}^0 is the interfacial tension when the voltage V is not applied, ε is the dielectric constant and d is the thickness of the insulating layer. When an electric voltage is applied, the electric charge changes the free energy on the dielectric surface, inducing a variation in the contact angle of droplet [5], i.e. a change in the surface wettability that becomes from hydrophobic to more hydrophilic (cfr. Fig. 3.7(c)). Such a change in contact angle is provided by the Lippmann-Young equation:

$$\cos\theta = \cos\theta_0 + \frac{\varepsilon V^2}{2d\gamma_{LG}} \quad (3.7)$$

where θ_0 is the contact angle in the absence of the electric field. This mechanism is used to split, generate, merge and direct droplets. EWOD mainly uses aqueous droplet which are conductive due to the addition of ions [4].

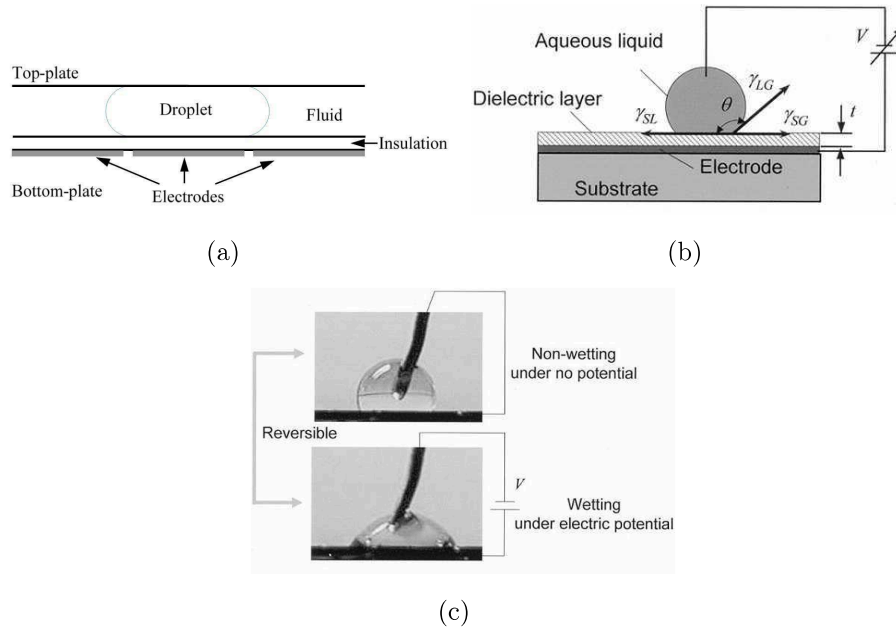


Figure 3.7: EWOD (*electrowetting-on-dielectric*): (a) configuration; (b) mechanism; (c) example of contact angle change. Reprinted from [5] ©2003 IEEE.

Thermocapillary

The thermocapillary effect or Marangoni effect, exploits the temperature dependence of the surface tension. In fact, a locally temperature gradient results in an surface tension gradient at the droplet interface;

hence, because a flow is always directed towards regions of higher surface tension, this occurrence affects the droplet motion. The local heating of droplets, achieved by a focused laser beam, is demonstrated in [98] to implement a complete platform for droplets manipulation (generation, merging, sorting).

Other active manipulation techniques

For the sake of completeness other active manipulation techniques should be mentioned: surface acoustic waves by piezoelectric transducers that generate localized pressure field, droplets pre-charging and magnetic fields used to manipulate magnetic particles [99].

3.4.3 Splitting

The splitting of droplets in microchannels is exploited for several purposes: to increase the capacity of a system and thus its throughput, to simultaneously generate droplets different in size, to produce sample replicates and also, as the droplets in many applications are used as a vessel for chemical substances, splitting allows to control the concentration of chemical species in every drop daughter generated by fission from a parent droplet [100].

Active

The splitting is performed by applying an external electric control, e.g. EWOD. The fission of a droplet is achieved by activating three or more electrodes in a row to elongate the droplet and then deactivating the middle electrode to reduce the contact angle. The activated regions

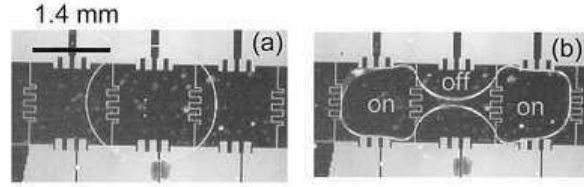


Figure 3.8: Droplet splitting by EWOD (*electrowetting-on-dielectric*). Reprinted from [5] ©2003 IEEE.

will attract the droplet until it is split in the central part as reported in Fig. 3.8.

Passive

Droplets splitting can be achieved passively by the use of symmetrical or asymmetrical T-junctions as in Fig. 3.9 [101, 102, 100]. These studies suggest that the break-up occurs only when a droplet is large enough. The break-up is due to the competition between the shear stress and interfacial tension on a droplet deformed at a junction, according to the Rayleigh-Plateau instability phenomenon (i.e. a cylindrical flow can reduce its total surface, and then break, when its length exceeds its circumference). When the continuous phase exerts a critical asymmetrical viscous stress on the droplet, causing an imbalance in its surface tension, the break-up occurs [100]. This behavior can be described by the capillary number Ca . When Ca is greater than the critical capillary number, C_{cr} , the break-up takes place. An expression for C_{cr} is given in [101]:

$$C_{cr} = \kappa \varepsilon_0 (1/\varepsilon_0^{2/3} - 1)^2 \quad (3.8)$$

where κ is a dimensionless fitting constant that depends on the contrast between the two viscous fluids and the geometry of the channel ($\kappa = 1$ for square channel) and $\varepsilon_0 = l_0/\pi w_0$ is the extension ratio of a droplet in the main channel, before it arrives at the junction as shown in Fig. 3.9. The size of the daughter droplets can be predetermined by making the two outlet channels asymmetric (i.e. having different hydrodynamic resistances). However, given that the presence of droplets in a microchannel modifies the resistance, this can cause erratic droplet break-up especially when multiple splitters are serially combined to repeatedly breakup droplets[103]. In [101] is found that the volume of the droplet daughter is inversely proportional to the resistance of the channels, whereas in [100] is demonstrated that it also depends on the size of parent droplet.

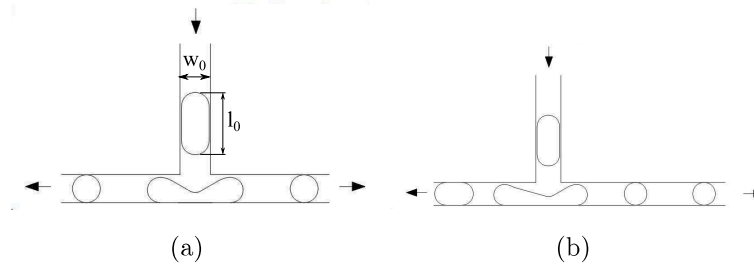


Figure 3.9: Geometry mediated droplets fission: (a) symmetrical configuration; (b) asymmetrical configuration. The parameters l_0 and w_0 are the length and width of the droplet before it arrives at the junction. These parameters are used in eq. (3.8) to calculate the critical capillary number at which the droplet break-up occurs.

3.4.4 Merging

Controlled coalescence of the droplets is a crucial operation, since it allows to perform combination between chemical substances that compose the droplets starting chemical and biological reactions in microfluidic devices. Such reactions are used in many applications which include the synthesis of biomolecules, kinetic studies, chemical synthesis, etc. In many reactions the reagents must be kept isolated until they reach suitable conditions, then the merging process must be controlled very precisely as a premature or late fusion can lead to false results. To promote droplets coalescence the droplets must be brought into close contact for a critical amount of time and wait for the thin film between droplets to be squeezed out. Indeed, when the droplets are in contact they form a thin bridge of liquid between them, due to the attractions between the molecules, the greater curvature of the meniscus around this bridge will cause an imbalance in surface tension that results in a rapid droplets merging. Therefore any technique that can transport or trap droplets is capable of bringing two drops together and merge them. For instance thermocapillary effect and SAW have been used to trap a droplet until a secondary droplet flows toward it [4].

However, droplets merging is not a straightforward issue because they must achieve temporal and spatial synchronization. Several passive and active techniques are developed to synchronize droplets before their fusion [104].

Active

The active fusion can be achieved using the EWOD technology by activating the middle electrode under a droplet and leaving off the lateral electrodes, [5], as shown in figure 3.10; note that even after all electrodes are switched off the shape of the meniscus of the merged droplet, is not circular, this is explained by the hysteresis of contact angle, that is one of the drawback of the EWOD.

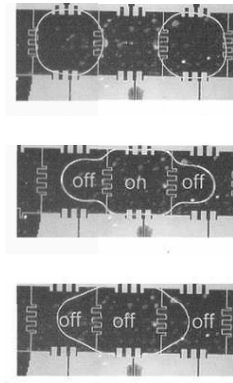


Figure 3.10: Droplet merging through EWOD. Reprinted from [5] ©2003 IEEE.

Another method for active merging is the electrocoalescence (EC) in which the fusion is achieved by applying an alternating voltage. In the presence of an electric field the behavior of a droplets can be assimilated to the perturbation of a dipole placed in its center, when two droplets approach they are attracted by a coulombic force, proportional to the square of the applied electric field, giving place to the

electrocoalescence [6]; a scheme of this device is shown in Figure 3.11.

In [105] the electrocoalescence is performed pre-charging droplets during their generation, through the application of a DC voltage. The device generate droplets of different chemical composition and of opposite charge. The droplets will join in the point of confluence of the two streams. The electrodes used to charge the droplets, after their formation, will also provide the electric field to force them along the flow lines, allowing their coalescence. With the application of an electric field droplets generation is perfectly synchronous and this ensures that the pairs of droplets will reach the point of confluence synchronically.

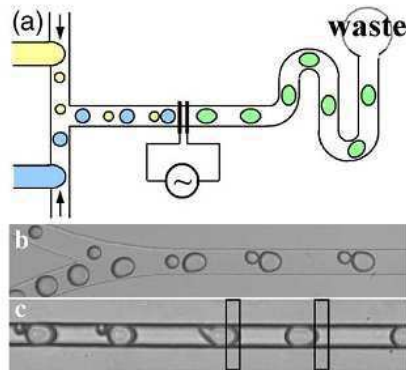


Figure 3.11: Electrocoalescence, diagram of the device: the water droplets of two different sizes are generated independently using a T-junction and are merged together in a single channel, when the smaller droplet reaches the larger one coalescence is performed by the application of an electric field by means of two electrodes. Reprinted with permission from [6]. Copyright 2006, AIP Publishing LLC.

Another active method exploits the dielectrophoresis (DEP). The device consists of micro-electrodes independently addressable through an interface. The merging is obtained activating adjacent electrodes and driving the motion of a droplet towards another until coalescence occurs [106].

Other methods use the overheating of two adjacent droplets through, for example, a laser [98]. This localized overheating produces depletion of surfactant molecules at the droplets interfaces breaking the thin film between the two interfaces, leading to coalescence. Overheating is also used for the generation and control of droplets motion by exploiting the thermocapillary forces [107].

Passive

The passive merging process is rather complex as it must ensure that the droplets are synchronized so that they can meet and join. This can be done by controlling the rate of volumetric flows and the geometry of the channel. The channel topologies, proposed in the literature, that allow the drainage of the continuous phase that separates the droplets promoting their fusion, are mainly two. The first technique is the design of an obstruction in the channel adding an obstacle or a narrowed channel as in [108]; in this way the leading droplets will be trapped providing sufficient time for a subsequent droplet to meet the previous one [99], an example is shown in figure 3.12(a).

The second one consists in a expansion region of a portion of the channel as in figure 3.12(b). A droplet in the expansion is slowed down and continuous phase is drained. Then, the droplets exit through a sudden contraction that increases the flow rate and creates the imbal-

ance required to break the thin film allowing fusion to take place.

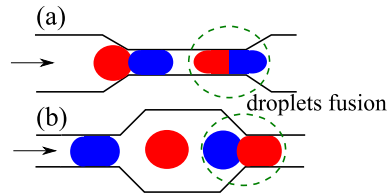


Figure 3.12: Geometry mediated droplets fusion can be achieved by: (a) stopping the droplet at a narrowed channel; (b) slowing down the droplet movement in a widening channel.

3.4.5 Mixing

The mixing of the reactants encapsulated into droplets is important for the study and the realization of chemical reactions and generally is the next step after merging. The problem to be addressed is how overcome the interfacial forces between two fluid flows to be able to carry out the mixing. For the condition of laminar flow in fact, when two streams come into contact, the mixing can not be turbulent but only diffusive. The property that allows two adjacent miscible fluids to flow in a distinct way then becomes an obstacle to get around.

Passive

There are two ways to achieve the mixing between two fluids in a passive device. In the first technique the reagents are introduced as laminar adjacent flows and then, using a symmetrical or asymmetrical junction, the continuous flow is broken into droplets. The reactants are

then mixed by diffusion or by convection induced by the surrounding flow or channel walls. The other technique is based on the merging of droplets discussed in the previous section.

When a droplet moves along a straight channel the mixing is facilitated by the flow recirculation that distributes reagents from the center of droplet to its edge [109]. When the concentration gradient is perpendicular to the direction of transport the mixing is not effective, whereas if it is parallel the mixing is effective; these two occurrences are shown in Figure 3.13 [7]. For droplets generated through a symmetrical junction, the reaction gradient is directly transferred from the laminar flow to them (Figure 3.14), while for droplets generated through an asymmetric system mixing is facilitated by an effect called *twirling*, which creates a vortex into droplets allowing an effective mixing. This effect shown in Fig. 3.15, however, is finished, and then significantly decreases the mixing time only for short droplets [7].

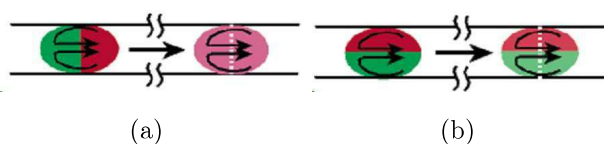


Figure 3.13: Effects of initial conditions on the mixing due to recirculating flow inside droplets that move in a straight channel. (a) The flow recirculation (represented by black arrows) effectively mix the solution of reagents which are initially localized in the front and rear halves of droplet. (b) The flow recirculation does not mix effectively the solution of the reactants initially localized in the left and right halves of droplet. Reprinted with permission from [7]. Copyright 2003 American Chemical Society.

The mixing can be facilitated and sped up by creating a more

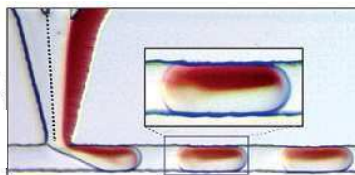


Figure 3.14: A symmetric system for droplets generation that transfers the concentration gradient of the continuous flow to the droplets. Adapted with permission from [7]. Copyright 2003 American Chemical Society.

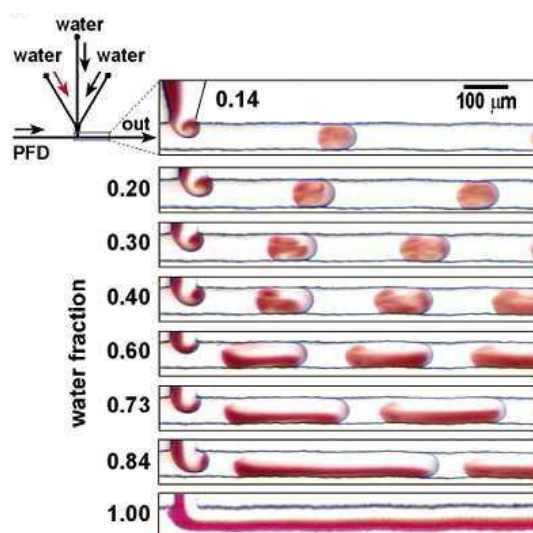


Figure 3.15: "Twirling" effect: facilitates the mixing but only occurs for small droplets. Reprinted with permission from [7]. Copyright 2003 American Chemical Society.

complex geometry of the channel for example with several serpentines as in Fig.3.16, in fact a droplet passing through curves is subjected to stretching, folds, reorientations that induce the chaotic mixing of encapsulated reactants [8, 110].

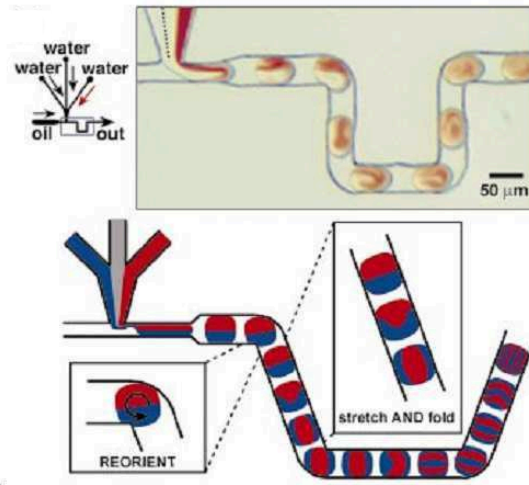


Figure 3.16: Diagram of mixing in droplets through a serpentine showing that the droplets are stretched, reoriented and folded, this allows a fast and effective mixing. Reprinted with permission from [8]. Copyright 2003, AIP Publishing LLC.

Active

Active mixing is obtained through the techniques already presented previously for merging: EWOD, DEP, etc. The electrical control allows to reduce the size of the device, since the droplets may be driven in any direction back and forth, whereas passive mixing needs long

and topologically complex channels as discussed above. In [111] an extensive study on the characterization of droplet merging by EWOD can be found.

3.4.6 Other operations

Holding droplets at a specific location in a microchip during flow can be used for several protocol steps. One step could be incubation, where a droplet needs to wait for a chemical or biological process to reach completion. Or a step in which droplets need to be analyzed over a longer time, this is easier if the droplets are not moving. Geometrical structures are the simplest method for droplets trapping. For example, the microfluidic parking networks perform the trapping at specific on-chip locations by exploiting the competition between the Young-Laplace and the pressure drop.[29]. It is clear that active methods as EWOD and pneumatic valves are intrinsically capable of trapping and releasing, since it controls all motions of the droplet [4].

Another important operation on droplets is sorting. This allows isolation of droplets of interest, synthesis of samples, filtering of contaminants. An active sorting technique can be implemented by control algorithms applied to the electrodes as in [106], [105]. The droplets sorting will be discussed in chapter 6.

3.5 Bubble Logic

The interaction of logic gates could be useful in droplet microfluidics to perform more complex routines automatically and determined by the current state of the microfluidic device.

Recent studies, extending previous preliminary works on hydrodynamic droplet behavior in microchannels, introduced the innovative concept of *bubble logic* consisting in steering hydrodynamically the flow of bubbles/droplets into a microchannel network by means of other properly timed bubbles/droplets [112, 10, 113]. The idea is to integrate chemistry with computation to provide flow control mechanism for microfluidic processors without off-chip components. A bubble that travels in microchannel can carry a double payload because represents one bit of information but also transports a chemical load inside it. Using such bubbles in [10] is demonstrated the nonlinearity, gain, bistability, synchronization, cascability and feedback required for a scalable universal logic family.

Examples of basic logic computing devices introduced in [10, 113], include an AND/OR gate and an INVERTER gate, a T flip-flop, a synchronizer, and an oscillator. The logic gates are based on a simple coding scheme: the presence of a droplet in the device corresponds to a binary value 1; no droplet in the device corresponds to a binary value 0. Figure 3.17 shows AND, OR, NOT gates that form a universal logical set. These device were designed exploiting the hydrodynamic principle stating that a bubble (or droplet) always flows in the channel with minimum instantaneous resistance. Another device reported in [10] is the bistable, in Fig. 3.19, able to trap and release individual bubbles, implemented as a flip-flop of type T (see Fig. 3.18). This is the basic unit of memory in the bubble logic. The hydrodynamic principles exploited for its design are the minimization of surface energy of a bubble and the Young-Laplace equation.

However, this logic implemented in low-Reynolds-number droplet hydrodynamics is asynchronous and thus prone to errors that prevent

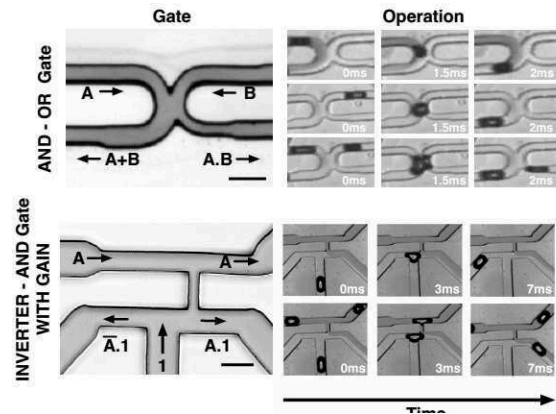


Figure 3.17: Microfluidic bubble Logic. A bubble in a channel represents one bit. **A** and **B** indicate the two inputs of the device. The top row shows a two-input AND-OR gate with two symmetrical input channels **A** and **B** and two asymmetrical output channels ($A + B$ and $A \cdot B$ computing the two outputs simultaneously). The bottom row depicts a universal $\overline{A} \cdot B$ gate with gain that can be used to switch a larger bubble by a smaller one. The device has two asymmetries, a T-junction at the bottom and a thin channel that provides a variable flow from the top contro channel [9]. The scale bar in the figure is $100\mu\text{ m}$. Reprinted from [10] with permission from AAAS.

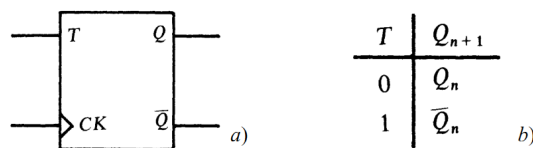


Figure 3.18: The T or "toggle" flip-flop: a) electronic circuit symbol e b) truth table

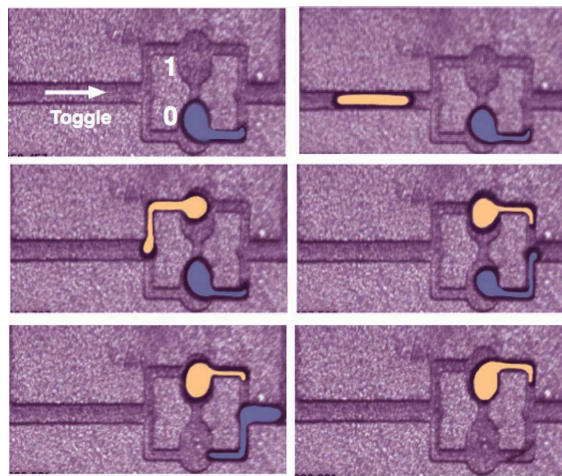


Figure 3.19: Microfluidic one-bit memory implemented as a toggle flip-flop. The gate stores its state indefinitely (zero for the blue bubble) until a toggle signal arrives (orange bubble, left to right). This switches the state of the flip-flop from zero to one, until another toggle bubble arrives. Adapted from [10]. Reprinted with permission from AAAS.

scaling up the complexity of logic operations. In a recent work [114] is presented a platform for error-free physical computation via synchronous universal logic by coupling of magnetic and hydrodynamic interaction forces between droplets. This platform uses as active control a rotating magnetic field that enables parallel manipulation of arbitrary numbers of ferrofluid droplets on permalloy tracks to develop logic gates.

In this context other experimental devices exploiting pure hydrodynamic manipulation of droplets have been realized to demonstrate the feasibility of simple computing and communication tasks entirely in the microfluidic domain: a coding/decoding scheme has been proposed in [11, 115]. In [11] information is encoded in the distance between consecutive droplets which flow through a cascade of two microfluidic circuits exhibiting the same topology so as to allow reconstruction of the information at the destination. Figure 3.20 shows a possible encoder/decoder from [11], an analog input signal is obtained by modulating the pressure of the dispersed phase in a continuous manner while a digital signal can be obtained using a electronically controlled valve for applying two pressure values to the dispersed phase which corresponds to 0 and 1. The first ring performs the encoding in the sequence of the time intervals between the droplets while the second ring performs the decoding.

All the above operations are realized by very simple devices, consisting of appropriate combinations of micro-channels. In this way, similarly to what happens for electrical signals, the controlled and the controlling quantity are homogeneous. Thanks to such homogeneity, bubble logic devices can be cascaded and even connected to form feedback loops, paving the way towards support of more complex functions

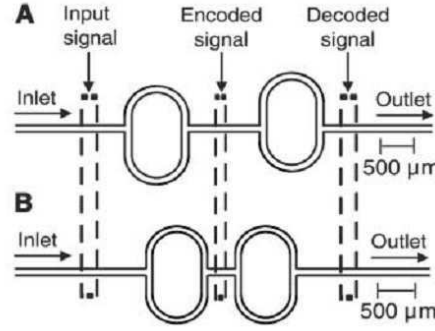


Figure 3.20: Encoding and decoding a signal. (A and B) Schematic diagrams of the encoder/decoder devices. Droplets arrived at the first loop separated by varying, aperiodic time intervals, which form a signal, and emerge from the first loop encoded in a period-2 fashion. From [11]. Reprinted with permission from AAAS.

[10]. Indeed, computing microfluidics, in which the droplets and the bubbles that flow through microfluidic channels represent information bits, can be used as a paradigm for scalable control mechanisms to manipulate this new class of materials, this technology may have a great impact on a large number of fields such as cell analysis, chemical assays, combinatorial chemistry, etc.

3.6 Droplet resistance

In order to appropriately control the droplet motion it is important to stress that the presence of a droplet in a microchannel increases the hydrodynamic resistance of such microchannel. In particular, the droplet induces an additive resistance R_D .

Although it is difficult to accurately predict the resistance added by a droplet in a channel, several studies confirm that the hydrodynamic resistance R' of a micro-channel with a rectangular section, containing n droplets can be approximated as [116, 34, 117, 118]

$$R' = R(\mu_r \phi + 1 - \phi) + n[3.15f(\mu_r)\frac{\gamma}{h}Ca^{2/3}\frac{1}{v \cdot w \cdot h}] \quad (3.9)$$

where

- $\mu_r = \frac{\mu_d}{\mu_c}$ is the ratio between the viscosity of the dispersed and continuous phase;
- R is the hydrodynamic resistance in case no droplets are currently in the micro-channel;
- Ca is the capillary number;
- $\phi = n \cdot L_D/L_C$ is the fraction of the micro-channel occupied by n the droplets, where L_C and L_D represent the lengths of the channel and the droplet, respectively;
- $f(\mu_r)$ is a function of the viscosity ratio varying between 1 and about 1.5 when μ_r spans from 0 to $+\infty$ [119];
- v is the velocity of the droplets.
- γ is the surface tension coefficient.

Approximate expressions for the hydrodynamic resistance R' can be found in two cases which are typical of several application scenarios:

- Case 1: when $\mu_r > 1$, as for example in the case of oil droplets dispersed in water;

- Case 2: when $\mu_r \ll 1$, as for example in the case of nitrogen bubbles dispersed in water.

Case 1

$\mu_r > 1$: in this case the resistance of a pipe containing droplets can be approximated by [120, 34]:

$$R' = R(\mu_r \phi + 1 - \phi) = \zeta L_C \mu_c (\mu_r \phi + 1 - \phi) / w \quad (3.10)$$

where $\zeta = \frac{\alpha}{\mu_c}$ and α is the expression defined in eq. (2.13).

Case 2

$\mu_r \ll 1$: in this case the term $\mu_r \phi$ in the eq. (3.9) can be neglected, whereas $f(\mu_r)$ can be approximated as $f(\mu_r) \approx 1$. Accordingly, by defining R_D as in [34, 121]

$$R_D = 3.15 \frac{\gamma}{h} C a^{2/3} \frac{1}{U \cdot w \cdot h} \quad (3.11)$$

where U is the droplet velocity, the hydrodynamic resistance can be approximated as follows:

$$R' \approx R(1 - \phi) + n R_D \quad (3.12)$$

If there is only one droplet in the channel, that is, $n = 1$, the eq. (3.12) can be rewritten as

$$R' \approx \alpha \left[L_C - L_D + \frac{3.15 \cdot (1 - 0.63h/w)}{12} C a^{-1/3} h \right] / w \quad (3.13)$$

SIMULATION TOOLS FOR MICROFLUIDICS

This chapter examines the resolution methods of the equations of fluid motion. The first part will deal with numerical methods and algorithms used to this purpose, the second part will devoted to a numerical simulator that implements such algorithms and methods: OpenFOAM, *Open Source Field Operation and Manipulation* [122]. Moreover, the OpenFOAM settings used to perform the numerical simulations presented in this dissertation will be detailed.

4.1 Computational Fluid Dynamics

Computational Fluid Dynamics, or CFD, is the set of numerical techniques allowing the resolution of the equations of fluid dynamics. The CFD is essential not only for the design of microfluidic devices, but also as a support to the study of complex physical microfluidic phenomena. The CFD is a wide field as much as fluidics and microfluidics. Since

this dissertation focuses on two-phases laminar flow, this section will provide a brief overview of the numerical methods implemented only in this area. In particular, the VOF method (*Volume Of Fluid*) will be discussed in more detail because it is implemented in the OpenFOAM platform.

4.1.1 Overview of numerical methods

Given the importance of the CFD it is not surprising that up to date many numerical methods have been implemented; each of these has positive and negative features, not only in terms of computational cost. This discussion will focus on a subset of these methods that allows the numerical simulation of multiphase flows resolving the Navier-Stokes equations. The classic three discretization methods used for the numerical solution of partial differential equations are:

- the Finite Difference Method (FDM);
- the Finite Element Method (FEM);
- the Finite Volume Method (FVM).

The FDM method is based on the direct approximation of the differential partial equations in finite difference equations, calculated taking a finite number of points of the integration domain. Therefore the original equation is transformed into an algebraic equation deriving difference operators, for example, by Taylor series.

The FEM method is based on the discretization of the investigated domain space in a finite number of surface elements, or volume

elements, according to the structure to be analyzed which can be planar or three-dimensional. These elements are characterized by a fixed number of nodes and at these points the unknowns are defined. In each of these domains the solution of the differential equation is approximated by the linear combination of functions called shape functions. The FVM is based on cell-averaged-values, this distinguishes it from the FDM and FEM, where instead the main numerical quantities are the local function values at the mesh points. The FVM method consists in the discretization of the domain in a finite number of cells referred to as control volume (VC), the integral form is obtained directly from the differential equation by integration over a control volume, thus the name finite volume. The differential equations are integrated in each control volume transforming them into surface integrals through the divergence theorem. The net flux through the volume is the sum of the integrals on the four surfaces of the VC. The value of the integrand is not, however, provided on the faces of the volume control and is determined by interpolation from the values at the center of the cell. Therefore, the FVM is a locally and conservative method, because the flux on each face of a subvolume is deleted by the contribution of the adjacent subvolume, since the contribution of adjacent surfaces always appears twice but with opposite sign.

However, the numerical methods to solve problems involving multiphase flows are not characterized by the discretization choice, but by the model used to describe the interfaces between the fluid phases and their temporal evolution. In fact, the interface modeling between different phases is a rather complex issue, because the interface can be irregular, involves mass-transfer, is free to deform and then it is not at a fixed location. Depending on how this issue is resolved the

numerical methods can be classified in [123, 124]:

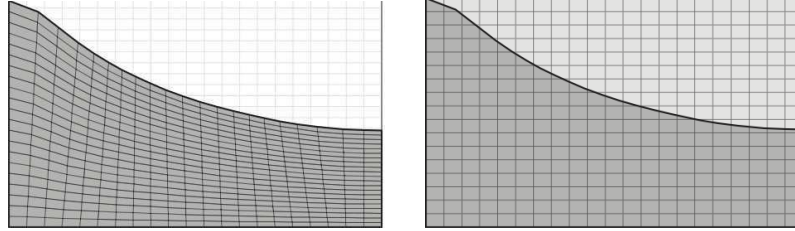
- ***Interface-tracking methods:*** *moving grid, front tracking, etc.*
- ***Interface-capturing methods:*** *level-set, volume of fluid, phase field, lattice-Boltzmann, coupled level-set and volume of fluid, etc.*

In the *interface tracking methods*, Fig. 4.1(a), the interface between the two phases is clearly defined and the grid elements lay completely or partially on it. During the evolution of the interface it is "followed" from the computational grid that needs to be updated as the flow evolves, i.e. grid and fluid move together. These methods are Lagrangian because the position of each point that lies on the interface depends on the time, and then from the past history of the system; therefore the time and position are dependent variables.

In the *interface-capturing methods*, Fig. 4.1(b), the interface between the two phases is not earlier defined, the computational grid is fixed while the interface evolves, hence it must be "captured"; this is achieved by using a characteristic function that is computed identifying the cells partially filled by the considered fluids. These methods are Eulerian because the position of the points of the interface is independent from time.

4.2 Interface capturing methods

The following section provides a brief overview of the interface-capturing methods, focusing on the VOF method which is imple-



(a) *Interface-tracking methods:* the interface, modeled as a moving boundary, is explicitly described by the computational grid.

(b) *Interface-capturing methods:* use an artificial scalar field for an implicit description of the interface.

Figure 4.1: Interface representation methods.

mented in OpenFOAM.

4.2.1 Phase field

The phase field uses a single parameter ϕ to characterize the entire structure, the set of values that this parameter assumes is the so-called phase field. Hence, a phase function $\phi(x, t)$ is introduced to represent the interface $\phi = 0$. Away from the interface, this function takes the value $\phi = +1$ for a phase and $\phi = -1$ for the other phase. The function ϕ in the region of the interface will vary slowly between these two values.

The evolution of the field is governed by the equation of Cahn-Hilliard that is a non-linear parabolic diffusive equation. This method is of the first order approximation, hence it requires a dense computational grid in the interface region [125].

4.2.2 Lattice-Boltzmann

The Lattice-Boltzmann Method (LBM) differs from the phase-field method in the discretization of the Navier-Stokes equations, in fact it is obtained directly through the discrete transport equation of Boltzmann. This considers a reticular geometry with gas particles restricted to move on a "lattice" of nodes and not on a continuum of sites. The fluid dynamics is assimilated to the behavior of these particles [126, 125, 127]. LBM is a mesoscopic approach to solve fluid flows by evaluating the evolution of particle distribution functions owing to advection and collision over a discrete lattice mesh.

4.2.3 Level set

In this method the interface is represented by the zero level of a function $\phi(\underline{x}, t)$ that represents the shortest distance from the interface. The values of this function are positives inside the interface and negative outside. The two phases are distinguished by using different signs. The function $\phi(\underline{x}, t)$ is in fact defined as $\phi(\underline{x}, t) = \pm d$, where d is the distance from the \underline{x} interface. The equation $\phi_t + \vec{u} \cdot \nabla \phi$ is used to calculate the interface motion, where ϕ_t is the time derivative of ϕ . The problem of this method lies in the discretization of the motion equation in fact, in the presence of flat surfaces or steps close to the interface, requires a reset of the function $\phi(\underline{x}, t)$ at each time step to assign an accurate value at the distance function to the interface. Nevertheless, the method does not guarantee the mass conservation. To solve this problem it is necessary to use high-order difference schemes that compromise the computational simplicity of this method.

4.3 VOF: Volume Of Fluid method

In this section the implementation of the VOF method in the OpenFOAM software [122] is presented. The *Volume Of Fluid* method was introduced by Hirt and Nichols in 1981 [128]. It belongs to the category of interface-capturing methods. The spatial domain is discretized in finite volumes (FVM), also called cells, and the variables are calculated at the center of each computational cell.

The algorithm is divided into two stages:

- **reconstruction of the interface** - the identification, in each cell of the computational domain, of the nearest interface via interpolation methods;
- **determination of the dynamic interface** at each time step to calculate the new position of the interface.

In the VOF method a single system of conservation equations is solved for the entire two-phase flow as a single fluid. These equations will be discontinuous at the interface between the two phases, because the properties of the two phases are different. The change of the fluids properties (such as density and viscosity) across the interface is described by a Heaviside function:

$$H = \begin{cases} 1 & \text{inside the interface} \\ 0 & \text{outside the interface} \end{cases} \quad (4.1)$$

Through this step function the two phases can be viewed as a single phase with properties determined by the values taken on the two sides of the interface, for example the density ρ function will be:

$$\rho(\mathbf{x}, t) = \rho_1 H(\mathbf{x}, t) + \rho_2 (1 - H(\mathbf{x}, t)) \quad (4.2)$$

where 1 and 2 are used to distinguish the two phases. The interface will be characterized by a non-zero value of the gradient of the step function. The phenomena related to the presence of the interface, such as the surface tension, are added to the Navier-Stokes equation by means of a interface term with a three-dimensional Dirac δ -function $\delta(\mathbf{x}) = \delta(x)\delta(y)\delta(z)$ [129]. For a Newtonian fluid the equations of mass conservation, momentum and the equation that relates deformations and shear stresses, are therefore:

$$\nabla \cdot \mathbf{U} = 0 \quad (4.3a)$$

$$\frac{\partial \rho}{\partial t} \mathbf{U} + \nabla \cdot \rho(\mathbf{U}\mathbf{U}) = -\nabla p + \nabla \cdot \tau + \rho \mathbf{g} + \int_{S(t)} \gamma \kappa' \mathbf{n}' \delta(\mathbf{x} - \mathbf{x}') dS \quad (4.3b)$$

$$\tau = \mu(\nabla \mathbf{U} + \nabla \mathbf{U})^T \quad (4.3c)$$

where t is the time, \mathbf{V} is the velocity field, τ is the stress tensor and \mathbf{g} is the gravity acceleration. The last term of eq. (4.3b) represents the contribution to the momentum due to the surface tension. It acts only on the interface, in fact the integral is calculated only over the surface of the interface $S(t)$, where κ is its the curvature and \mathbf{n} the normal vector of the interface. The equation (4.3) is therefore valid for the entire flow field including the interface (the alternative would be to write the conservation equations for each fluid and match them

at the separation interface). However, through the interface cannot exist a discontinuity as defined in eq. (4.1), because there is a smooth transition region between the two phases. Therefore a function called volume fraction is used as indicator function to mark the different fluids in each cell of the computational domain (see Fig. 4.2). The volume fraction α is defined as:

$$\alpha = \begin{cases} 1 & \text{for the volume occupied by the phase 1} \\ 0 < \alpha < 1 & \text{in the volume occupied by the interface} \\ 0 & \text{for the volume occupied from phase the 2} \end{cases} \quad (4.4)$$

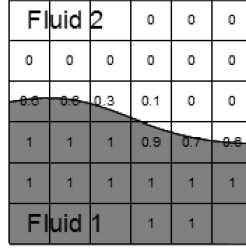


Figure 4.2: Volume fraction $\alpha = \frac{V_1}{V_1 + V_2}$, where V_1 and V_2 are the volumes occupied by phase 1 and 2, respectively.

Since the function α is associated with each of the two phases and propagates with them, is a Lagrangian invariant therefore the transport equation for α can be written as [129]:

$$\frac{\partial \alpha}{\partial t} + (\mathbf{U} \cdot \nabla) \alpha = 0 \quad (4.5)$$

where \mathbf{U} is the velocity field.

In this way the properties of the two phases, specifically the density ρ and the viscosity μ , can be expressed as function of $\alpha = \alpha(\mathbf{x}, t)$:

$$\rho(\mathbf{x}, t) = \alpha\rho_1 + (1 - \alpha)\rho_2 \quad (4.6a)$$

$$\mu(\mathbf{x}, t) = \alpha\mu_1 + (1 - \alpha)\mu_2 \quad (4.6b)$$

The equations (4.3) should be resolved together with the equation (4.5). The numerical solution of these equations requires the following techniques:

- a compression technique for the interface α in order to maintain its value strictly between 0 and 1;
- a technique for calculating the contribution of surface tension, that is, for the computation of the integral in the eq. (4.3b).

4.3.1 Interface Compression

As discussed the interface is represented as the jump from 0 to 1 of the volume fraction (or indicator function, note that often the value 0.5 for the contour is used). This leads to a computational problem for the approximation of the gradient of α (i.e. the advection of a discontinuous function) which results in an inaccurate reconstruction of the interface with over and under-estimations. The method implemented in OpenFOAM to maintain a sharp interface is to introduce a bounded compression term into the indicator function equation (4.5):

$$\frac{\partial \alpha}{\partial t} + \nabla \cdot (\mathbf{U}\alpha) + \nabla \cdot (\mathbf{U}_r\alpha(1 - \alpha)) = 0 \quad (4.7)$$

where \mathbf{U}_r is an artificial velocity suitable to push the volume fraction toward the free surface (it is perpendicular to the interface and directed toward it). The calculation of \mathbf{U}_r is carried out considering the absolute value of the velocity in the transition region. In this way the compression velocity never gets zero and ensures a sharp interface. The multiplication for $\alpha(1-\alpha)$ ensures that the compression term acts only in the region of the interface ($0 < \alpha < 1$).

4.3.2 Calculation of surface tension

The issue in calculation of the surface tension is that the interface is not explicitly tracked but it is reconstructed, so the integral in eq.(4.3b) cannot be evaluated and must be approximated. This is achieved by using the *continuum surface force* model (CSF). This model represents the effects of surface tension as a volumetric force acting within the transition region [129]:

$$\int_{S(t)} \gamma \kappa' \mathbf{n}' \delta(\mathbf{x} - \mathbf{x}') dS \approx \gamma \kappa \nabla \alpha \quad (4.8)$$

where κ is the interface curvature. The curvature is calculated using \mathbf{n}^* , the unit vector normal to the interpolated interface α^* :

$$\kappa = -\nabla \cdot \mathbf{n}^*, \text{ with } \mathbf{n}^* = \frac{\nabla \alpha^*}{|\nabla \alpha^*|}. \quad (4.9)$$

The total surface tension force over a closed surface must be zero. The problem of VOF is that, considering $S(t)$ as closed surface: $\int_{S(t)} \mathbf{n} dS \neq 0$, this can lead to an unphysical non zero resultant force. This problem does not exist in interface tracking methods because they use a computational grid moving with the surface. How-

ever, these methods does not guarantee the mass conservation of each fluid. The outlined problem in VOF can be resolved by using a moving computational grid.

To facilitate the expression for the pressure boundary conditions, the dynamic pressure p_{rgh} is defined as the total pressure p less hydrostatic pressure $\rho \mathbf{g} \cdot \mathbf{x}$:

$$p_{rgh} = p - \rho \mathbf{g} \cdot \mathbf{x} \quad (4.10)$$

Taking into account all the above discussions and by using some simple mathematical artifice to simplify the formulation, the conservation momentum equation resolved by the VOF method can be written as [129]:

$$\frac{\partial \rho}{\partial t} \mathbf{U} + \nabla \cdot (\rho \mathbf{U} \mathbf{U}) = -\nabla p_{rgh} + \nabla \cdot (\mu \nabla \mathbf{U}) + (\nabla \mathbf{U}) \cdot \nabla \mu - \mathbf{g} \cdot \mathbf{x} \nabla \rho + \gamma \kappa \nabla \alpha \quad (4.11)$$

The discretization of this equation, required to solve it numerically, will be addressed in the next section. Indeed, it is important to understand how to set the OpenFOAM simulator. In general, each term is approximated by using the Gauss theorem and replacing integrals by finite sums.

4.4 OpenFOAM settings

Open Source Field Operation and Manipulation (OpenFOAM) is a CFD software released under the GNU (*General Public License*) and written in C++. The code is open, so freely available and modifiable.

4.4.1 Code and solvers

OpenFOAM is a library written in C++ used to create executables, i.e. applications. The applications are divided into two categories: solvers designed to solve a specific problem and utilities for pre- and post-processing. OpenFOAM is distributed with a set of precompiled applications but these can be also created by using the freely available libraries. The overall structure of OpenFOAM is shown in Fig. 4.3.

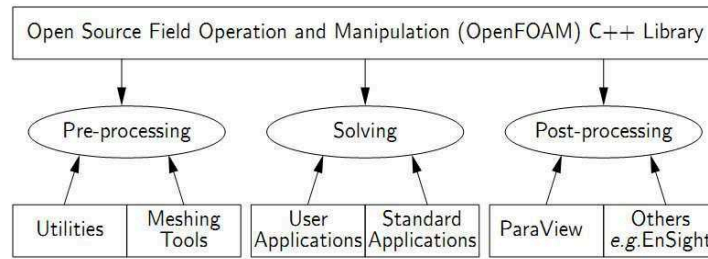


Figure 4.3: OpenFOAM software structure.

There are many available standard solvers, depending on the problem to solve the user can choose the appropriate solver. The solvers used to perform the simulations presented in this dissertation are two: *interFoam* and *interDyMFoam*; both solve multiphase flow for incompressible fluids by implementing the VOF method, they are distinguished only because *interFoam* uses a fixed computational grid whereas *interDyMFoam* an adaptive moving grid.

The first task for a solver is the discretization of the problem in all its components, namely:

- the discretization of the computational domain, this is achieved

by decomposing the domain into cells and storing the relationship for each set of cells;

- the discretization of the equations in space and time;
- the discretization of the time into time steps that can be either fixed or dynamic.

To run a simulation in OpenFOAM the files containing the solver specifications choices for the discretization must be set. In the next section will be reported the set up utilized to perform the simulations presented in the following chapters of this dissertation.

4.4.2 Solution domain discretization: Mesh

OpenFOAM implements the FVM method for the discretization of the investigated geometry. The computational grid, also called *mesh*, is the set of cells (or control volumes) in which the initial domain is divided. Based on the problem to investigate, different types of cell and mesh can be employed. The cell shape can be a: tetrahedron, hexahedron, pyramid, and wedge for the 3D geometries or triangle and quadrilateral for 2D geometries. The mesh types are:

- **Structured Mesh**

A mesh is structured when the position of each cell can uniquely determined from a set of indices on the basis of a fixed ordering relationship. The cells of a structured mesh can be thought as the elements of an array. For example, in 2D (3D) to each cell corresponds a pair i, j (a triplet i, j, k) of indices. The cell shapes used in this mesh are rectangular (2D) or hexahedral

(3D) (see Fig. 4.4). This mesh cannot be used for very complex geometries.

- **Unstructured mesh**

A mesh is called unstructured when its cells cannot be ordered as the elements of an array: the location of a cell cannot be determined by the neighboring cells. So, the cells shape may be of any type also triangles (2D) or tetrahedra (3D) (see Fig. 4.5). Unstructured grids allow to better describe complex geometries. It is also possible to vary the density of the grid in accordance with the gradient of the solution: the mesh is more dense where needed to obtain more accurate results, for example in areas where the turbulence is modeled, or where physical phenomena of interest occur, or where there are corners and edges. This, obviously results in an additional computational cost in terms of CPU and memory.

OpenFOAM allows the use of both these types of computational grid. The grid has a significant impact on: the rate of convergence (or even lack of convergence), the solution accuracy, and the computational cost. Then, the choice of the type and the number of cells of the mesh is crucial.

The pre-processor utility *blockMesh* is used in OpenFOAM to create mesh by the description of the domain geometry. However, both the geometry and mesh can be generated using other external programs (e.g. CAD, Salome, Gmsh) and then imported into the OpenFOAM software. The mesh generated by *blockMesh* is structured but can be refined in regions of interest. In the file *blockMeshDict* the

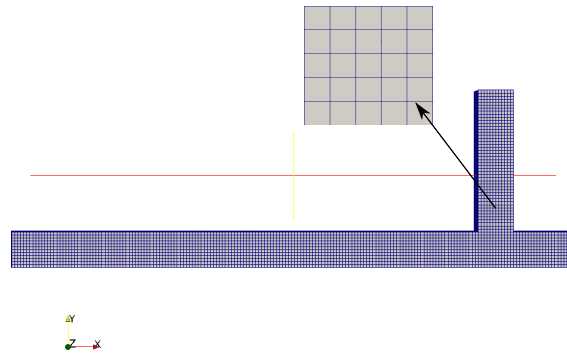


Figure 4.4: Example of structured mesh for a T-junction geometry.

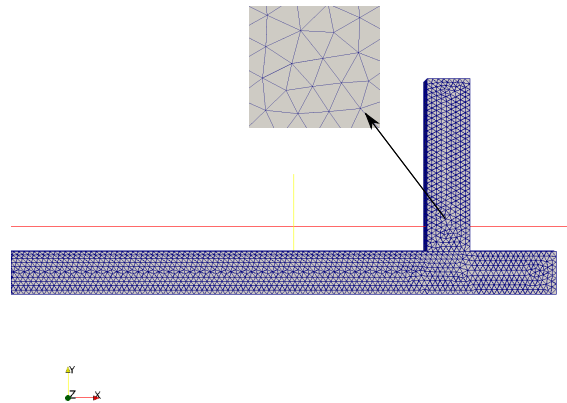


Figure 4.5: Example of unstructured mesh for a T-junction geometry.

spatial domain is described and divided into blocks of any form, specifying the number of cells for each block. The blocks must not intersect and their coordinates need to be specified according to the guidelines imposed by the utility, as explained in the manual [122]. To get an unstructured mesh there are two options: to import the mesh by an external application or use the utility *snappyHexMesh*. The unstructured mesh in Fig. 4.4 is obtained from another open source software: Salome[130].

4.4.3 Time discretization

The temporal discretization is described in the *controlDict* file, in which the time step can be specified by the keyword `deltaT`. To ensure that the solution converges and its accuracy, the value of the time step chosen must ensure that the Courant number is always less than 1. This condition for the stability of a numerical scheme is known as the CFL condition (Courant- Friedrichs-Lewy). It states that the time taken by a particle to cross a cell must be less than the time step in the calculation, this ensures that the scheme may access the information required to form the solution. Otherwise the simulation may produce incorrect results and eventually diverge during the iterative process. The Courant number for a single cell is then defined as:

$$Co = \frac{\delta t |\mathbf{U}|}{\delta x} \quad (4.12)$$

where δt is the time step, $|\mathbf{U}|$ is the absolute value of the velocity through the cell, and δx is the cell size in the direction of the velocity. The time step δt must be calculated for the worst case, which means to consider the smallest cell size and the maximum flow speed through

this cell. Then, the proper δt is obtained by reversing the eq. (4.12) with $Co = 1$. However, in some problems this calculation cannot be simple, in these cases it is better to use the automatic adaptation of the time step by the keyword `adjustTimeStep` in the *controlDict* file. In this approach the maximum value for Co to be used in determining the δt must be specified.

Of course a number of Courant small will affect the simulation time. In the simulations reported in this dissertation, the value of the Courant number was set to $Co = 0.2$ for both phases.

4.4.4 Equations discretization schemes

The aim of equation discretization is to transform the governing equations into a corresponding system of algebraic equations. The solution of this system approximates the solution to the original equations at some pre-determined locations in space and time [129]. The solver *interFoam* uses MULES (*multidimensional universal limiter for explicit solution*) method to solve explicitly the transport equation of the volume fraction but by limiting the flow. This method allows to maintain the volume fraction bounded in the interval between 0 and 1, therefore it ensure that the sum of all volume fractions in each cell is always less or at most equal to 1, this regardless of underlying numerical schemes adopted, mesh structure, etc.

The discretization schemes, for the terms in the Navier-Stokes equation (4.11) and in the volume fraction transport equation (4.5), can be chosen among those implemented in the code, according to what is appropriate for the considered problem; they must be indicated in the dictionary *fvSchemes*. The choice of these schemes must be particu-

larly accurate to ensure the convergence of a simulation. In particular, within the file *fvSchemes*, there is a sub-dictionary, **divSchemes**, in which are indicated the numerical schemes for the divergence calculation of the convection terms in equations (4.5) and (4.11). The keywords used to indicate each term are:

- `div(rho*phi,U)` for the term $(\nabla \cdot (\rho \mathbf{U} \mathbf{U}))$;
- `div(phi,alpha)` for the term $\nabla \cdot (U \alpha)$;
- `div(phirb,alpha)` for the term $\nabla \cdot (U_r \alpha)$.

Discretization schemes setting

In the following the numerical schemes used to perform the simulations will be reported. For their choice a study was carried out on the available OpenFOAM documentation [122] and on the literature about numerical schemes.

- Time derivative: Euler implicit time differencing scheme;
- gradient: Gauss scheme with linear interpolation between centers of cells and centers of the faces (face=boundary of a cell);
- term $(\nabla \cdot (\rho \mathbf{U} \mathbf{U}))$: Gauss scheme with upwind interpolation;
- term $\nabla \cdot (U \alpha)$: Gauss scheme with vanLeer interpolation;
- term $\nabla \cdot (U_r \alpha)$: Gauss scheme with interpolation of the field α by the method of interface compression;

- Laplacian: Gauss scheme with linear interpolation for μ and surface normal gradient of type corrected (i.e. with explicit non-orthogonal correction);
- interpolation scheme: linear;
- surface normal gradient: explicit non-orthogonal correction scheme.

Among these numerical methods, those concerning the terms of convection will be briefly described because, as already mentioned, they are the most critical. For the discretization of the convection divergence terms $(\nabla \cdot)$, is needed an interpolation scheme to calculate the velocity values at the cell faces (see Fig. 4.6). A wide choice of interpolation schemes is provided by OpenFOAM, the simplest solution is the interpolation from cell centers to face centers, but this often leads to numerical instability. By using linear interpolation, referring to the figure 4.6, the value at the face centers is obtained as follows:

$$\phi_f = f_x \phi_P + (1 - f_x) \phi_n, \text{ with } f_x = \frac{\overline{fN}}{\overline{PN}} \quad (4.13)$$

where ϕ refers to the flux $\phi = \rho U$ and ϕ_f is the face field. Another interpolation method is the upwind that guarantees boundedness of the solution, but it is only first order accurate. This method does not interpolate the values but it assigns as value for a face center the center value of the upstream cell according to the direction of the flow:

$$\phi_f = \phi_P \text{ for } F \geq 0 \quad (4.14)$$

$$\phi_f = \phi_N \text{ for } F \leq 0 \quad (4.15)$$

where F is the flow at the interface. The upwind method is stable only if the CLF condition is satisfied. Also the upwind method of second order can be used, in which the value for a face center is obtained by using a series expansion of the variable ϕ around the upstream cell center.

The vanLeer method is a combination of linear and upwind methods.

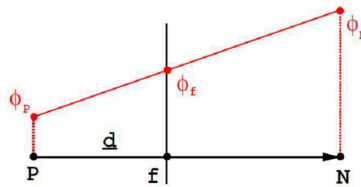


Figure 4.6: Interpolation from values of cell center to face center: f is the face, P and N are the centers of two cells in which the solution is known. Examples of interpolation schemes available in OpenFOAM are: upwind, linear, vanLeer.

Linear-solver settings

The linear solvers to be used to solve each matrix equation generated by discretization, must be indicated in the dictionary *fvSolution* together with their tolerances values and the number of correctors and iterators for the PISO cycle (*Pressure Implicit with Slipping of Operators*).

The PISO algorithm is an iterative procedures for solving equations for velocity and pressure used for transient problems. It is based on evaluating some initial solutions and then correcting them. In fact, to

solve the Navier-Stokes equation it is needed an independent equation for pressure that the solver obtains finding the Poisson equation for the pressure. Since the Navier-Stokes and Poisson equations are coupled, they must be solved simultaneously. This can be done through the PISO iterative algorithm that solves the momentum equation based on the value of the pressure field at the previous instant. The iterations within a time step are called *outer iterations*.

The momentum equations can be solved correctly only when the correct pressure field is known or estimated, otherwise the resulting velocity field will not satisfy the continuity equation. For this purpose the PISO algorithm uses the so called *correctors*. The number of iterations and correctors not only affects the result of simulation, but also its convergence. In particular, the simulations carried out were convergent and accurate by choosing a number of iterations equal to 2 and a number of correction equal to 3.

4.4.5 Boundary conditions

To solve the equations appropriate boundary conditions must be imposed. The types of boundary conditions used in the 3D simulations are shown in table 4.1 referring to the boundaries reported in Fig.4.7 that shows an example of simulated geometries.

In the following a brief description of the boundary conditions used to perform the simulations presented in this thesis is provided.

- `fixedValue`: assigns a specified value;
- `zeroGradient`: normal gradient zero at the boundary;
- `outletInlet`: is a `zeroGradient` condition for pressure when \mathbf{U}

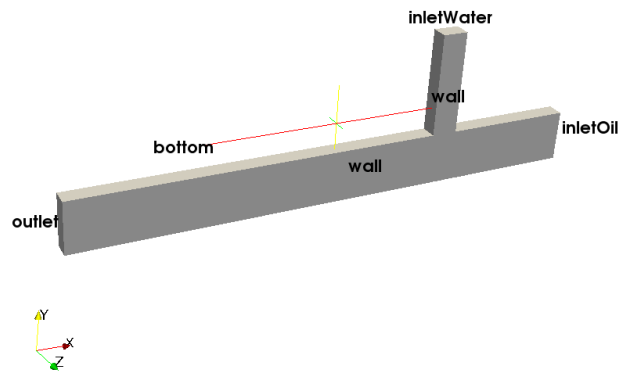


Figure 4.7: Example of a simulated geometry: **inletWater** is the inlet of the dispersed phase; **inletOil** is the inlet of the continuous phase; **outlet** is the outlet of the device; **bottom** is the back of the device; **wall** are the remaining boundaries.

	α	p_{rgh}	U
<i>inletWater</i>	fixedValue	zeroGradient	flowRateInletVelocity
		outletInlet	pressureInletVelocity
<i>inletOil</i>	fixedValue	zeroGradient	flowRateInletVelocity
<i>outlet</i>	zeroGradient	fixedValue	zeroGradient
<i>walls</i>	constantAlphaContactAngle	fixedFluxPressure	fixedValue
		partialSlip	
<i>bottom</i>	symmetryPlane	symmetryPlane	symmetryPlane

Table 4.1: Example of boundary conditions used to perform 3D simulations of the T-junction generator in Fig. 4.7; α is the volume fraction, U the velocity field and p_{rgh} is the pressure in eq.(4.10).

points outward, fixedValue when \mathbf{U} points inward. The fixed value to be assigned must be provided, this condition is used to impose an inlet pressure;

- flowRateInletVelocity: allows to assign as input for \mathbf{U} a volumetric flow rate;
- pressureInletVelocity: when a pressure value is assigned as input, \mathbf{U} is evaluated from the flux, normal to the patch;
- constantAlphaContactAngle: assigns a specified constant value to the contact angle;
- fixedFluxPressure: adjusts the pressure gradient so that the boundary flux matches the velocity boundary condition;
- partialSlip: assigns a condition of partial slip to the wall according to an assigned value ranging between 0 and 1,

where 0 imposes the *slip* and 1 the *no-slip*. The condition of *no-slip* can also be assigned through the condition `fixedValue` by imposing the value 0 for \mathbf{U} ;

- `symmetryPlane`: defines a symmetry. This condition is used if the investigated geometry is symmetric, in this case only half side of the domain is modeled.

In the simulations the value of the volume fraction was assigned as follows:

$$\alpha = \begin{cases} 1 & \text{for the dispersed phase} \\ 0 & \text{for the continuous phase} \end{cases} \quad (4.16)$$

To initialize α was used utility `setFields`. It should be noted that OpenFOAM offers the possibility to run the computation in parallel on multiple processors or on multiple networked machines. The related utility is `decomposePar`.

The values for the fluid parameters can be specified in the `transportProperties` file; note that OpenFOAM uses the kinematic viscosity defined as the ratio between the dynamic viscosity and the fluid mass density $\nu = \frac{\mu}{\rho}$.

CHAPTER
FIVE

HYDRODYNAMIC CONTROLLED
MICROFLUIDIC NETWORKING

Microfluidic devices, and Lab-on-Chips (LoCs) in particular, have recently attracted the interest of researchers for the huge number of application scenarios they offer ranging from point-of-care diagnostics to biochemical research. However LoCs are today not flexible and very static in the sense that they perform only simple and fixed operations. In this chapter the idea of a *microfluidic communication network* is discussed for providing programmability to such devices. It overcomes the limitations of traditional LoC by supporting dynamic addressing of various microfluidic elements aimed at executing different tasks. For this reason this chapter explores the basic communication facilities that a microfluidic programmable device should support and the methodologies that can be used to prosecute this challenging target. In particular, the approach proposed in this chapter is to use a sim-

ple cheap and purely hydrodynamic technology to support switching capabilities in a network of microfluidic devices, this results in the definition of a Hydrodynamic Controlled microfluidic Network paradigm (HCN).

5.1 Challenges and motivations

A LoC is a microfluidic device that implements a specific biochemical protocol for the analysis or experiment to carry out. Droplets in LoCs are used to transport samples inside the continuous phase, so that each of them interacts with appropriate substances in highly controlled conditions. Each droplet unit operations, reviewed in chapter 3, corresponds to a step of a biochemical protocol such as generation, mixing, and incubation as shown in Fig.5.1. LoCs are usually realized through monolithic devices: each LoC is a pre-set fixed serie of one or more unit operations, connected by microfluidic channels, to suite the requirements of a specific protocol, some examples are reported in Fig. 5.2.

A large number of attempts have been made in the literature to define a framework, including both hardware and software features, realizing programmable Lab-on-Chips (*Programmable LoCs*) able to execute a large number of different chemical and biological analyses and synthesis within a single microfluidic device [24, 23]. Similarly to the approach pursued in the *systems-on-a-chip* domain, programmable LoCs can be realized as a set of basic LoC (or *microfluidic elements* μ fE), executing one or two unit operations (e.g. injection and mixing), built-in the same microfluidic device and interconnected with each

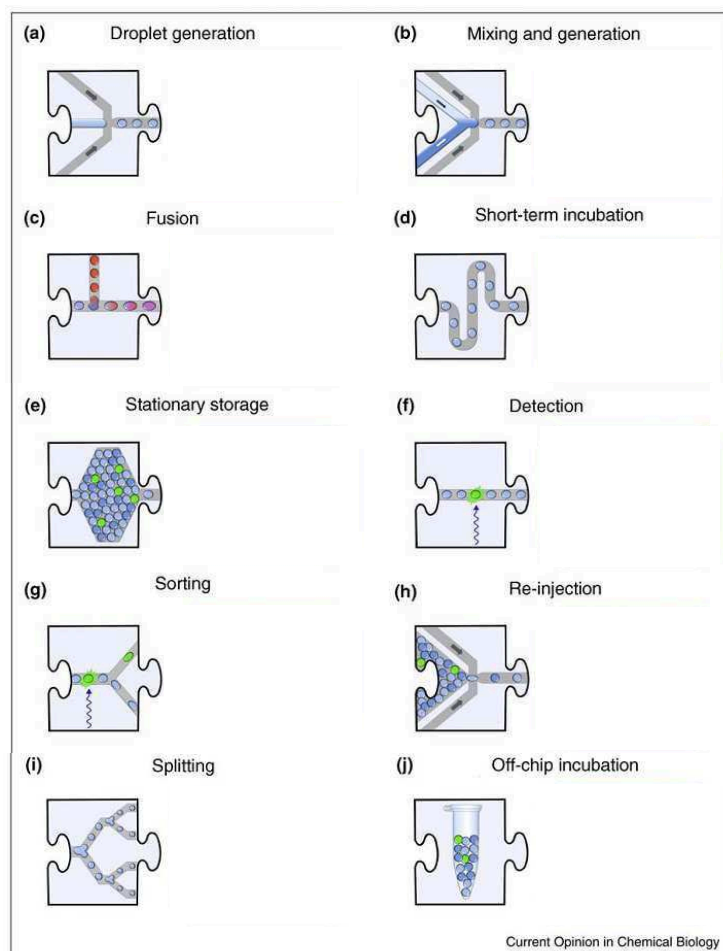


Figure 5.1: A toolbox of unit operations for droplet microfluidics. This overview shows one selected example of each module for the manipulation of microfluidic droplets. These modules can be integrated like jigsaw pieces to suit the requirements of specific biological experiments. It should be noted that this display is far from comprehensive: alternatives exist for many of these modules and more will certainly arise in the future. Criteria for their future evaluation will be fidelity, ease of use and interoperability. The modules are: (a) droplet generation; (b) mixing and generation; (c) fusion; (d) short-term incubation; (e) stationary storage; (f) detection; (g) sorting; (h) re-injection; (i) splitting; and (j) off-chip incubation. Adapted from [12] Copyright 2010, with permission from Elsevier.

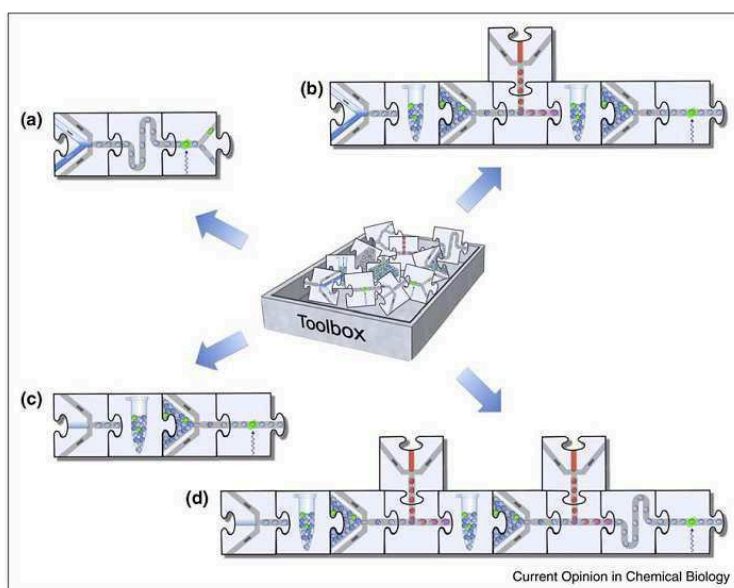


Figure 5.2: A summary of integrated microfluidic workflows. Recently published workflows for biological experimentation are represented as combinations of jigsaw pieces from 5.1. (a) Directed evolution of yeast cells; (b) in vitro enzyme expression of DNA; (c) sensitive detection of cell-surface biomarkers on compartmentalized single cells using enzyme amplification (ELISA assay); (d) toxicity screening. Reprinted from [12] Copyright 2010, with permission from Elsevier.

others [16]. A challenging requirement of these systems, therefore, is the ability of accurately controlling the exchange of microfluidic samples and information between the basic microfluidic element.

Nowadays, in these microfluidic systems, active control of droplets movements is based on microelectronic technologies integrated inside the microfluidic device such as EWOD and dielectrophoresis, as discussed in chapter 3.4. Realization of such control systems requires a complex multilayer microfabrication process; also, they are not suitable for certain biological settings due to problems of biocompatibility of electrical signals on cells or biomolecules [105, 131, 31].

An alternative approach is based on pure hydrodynamic control of droplets which flow in a microfluidic device discussed in par. 3.4. The main design parameters involved in these techniques are channel geometries and hydrodynamic forces. Hydrodynamic droplets manipulation, therefore, does not require in-chip electronics and only relies on the use of actuators (pumps and reservoirs) at the edge of the chip, without requiring complex and costly production processes. The introduction of the innovative concept of bubble logic [10], discussed in section 3.5, have shown that the design of microfluidic networks aimed at supporting flexible, cheap and scalable programmable microfluidic systems based only on hydrodynamic control is technologically feasible. A first step in this direction is proposed in [132, 15, 133] where a paradigm for a microfluidic communication network is defined.

The availability of such solutions have inspired other works on the design of a microfluidic communication system: in [134] experiments are conducted to show the feasibility of data transmission in a such system and a protocol stack for microfluidics communications is developed. Starting from the physical layer, feasible modulation schemes

for data transmission suitable for microfluidics communications are examined in [134] by applying two modulation schemes for signal transmission: on/off keying (in which the bit 1 is represented by dispersed phase, while the bit 0 is represented by a continuous phase of fluid) and communication by silence (in which the payload is represented as distance between two droplets). The noise contributing to the overall system, caused from flow rates fluctuations, is investigated. The performances are evaluated by using data obtained through MATLAB software simulations. The experiments reveal that communication by silence is significantly better than on/off keying. However, the results show that both modulation schemes are feasible for signal transmission.

In [135] the design of a microfluidic communication network with a bus topology, is analyzed where multiple microfluidic elements are connected to a main channel by means of passive switching elements. A mathematical model of the system and the rules to be followed for proper design and dimensioning of such a microfluidic network are presented. Moreover, a preliminary performance analysis that gives some insights into the complex interrelations among the different elements of the microfluidic network is provided.

The idea developed in this thesis is to implement an innovative flexible and modular microfluidic networking technology providing communication capabilities to microfluidic devices, such as Lab-on-Chips (LoCs), combining the LoC specific functionalities in more powerful and competitive microfluidic systems. This can be of primary interest in case of biomedical applications where different elements could be able to perform specific operations and exchange the result of such elaborations. The resulting networked LoC paradigm, named *Hy-*

hydrodynamic Controlled microfluidic Network (HCN), extends classical communication concepts to the microfluidic domain by exploiting hydrodynamic microfluidic effects. In the remainder of this chapter the HCN requirements and the resulting communication functional architecture will be introduced; also appropriate schemes for information encoding in the microfluidic domain will be addressed. In subsequent chapters specific functionalities of the HCN will be designed and assessed, while in the last chapter an implementation of HCN as a whole will be analyzed.

5.2 Overview and architecture

Consider a microfluidic system that includes a certain number M of elements denoted as μfE_i , $i \in 1, 2, \dots, M$, respectively. A *microfluidic element* μfE is a microfluidic chip (i.e. a LoC) which performs one or more specific microfluidic operations on liquid samples and is identified by an address in the HCN network. Basic operations are, for example, droplets' generation, fusion, mixing, etc. Any microfluidic application requires a given sequence of functions to be performed by the networked μfE . Accordingly, samples to be processed must traverse an appropriate sequence of μfE s in the system where the output of a μfE may be given as input to another μfE . The purpose of HCN is to enable programmable, flexible, and dynamic setting of the sequence of μfE that will be traversed by a sample encapsulated into a droplet.

The most simple HCN architecture which can support the above discussed networking functionalities consists of a bus topology shown in Fig.5.3. In this architecture the droplets are generated by boundary

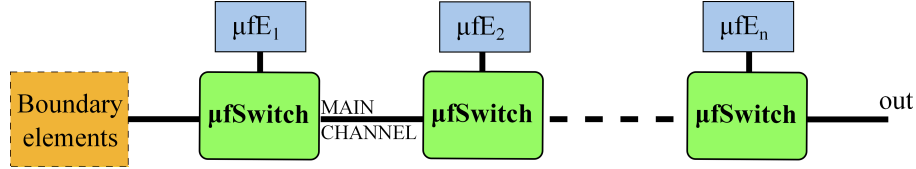


Figure 5.3: Bus Topology of HCN.

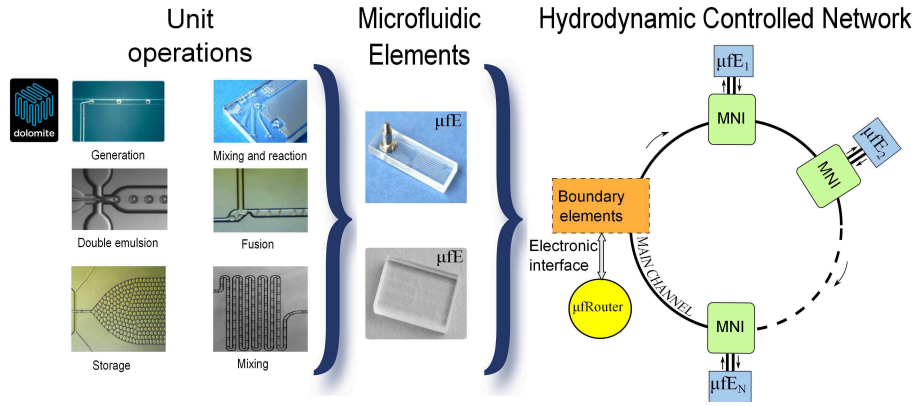


Figure 5.4: Ring topology of HCN. The left part of the picture shows microfluidic chips commercially available from <http://www.dolomite-microfluidics.com>

elements and travel along a main channel. Each μfE is connected to the bus by a related $\mu fSwitch$, this is a device able to forward droplets toward the intended μfE .

A more complex envisioned HCN consists of a physical ring topology implementing a logical star topology as shown in Figure 5.4. This architecture uses a request/response interaction model among the μfEs in which a *central entity* sends each sample to a specific μfE . When the corresponding operation is completed, the μfE will send the processed sample back to the central entity. The central entity implements a

manager role which incorporates:

- the system logic necessary to perform job scheduling;
- the functions needed to construct the droplets patterns which will be sent through the HCN in such a way that samples are delivered to the correct μfE .

Moreover, the central entity is in charge of detecting the bio/chemical reactions executed by the μfEs on the samples when they arrive through the main channel. For this reason it will be labeled as *microfluidic router* (μ_R).

It is evident that μ_R contains boundary elements, such as pumps and sinks, which are controlled using standard electrical/electronic technologies, that is, the source and the destination of all droplets are integrated in μ_R . The microfluidic router μ_R generates *microfluidic packets* consisting of droplets which contains the samples to be processed and encodes in the packet the forwarding information.

To perform complex multi-step protocol μ_R , after receiving the droplets processed by a μfE , should be able to re-inject these droplets into the HCN to perform further operations. A microfluidic router should be realized through mechatronics technologies to allow fully automated droplets processing. However, it could be also a simple passive flow focusing generator (see Fig. 3.5(b)) connected to off-chip syringe pumps for droplets production. In this case, the droplets processed through the HCN can be collected in a output storage chamber. From the storage chamber the pre-processed droplets can be re-injected into the HCN through the same passive flow-focusing geometry controlling the inter-droplet distance by the modulation of the

input flow rates. Many examples of droplets re-injection system can be found in literature as in [13, 136, 137]. Indeed, this is a common microfluidic operation necessary when an emulsion formed in a previous step must be injected into a microfluidic device for additional processing as shown in Fig. 5.5.

In the HCN, similarly to what is done in the Network-On-Chip domain, it is assumed that a networking element – called *Microfluidic Network Interface* (MNI) – is attached to each microfluidic element to perform the operations required for efficient and reliable exchange of droplets with the other elements.

The MNI is responsible for the operations needed to detect the destination address encoded in the microfluidic packets, and for switching the microfluidic packets accordingly. Furthermore, the MNI should insert the droplets leaving the μ fE in the main channel, avoiding collisions with other droplets. In other words the MNI is responsible for performing *switching* and *medium access control* (MAC) functionalities.

As discussed below and in [15, 16], the set of functions to be implemented in a microfluidic communication network, such as HCN, are:

- **information representation**, which is required to encode the address of the intended destination in the pattern of droplets traveling through the HCN;
- **switching and signaling**, which is employed to forward droplets toward the appropriate LoC;
- **medium access control**, which is needed to avoid the fusion

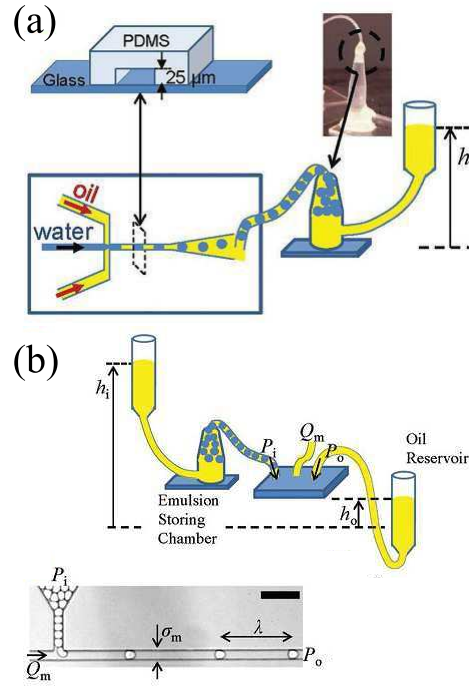


Figure 5.5: Example of a re-injection system: (a) an emulsion is produced by a flow focusing device and delivered into storage chambers connected to reservoirs. The collecting, storing, and re-injecting of droplets is controlled by applying gravity-driven hydrostatic pressure to reservoirs; (b) apparatus for droplet re-injection and its optical micrograph. Reprinted from [13] with permission of The Royal Society of Chemistry.

(i.e., coalescence) between droplets when they enter the Output bus after leaving the LoCs.

Before dealing with the design of both a single MNI and the HCN as a whole, the following paragraph provides an overview of the schemes proposed to encode information and perform switching. The MAC functions and their implementation will be discussed extensively in chapter 7.

5.3 Information Encoding

In droplet microfluidic systems, information encoding in the droplets' pattern can be performed according to several possible methodologies [15]. In particular, four different approaches have been identified:

Presence/Absence (DPAE) The most intuitive way to represent information proposed in [10] and utilized in [138] is based on presence encoding [138] and relies on the occurrence of a droplet at a certain point in time and space. This occurrence corresponds to the logic value '1', whereas absence of the droplet corresponds to the logic value '0'. In the following such approach to information representation will be referred as "*Droplet Presence/Absence encoding* (DPAE)" scheme.

Size (SE) Another way of encoding information is based on the capability of generating (and then distinguishing) droplets of different size. This approach, utilized in [139, 140], will be referred as "*size encoding* (SE)".

Distance (DE) An alternative approach, proposed in [11] and explicitly utilized in [15], consists in representing information into the distance between consecutive droplets. This approach will be referred as “*distance encoding* (DE)”.

Composition (CE) Information is encoded in the substance composing the droplets. This approach will be referred as “*composition encoding* (CE)”.

5.4 Signaling

To support the exchange of appropriately processed samples, i.e. droplets, from a microfluidic element to another two problems have to be addressed: i) information related to the identity of the element which should perform droplet manipulation needs to be appropriately encoded into a set of droplets; ii) each element should be able to reliably identify droplets that are addressed to itself and discard those addressed to other elements. Therefore, the problem of signaling and switching has to be addressed.

Concerning the signaling problem, some concepts mainly inherited by the telecommunications networks literature will be recalled. More specifically, denoting as *service* the droplet manipulation that is required at a given microfluidic element, the term *signaling* implies the exchange of *appropriate messages* needed for the support of the required service. Accordingly, the *signaling system* consists of the network elements needed to exchange these messages.

The MNI, i.e. one of such network elements, must be able to determine if a droplet is addressed to its corresponding μ fE or not according

to the use of appropriate signaling information. The droplets encapsulating a chemical load such as reagents and samples, that have to be directed and routed, are denoted as *payload droplets*. The droplets used to control the correct routing of payload droplets are denoted as *control droplets*.

Similarly to what is done in traditional telecommunications networks when network elements should communicate, signaling can be either *channel associated* or on *common channel*. In case of channel associated signaling, this is transferred using the same transmission facility used for transmitting the information itself. In case of common channel signaling, instead, control signals and data are transmitted over separate facilities.

These two cases are shown in Fig.5.6 where the system architecture is reported. Here a separate dotted signaling ring is represented which connects, in parallel to the information ring, all the *MNIs*. The dotted line is used to highlight that, in case of common channel signaling a separate ring is used, while in case of channel associated signaling it is not.

This paragraph describes how these two types of signaling schemes can be supported identifying appropriate suitable encoding techniques. Moreover, for each of them, a possible MNI¹ design is illustrated.

5.4.1 Common channel signaling

The common channel signaling scheme employs two different physical channels: one channel to transmit the addressing information (i.e.

¹In the rest of this chapter will be considered only the switching functionality of the MNI and not the MAC one.

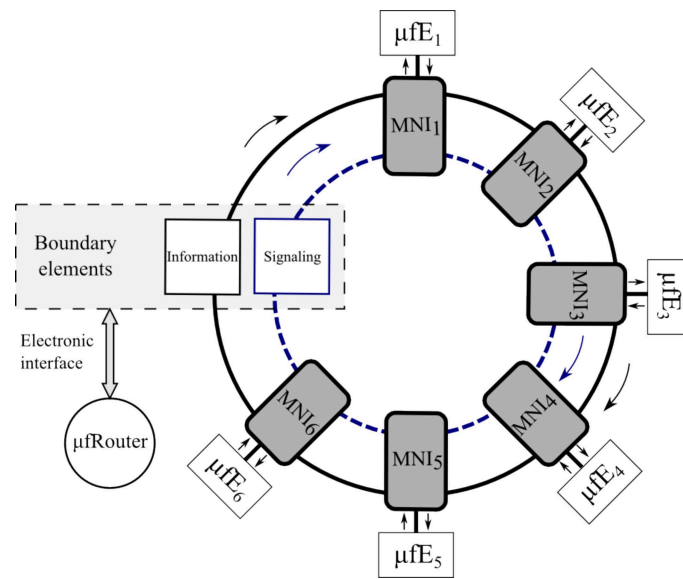


Figure 5.6: Proposed system architecture for HCN when using channel associated or common channel signaling. The dotted line represents a distinct channel in which the signaling information, e.g. control droplets, is carried out when the common channel signaling architecture is adopted.

signaling) for all the MNIs and an independent microchannel for the delivery of payload droplets, The identified encoding schemes which can be used in this architecture are: DPAE and CE. Devices that implement these schemes already exists in literature, they are called sorters, and are employed to direct the droplets motion, therefore they can be used to implement the switching functionality of the MNI. In both these cases the MNI consists of a bifurcation at which a droplet takes a route depending on the signaling information.

Presence/absence of droplet A possible MNI that employs the DPAE scheme is the AND bubble logic gate in [10] reported in section 3.5. This device performs the functionalities of a boolean AND gate driving the droplets into a microchannel by means of other properly timed control droplets. The detailed scheme is focused in the zoom in Fig. 5.7 (left). There are two distinct channels: a signaling channel A where the control droplets flow and an input channel B where the payload droplets move. The device consists of an asymmetric T-junction and a narrow channel that connects this T-junction to the control channel. The control droplets are used to switch, if needed, a payload droplet at each junction. When a droplet in the signaling channel clogs up the connecting channel, the flow in this channel is turned off and a droplet at the bifurcation enters the wider channel, because it exhibit the minimum resistance. Whereas, when no droplet is present in the signaling channel, the flow in the connecting channel switches the droplet in the opposite direction. This method requires an extremely precise control of droplets flow for perfect synchronization between the train of control droplets and the payload droplets arriving at each bifurcation. Each AND gate represents the MNI of a

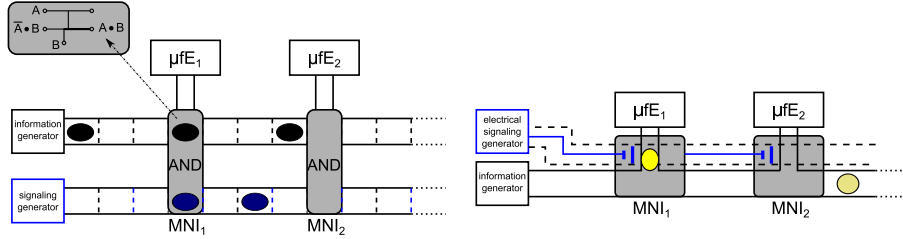


Figure 5.7: Possible MNI designs for a microfluidic communication network with common channel signaling: MNI implementing DPAE scheme (left); MNI implementing CE scheme (right).

single element where the output $A \cdot B$ of each gate is connected to a μfE element and the output $\bar{A} \cdot B$ is connected to the input channel of the next MNI.

Droplet composition The other case in which common channel can be used is to implement the CE scheme. In this case an active methodology is needed where droplets switching relies on the use of peripheral power sources. A possible MNI based on this scheme is the droplets sorter by composition reported in [141] and illustrated in Fig. 5.7 (right). In this device droplet sorting is achieved by dielectrophoretic (DEP) forces activated according to fluorescence intensity emitted by a droplet. The fluorescence depends on the presence of enzymatic activity in the encapsulated sample, that is from the droplet composition. As already reported in par. 3.4.2, the DEP forces arise from the interactions between a polarizable particle and a non-uniform electric field. The device is an asymmetric junction where the second of two electrodes is placed adjacent to the narrower branch. When no voltage is applied across the electrodes the droplet flows in the wider

channel. Switching of the droplet in the narrower channel is achieved by application of AC voltage across the electrodes, so that the dielectrophoretic force pulls the droplet into the direction of the electric field, i.e. into the narrower arm. Therefore, the signaling information for this device is triggered by the fluorescence of the droplet analyzed by using an optical setup.

5.4.2 Channel associated signaling

In the channel associated signaling, the signaling shares the same channel as the data flow. So the address signaling information is transmitted over the same channel of the payload droplets. In this case to route a droplet to its destination, the address information has to be encoded into the payload droplets pattern. The two encoding scheme suitable for the implementation of a channel associated signaling architecture are the DE and SE.

Size of droplets It is possible to design a MNI that implements this encoding scheme by exploiting the device for droplet sorting proposed in [142]. This device shown in Fig. 5.8(b), consists of a Y-junction having an upper branch with a larger resistance as compared to the lower branch. A groove in the microchannel starts from the bifurcation leading to the upper branch. This groove is employed to drive the smaller droplets into the upper branch. The height of the channel is thinner than the diameter of generated droplets so these are flattened with a high surface energy. When a droplet is trapped into the guiding groove it has less surface energy than the flattened droplet because it will expand into the groove. In this way the droplets are guided to

travel along the driving track. However the amount of this driving effect depends on the droplets' size and the groove width. For a fixed groove width, smaller droplets are more prone to be trapped so will be confined to move along the groove; on the contrary, larger droplets tend to be less trapped and will move towards the lower channel supporting higher flow rate. This device can be utilized as an MNI to perform switching by size. To accomplish this goal these devices can be cascaded by designing each MNI with a groove width lower than the one of the following MNIs. Thereby tuning the droplet size at the generator, upon varying the flow rate of continuous and dispersed phases, a specific μfE can be addressed. In order to clarify this, let us assume to have two device in series where the branch with smaller resistance is connected to the next MNI in the ring and the branch with the groove is connected to the related μfE . The microfluidic router which wants to address the i -th μfE will generate a droplet of a size such that it is more likely to be trapped only in the groove of the i -th MNI.

Another possible implementation of a MNI for the SE scheme is reported in [135, 143] and shown in Fig. 5.8(a). In this case, each of the branches connecting a μfE to the main channel is designed to have a different resistance. To deliver a droplet to the i -th μfE this device uses two very close droplets: a *header* and a payload droplet. The *header droplet* is used as control droplet to divert the payload droplet to the intended destination and it will not be processed by a μfE but discarded from the system through the output port. The MNI is an asymmetric bifurcating junction in which the payload droplet will be diverted at the i -th MNI if the header droplet has a size (i.e. a resistance) large enough to cause a reversion of the leading flow at the

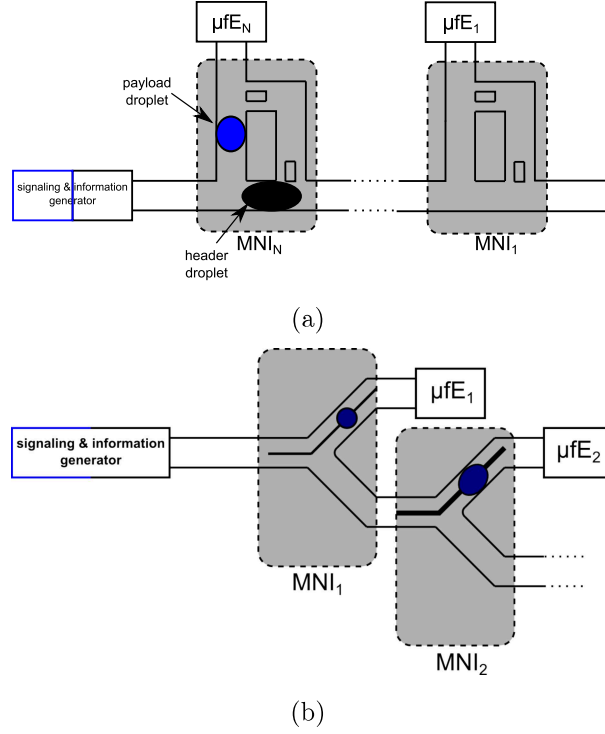


Figure 5.8: Possible MNI designs for a microfluidic communication network with channel associated signaling based on droplet size encoding scheme.

i -th bifurcation. On the contrary, the payload droplet will follow the header droplet in the main channel.

Distance between consecutive droplets When using this scheme addressing information are encoded in the distance between consecutive droplets. To appropriately route the payload droplet this scheme employs another droplet denoted as the *header droplet* for network signaling, as in the SE scheme. The destination address of the i -th

MNI can be encoded in the distance between these two consecutive droplets. The design of this MNI, shown in Fig.6.1, will be detailed in the next chapter.

5.5 Distance encoding scheme

In the following² of this thesis the distance between droplets, i.e., DE, will be employed for address encoding; according to this choice the design of a MNI and an implementation of the HCN with channel associated signaling will be presented. Reasons for using DE rather than the other identified encoding schemes can be summarized as follows:

- **DE vs. DPAE:** DPAE requires strict synchronization in the microfluidic circuit and thus involves complex design. In the near future, simplicity will be the key requirement for networked microfluidic systems and therefore, it is more appropriate to use asynchronous transmission as in DE.
- **DE vs. SE:** at the source, the control of the distance between droplets will be easier than the control of the droplets size. In fact, a large number of physical phenomena may cause severe discrepancies between the desired droplet size and the actual one [144, 145]. Moreover, recent papers [146, 87] report experimental studies which demonstrate that DE is more robust than SE, also if both techniques can achieve relatively low bit error probability in the considered scenarios.

²Some parts of the work presented in this section was published in [3]©2015 IOP Publishing Ltd

- **DE vs. CE:** CE needs active manipulation techniques that imply additional costs and a more complex fabrication process of the microfluidic chip.

In order to compare distance and size encoding, a set of experimental measurements were carried out. The experiments were performed using the microfluidic T-shaped droplet generator device shown in Figure 5.9, fabricated through 3D printing techniques as described in [3]. The cross-section of the channel is $200 \times 400 \mu\text{m}$. Droplets are formed where the stream of dispersed phase is sheared by the continuous phase that flows from the perpendicular channel (see Figure 5.9).

The chip was realized using VisiJet[®] Crystal [147], a proprietary transparent photopolymer USP Class VI certified. High oleic sunflower seed oil purified in water steam stream (Organic Oils S.r.l.), with dynamic viscosity $\mu \cong 0.049 \text{ Pa s}$, and a density $\rho \cong 916 \text{ Kg/m}^3$, was used as continuous phase and deionized water colored with a blue food dye was used as dispersed phase ($\mu \cong 0.001 \text{ Pa s}$, $\rho \cong 1000 \text{ Kg/m}^3$). No surfactants were added to the phases to facilitate the droplet formation. The fluids were injected into microchannels via side connectors through flexible plastic tubes sealed with glue by using two independent syringe pumps (New Era NE-1002X) to automatically control the flow rates Q_d and Q_c of the dispersed and continuous phase, respectively.

The microfluidic chip was fabricated by a high resolution 3D-printer (ProJet[®]HD3500,3DSystems) [147]. This printer is based on the MJM (Multi Jet Modeling) technology using a print head that jets the photopolymer and the supporting material (wax) layer by layer.

Each layer is cured by UV light and after printing the supporting material is removed by an ultrasonic cleaner and hot air drying. Currently this technology offers the best level details (resolution: 656 x 656 x 1600 DPI (xyz); 16 μ m layers) [3].

The droplets size and inter-distances were measured using an optical detection system consisting of a laser beam, two optical lenses and a light-sensor connected to a microcontroller (Arduino board). The sum of the flow rate of the two phases, i.e. the total input flow rate $Q_0^{(1,S)}$, were progressively varied in a range that corresponds to low capillary numbers ($Ca < 0.002$) to allow the formation of droplets in squeezing regime (see section 3.3).

Figure 5.10 shows the corresponding evolution of the variance of the droplet size and the inter-droplet distance. In the above figure observe that for small values of total flow rate the variance of droplet size is low. Upon increasing the total flow rate, the variance of the droplet size raises significantly. Conversely, as a threshold value is approached, the variance of the distance between droplets decreases rapidly, and below that threshold the droplets are more regularly spaced. Therefore, the encoding technique that allows to maximize the throughput is distance encoding; in fact the higher is the input flow rate, the higher is the transmission speed and in turn, the throughput.

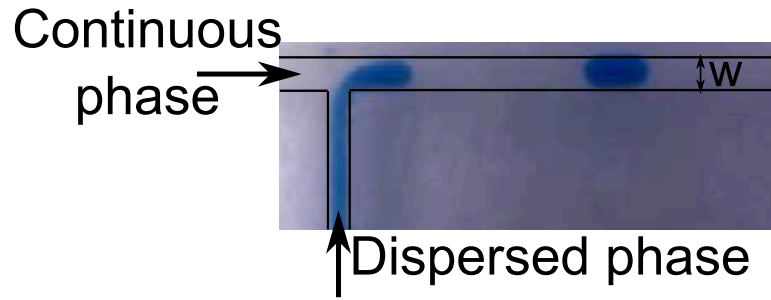


Figure 5.9: T-shaped droplets generator [3].

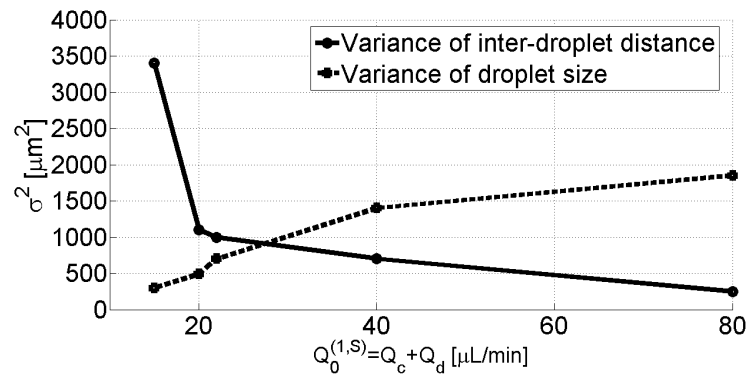


Figure 5.10: Variance of droplet size and droplet inter-distance vs. the total flow rate.

DROPLETS SWITCHING

This chapter ¹ provides the design rules for a microfluidic circuit implementing the switching function based on the distance encoding scheme. The feasibility of this approach is assessed reporting the results of performed numerical simulation and laboratory tests implying the process of construction of the switching device.

6.1 Background

To fulfill the need of a versatile, simple, and cheap programmable droplet-based LoC, it is crucial to be able to control and direct droplets' motion. As a result, many methods have been developed to manipulate individual droplets guiding them along a desired path; these mainly rely on sorting/switching devices and microfluidic logic

¹The work presented in this chapter was published in the following articles:[14] ©2014 ACM; [15] ©2013 IEEE

gates.

Droplets sorting and/or switching, in general, are coupled with detection methods to extract specific sub-populations of droplets. For example, based on their chemical content or size, the droplets are guided towards one branch of a bifurcation. Switching can be performed actively or passively. Active methods use valves [148], dielectrophoresis (DEP) [149], electric forces [105], thermocapillary effect [150] and surface acoustic waves (SAW) [151] to manipulate droplets for selective sorting or switching. These manipulation methods provide a precise control of droplets flow but suffer the drawbacks of being an active method, such as need for external electronic and optic control, and need for a complex multilayer fabrication process. Conversely, passive methods do not require in-chip electronics and complex and costly production processes.

However, guiding the droplets using passive methods is a complex problem that requires understanding of droplet motion dynamics through networks of microchannels. The complexity lies in the fact that the presence of droplets in a microchannel affects the pressure field and modifies the flow field in the microchannel network in a time-dependent way [152, 35, 153].

A new passive methodology to guide droplets has been recently proposed [15]: this is a switch able to selectively drive a droplet along a desired path based only on the programmable control of inter-droplet distance. Unlike existing solutions, the presented approach is independent of the properties of the droplet, such as size or chemical content, requires a simple one-step fabrication process and can be cascaded with consequent potential applications in both parallel or controlled protocols. Indeed, the proposed device can be integrated to create a

microfluidic communication network, the HCN, in which each droplet can be directed towards a different intended destination for further processing. For example, it can be useful to create a multi-purpose chip that can be employed for different types of experiments allowing to select the serial set of basic operations to perform; also it allows to execute in parallel, biochemical analyses and syntheses that require different reaction or incubation time, such as measurements of enzymatic kinetics [154] and determination of clotting time [155]. Usually, parallel processing in passive microfluidic droplet-based devices is achieved by splitting droplets [101, 156] at a junction or equally distributing the droplets on two paths [112]; however these devices lack programmability.

The inter-droplet distance has already been used as a mean to encode information [11, 157] and to design a hydrodynamic filter able to direct a train of droplets into the shortest branch of a bifurcation [158]. Based on the above relevant results, in the designed switch, droplets are hydrodynamically directed by exploiting only information encoded into the distance between them while flowing in the microfluidic channels.

6.2 Switch design

The approach proposed in the previous chapter is inspired by communication solutions fully consolidated in data transport. There, in order to exchange information between entities, data structures referred to as *packets* are defined. Each packet consists of a *header* and a *payload*: the *header* encodes signaling information such as the address of the

receiving entity; the *payload* contains the information to be manipulated by the receiving entity (e.g. the sample which is the object of the biochemical process.). In particular, in the proposed switch the distance between the header and the payload droplets determines the path that the second droplet will take at a bifurcation; so, by using a data transport terminology, the destination address of the payload droplet is encoded in the distance D_{HP} between the header droplet and the payload droplet. In other words the switching functionality will exploit D_{HP} in the same way a switching device in a data network uses the address information for guiding the packet towards the correct network user. For this reason the device acts as a "microfluidic switch" able to guide any (payload) droplet towards the appropriate destination branch of the microfluidic system.

Notice that header and payload droplets can be generated of alternate composition. This can be achieved either through active Droplet-on-Demand (DoD) generators, see section 3.3, or passive devices. For example, in [159] a passive system is proposed to create droplet pairs by generating alternating droplets, of two sets of aqueous solutions in a flow of immiscible carrier fluid.

The switching device consists of a T-junction geometry highlighted in Figure 6.1. The asymmetric branches 1 and 2 of the junction are connected by a bypass channel having a low hydrodynamic resistance that balance the pressure between the connected points at the two branches. It is designed in such a way that droplets do not enter it. Effect of the bypass channel is to make the behavior of the droplets inside the T-junction dependent on the geometric characteristics of branches 1 and 2 only, and independent of what is happening outside the T-junction [112] so allowing to cascade several microfluidic

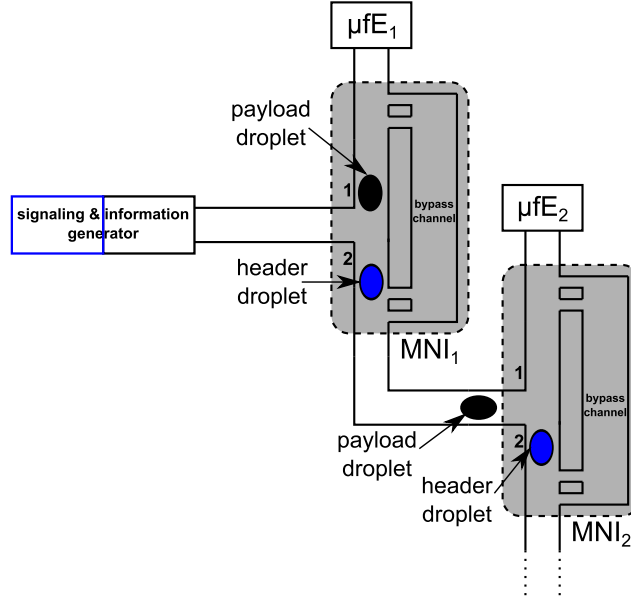


Figure 6.1: Distance-based switch [14].

switches. This property of the bypass has been demonstrated in [15] by studying the electrical equivalent circuit of the switching device shown in Figure 6.2.

The distance-based switch works as follows: when the header droplet arrives at the bifurcation, it chooses the shorter branch 2 because it has the lower hydrodynamic resistance R_2 . A payload droplet arriving at the bifurcation will enter the branch 1 if the header droplet is still in the branch 2 and will be delivered to the i -th μfE . This occurs because the presence of a droplet in a channel increases its resistance. On the other hand, if the header droplet left the branch 2, the payload droplet will enter in this branch following the header droplet; so they will be both forwarded to the next switch. Therefore in order to appropriately control the direction taken by the payload droplet when

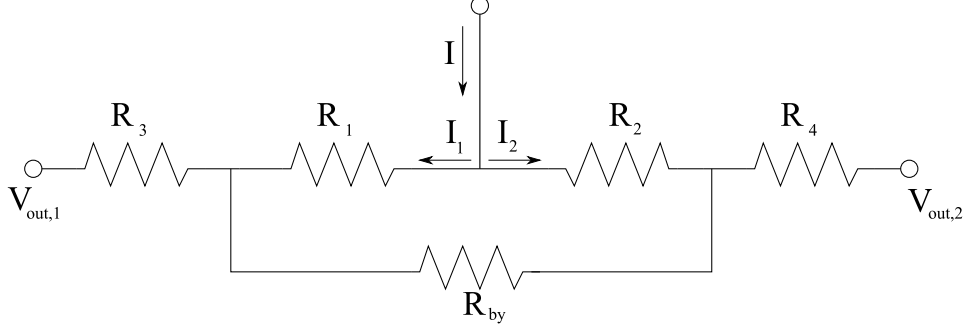


Figure 6.2: Electrical equivalent circuit of the distance-based switch [15, 14].

it arrives at the bifurcation point, is required that the presence of the header droplet in branch 2 inverts the sign of the inequality between the hydrodynamic resistances of branches 2 and 1. Thus, the following relationships must hold

$$\begin{cases} R_2 < R_1 \\ R'_2 > R_1 \end{cases} \quad (6.1)$$

where R'_2 is the increased resistance in branch 2 due to the presence of a header droplet.

In order to impose the relationship, $R_2 < R_1$, the results of the theoretical framework in section 2.3 are exploited. In fact, given that the hydrodynamic resistance of a rectangular microchannel $R = \frac{\Delta p}{Q} \approx \alpha \frac{L}{w}$ (with L and w the length and the width of the microchannel), in order to have $R_2 < R_1$, the length of branch 2 must be smaller than the length of branch 1, $L_2 < L_1$.

Approximate expressions for R'_2 can be found by considering the eq. (3.10) for $\mu_r > 1$ and eq. (3.13) for $\mu_r \ll 1$, when only a droplet is in the branch 2 of the switch. Accordingly by setting $h/w = 1/2$, the following relationships for the switch design must hold for the two

cases [15].

$\mu_r > 1$ The conditions in eq. (6.1) can be equivalently rewritten as

$$\begin{cases} L_2 < L_1 \\ \zeta[\mu_c L_2 + L_D(\mu_d - \mu_c)] > \zeta\mu_c L_1 \end{cases} \quad (6.2)$$

So it follows that the switch design must satisfy the following condition:

$$0 < L_1 - L_2 < L_D \left(\frac{\mu_d}{\mu_c} - 1 \right) \quad (6.3)$$

$\mu_r \ll 1$ The conditions in eq. (6.1) can be equivalently rewritten as

$$\begin{cases} L_2 < L_1 \\ \alpha(L_2 - L_D + 0.18Ca^{-1/3}h) > \alpha L_1 \end{cases} \quad (6.4)$$

So it follows that in this case the switch design must satisfy the following relationship:

$$0 < L_1 - L_2 < 0.18Ca^{-1/3}h - L_D \quad (6.5)$$

Moreover, as a further design guideline, droplet break-up at the bifurcation point of the switch must be prevented. To this purpose, the following condition must hold (see section 3.4.3):

$$L_D < \pi w \quad (6.6)$$

Also, it is important to observe that the distance between a header and a payload droplet changes as they traverse a switch. Such changes should be considered to correctly address a switch.

Suppose that the distance between two droplets entering the switch is $D_{HP}^{(1)}$. The velocity of the droplets in the branch leading to the bifurcation point of the switch is v (i.e. the input velocity) whereas v_2 is the velocity of the droplets in branch 2. The distance $D_{HP}^{(2)}$ between a payload droplet at the switch bifurcation while the corresponding header droplet is flowing in the branch 2 will be equal to

$$D_{HP}^{(2)} = v_2 \cdot \frac{D_{HP}^{(1)}}{v} \quad (6.7)$$

The velocities v and v_2 are proportional to the flow rate in the corresponding branches; specifically, the following relationship holds:

$$Q_2 \approx \frac{L_1}{L_1 + L_2} \cdot Q \quad (6.8)$$

By using eq. (6.8) in eq. (6.7) an approximation for $D_{HP}^{(2)}$ is given by

$$D_{HP}^{(2)} \approx D_{HP}^{(1)} \frac{L_1}{L_1 + L_2} \quad (6.9)$$

It should be noted that to drive the payload droplet toward the outlet 2 of the switch the required condition is

$$D_{HP}^{(2)} < L_2 \quad (6.10)$$

In chapter 8 will be analyzed a cascade of switches connected in series and the rules for a proper addressing of each switch will be detailed.

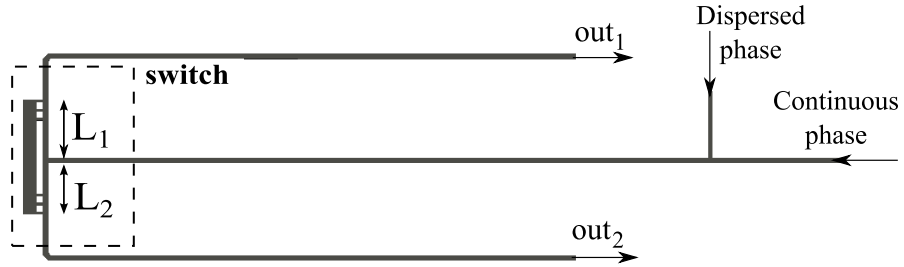


Figure 6.3: Switch simulated geometry [14].

6.3 Methods and materials

6.3.1 Computational Fluid Dynamic analysis

To assess the device functioning computational fluid dynamic (CFD) analysis was carried out using OpenFOAM software [122]. In order to show how and if the designed switching device can correctly work, 3D simulations of the device depicted in Figure 6.3 were performed. The viscosities and densities of the dispersed and continuous phases were set according to the physical properties of the fluids used experimentally and reported in section 6.3.4 with the interfacial tension between the two phases $\gamma = 0.0365$ N/m. Moreover, a static contact angle of 140° between the two phases was imposed.

6.3.2 Switch layout

For the considered fluids $\mu_r \cong 0.7$, then the above discussed approximations to calculate R'_2 cannot be applied. Therefore, to design the device layout the eq. (3.9) must be taken into account to satisfy the relationship in eq. (6.1). A length $L_D = 700\mu m$ for the generated droplet is chosen to met the no break-up condition in eq. (6.6). A capillary number $Ca = 0.0001$ is considered because the droplet must be generated in squeezing regime to ensure monodispersion and even spacing (see section 3.3). Furthermore, microchannels cross-section is set to $h/w = 1/4$. By substituting these values in eq.(3.12) to calculate R'_2 , and imposing $R'_2 > R_1$, the following expression is obtained:

$$L_1 - L_2 < 373\mu m \quad (6.11)$$

According to this relationship the lengths of the two branches of the switch are set to: $L_1 = 4.25 \text{ mm}$ and $L_2 = 3.9 \text{ mm}$ with $L_1 - L_2 = 350\mu m$.

6.3.3 Device fabrication

A prototype of the device described above has been realized and is shown in Figure 6.4. This microfluidic device is fabricated in polydimethylsiloxane (PDMS) polymer according to the fast prototyping technique described in [160] and in section 3.1. Briefly, PDMS channels bearing circular reservoirs at the ends of each channel were created by replication from masters in polyvinyl chloride. Replicas were formed from a 1:10 mixture of PDMS curing agent and pre-polymer (Sylgard 184, Dow Corning, USA). The mixture was degassed under

vacuum, poured onto the master in order to create a layer with a thickness of about 3-4 mm, and then left polymerizing for 48 h at room temperature on a plain surface. The PDMS mold bearing the negative pattern of the masters was peeled off from the master surface and repeatedly washed with ethanol, ultra-pure water, and dried before use. PEEK tubes (UpChurch Scientific) were inserted in the circular. The irreversible adhesion of PDMS molds on microscope cover glasses was obtained after 30 s air plasma etching of cleaned surfaces. Processing of surfaces with air plasma was carried out by using a Femto Diener Electronics plasma cleaner system using a 40-kHz generator. After the air plasma etching, treated surfaces were quickly placed in contact with each other and the new device placed at 60 °C for 30 min. The device includes a T-shaped droplet generator (see Figure 6.4) in which the stream of dispersed phase that flows from the vertical channel, is sheared by the continuous phase that flows from the horizontal channel. The prototype transverse dimensions ($w = 400\mu m$ and $h = 100\mu m$) are the smallest that can be obtained because of fabrication constraints. These dimensions are the same of the simulated geometry. The width of the vertical channel in the T-shaped generator is $w_d = 200\mu m$.

6.3.4 Experimental setup

The used fluids are a fluorinated oil, FC-3283 ($\mu_c = 1.3 \text{ mPa}\cdot\text{s}$, $\rho_c = 1820 \text{ kg/m}^3$) and an aqueous flow ($\mu_d = 1 \text{ mPa}\cdot\text{s}$, $\rho_d = 1000 \text{ kg/m}^3$) added with a color dye. A surfactant (PFO) is added to the continuous phase to lower the interfacial tension facilitating droplet formation and stabilization of the emulsion.

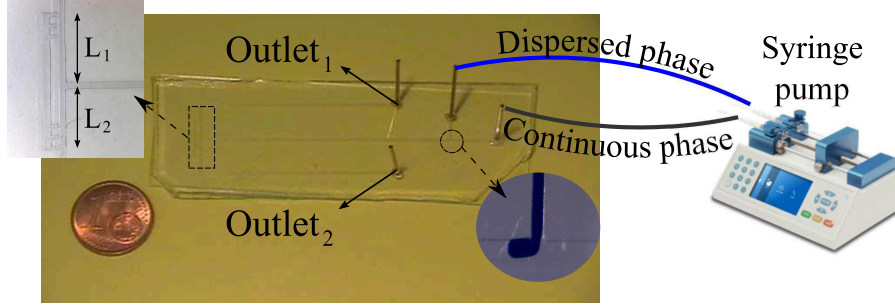


Figure 6.4: Prototype of the switching device [14].

The tests were carried out using syringe pumps (Harvard Apparatus) to inject the two fluids in the microchannels and varying the inter-droplet distance by changing the flow rate of the dispersed phase and the continuous phase. Pharmed BPT tubing (ID 0.25 mm, Cole Parmer) were used to connect syringes to microfluidic device inlets. The data were extracted from camera images of droplets.

6.4 Results and discussion

6.4.1 Simulation results

In Figures 6.5 and 6.6 the behavior of the distance-based switch in two cases is shown. In the first case, the payload droplet must be delivered to out_1 , whereas in the second case the payload droplet must be delivered to out_2 . The flow rate of the continuous and the dispersed phases has been set to generate consecutive droplets at a distance such that, when the payload droplet arrives at the bifurcation point, the header droplet is still in branch 2 ($Q_d = 0.6 \mu\text{L}/\text{min}$, $Q_c = 6 \mu\text{L}/\text{min}$) or has already left this branch ($Q_d = 0.2 \mu\text{L}/\text{min}$, $Q_c = 8 \mu\text{L}/\text{min}$)

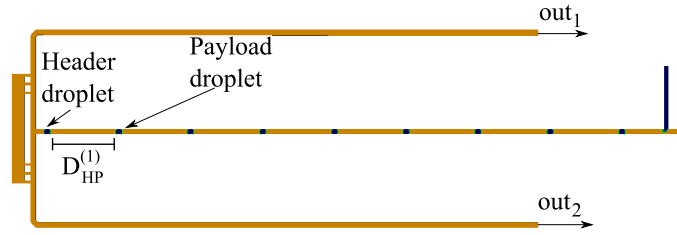
according to the relationship in eq. (6.10).

To further verify the device functionality and show how the bypass channel is able to equalize the pressure between the connected branches, the streamline patterns is reported in Figure 6.7: when a droplet travels along branch 2 the flow in the bypass channel is from 1 to 2, while it is inverted if a droplet travels along branch 1.

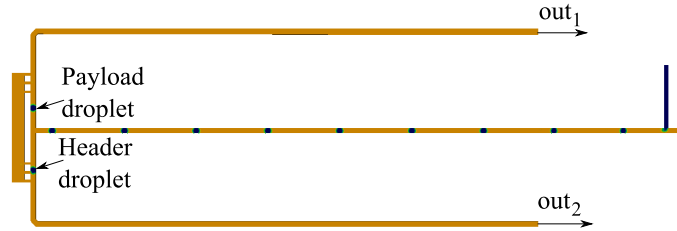
6.4.2 Experimental testing

The validity of the theoretical model in [15] and the feasibility of the switching function have been assessed through an experimental testing of the simulated device geometry. Two regimes have been obtained depending on inter-droplet distance: an alternating regime in which two consecutive droplets follow an opposite path and a filtering regime in which both are switched in the branch 2. In Figures 6.8 are shown two snapshots of the device working in alternating regime, note that the distance between two consecutive droplets (header and payload) is such that when a droplet arrives at the bifurcation, the previous one is still inside the branch 2. In Figures 6.9 are shown two snapshots of the device working in filtering regime; note that the distance between two consecutive droplets (header and payload) is such that when a droplet arrives at the bifurcation, the previous one has already left the branch 2.

However, the performed tests show that, also for fixed values of Q_c and Q_d , the inter-droplet distance is not constant, but varies within a range of values as illustrated in Figure 6.10; this may be avoided by adding a fluidic resistor as explained in [11]. So, the switching device in addition to guarantee a correct functioning based on inter-droplet

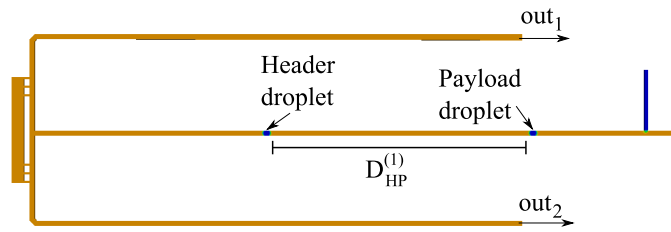


(a) Condition before the header droplet arrives at the bifurcation point.

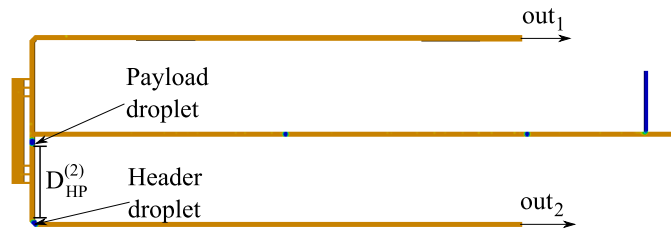


(b) Condition after the payload droplet leaves the bifurcation point.

Figure 6.5: Simulation results for the case in which the payload droplet is addressed to the out_1 [14].



(a) Condition before the payload droplet arrives at the bifurcation point.



(b) Condition after the payload droplet leaves the bifurcation point.

Figure 6.6: Simulation results for the case in which the payload droplet is addressed to the out_2 [14].

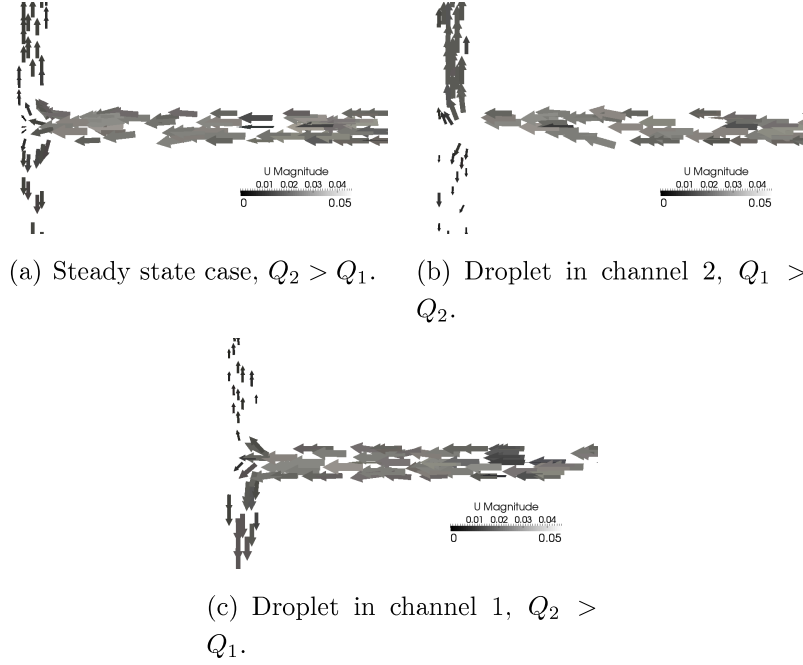
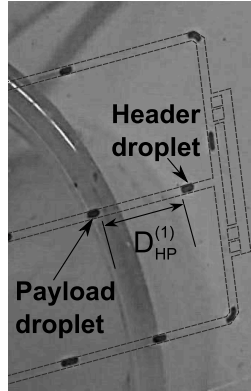
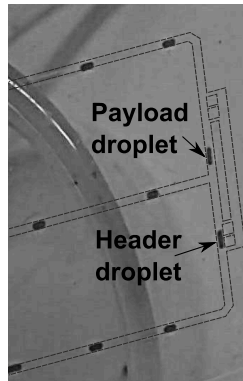


Figure 6.7: Simulation results of streamline pattern in the bypass channel at different droplet positions [14].

distance, should be robust against these variations. First, the case is considered in which the payload droplets have to be directed to out_2 and the header droplet to out_1 , that is the filtering regime. In order to evaluate the performance of the switching device and verify the validity of the eq. (6.9), the experimental parameters have been set to $Q_d = 0.6 \mu\text{L}/\text{min}$ $Q_c = 6 \mu\text{L}/\text{min}$. Then, measurements of the distance between two consecutive droplets have been performed before the bifurcation ($D_{HP}^{(1)}$) and after the bifurcation ($D_{HP}^{(2)}$), when the payload droplet reaches the bifurcation whereas the header droplet is

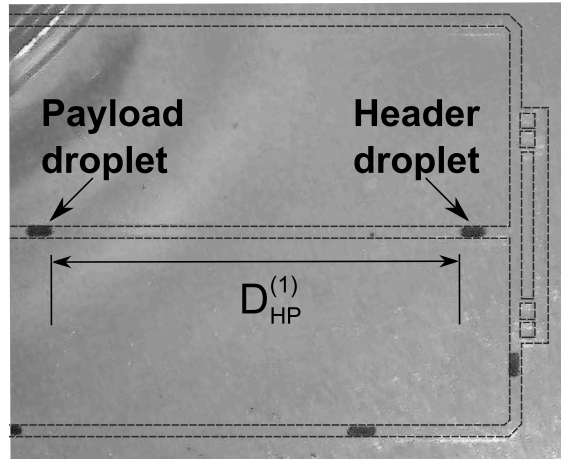


(a) Alternating regime: condition before the header droplet arrives at the bifurcation point.

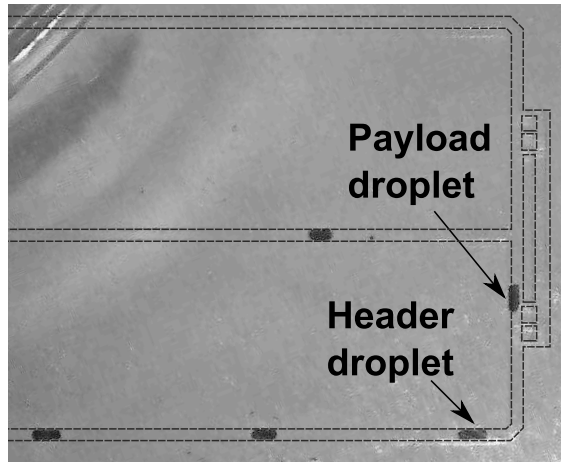


(b) Alternating regime: condition after the payload droplet leaves the bifurcation point.

Figure 6.8: Experimental results for the case when the payload droplet enters branch 2 [14].



(a) Filtering regime: condition before the header droplet arrives at the bifurcation point.



(b) Filtering regime: condition after the payload droplet leaves the bifurcation point.

Figure 6.9: Experimental results for the case when the payload droplet enters branch 1 [14].

flowing into branch 2. As shown in Figure 6.10, despite the variations of inter-droplet distances, the inequality (6.10) is satisfied; it is expected that the device operation is robust against these variations. To verify this, Figure 6.11(gray plot) shows the probability of correct path choices for the different values of the distance between droplets. The probability decreases from 75% to 25% as the inter-droplet distance increases. For distance $D_{HP}^{(1)} < 1$ mm (not shown) the reliability of the device is low because of coalescence and consequent break-up events at the bifurcation point. In the same Figure 6.11 (black plot), the performance evaluation is reported for the case in which the header droplets and the payload droplets should be directed both to the out_2 . These results have been obtained by setting $Q_d = 0.2$ $\mu\text{L}/\text{min}$ and $Q_c = 8$ $\mu\text{L}/\text{min}$: the resulting inter-droplet distance in these conditions is higher than 7.5 mm. The accuracy increases from 50% to 87% as the inter-droplet distance increases. This is because of the imperfections in the micro-channel at the junction between the two branches and the bypass channel. They are mainly related to the first phase of the fabrication process, i.e. the creation of the mold pattern by means of a cutting plotter. These imperfections randomly slow down a droplet; this deceleration affects the inter-droplet distance and leads to an incorrect path choice by the next droplet. So, taking into account these problems, the measured results for the switch accuracy were reasonably compliant with those expected by the simulation results.

The testing of the presented switch confirms that this device offers a robust method to control the droplets motion and will be employed in chapter 8 in the implementation of a microfluidic network.

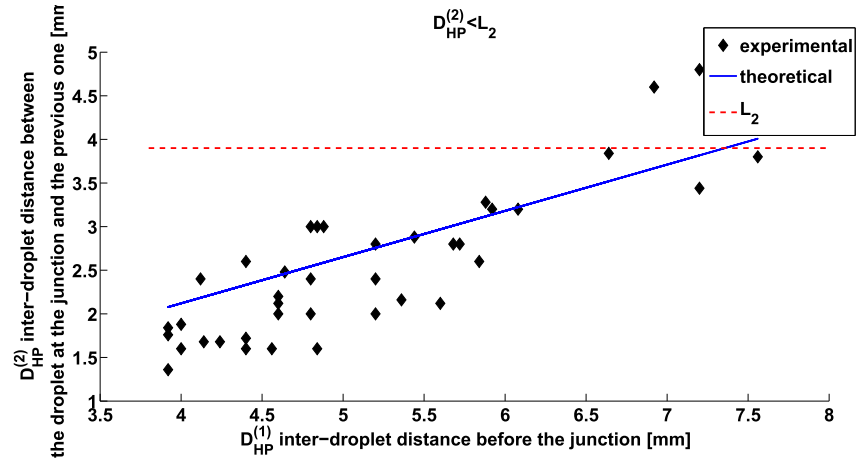


Figure 6.10: Theoretical vs. experimental results for inter-droplet distances in the alternating regime [14].

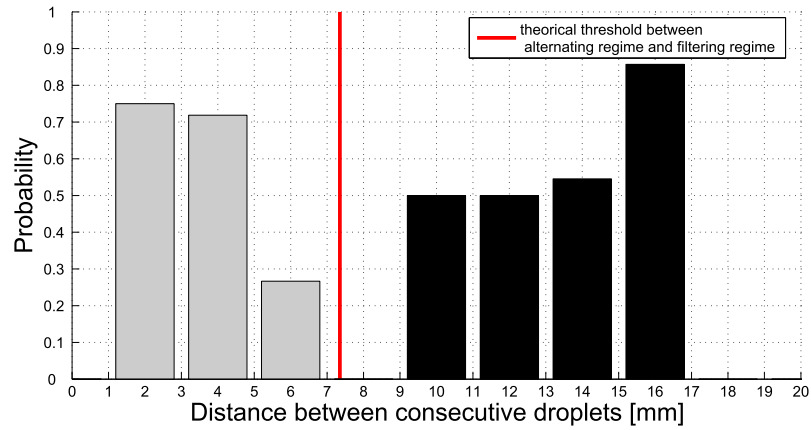


Figure 6.11: Probability of switching success versus the inter-droplet distance [14].

MEDIUM ACCESS CONTROL IN MICROFLUIDIC CHANNELS

In this chapter¹ the design of another important network element is presented. It is a device that provides a channel access control mechanism to avoid the coalescence, due to undesired collisions, between droplets that come from different microfluidic elements and flow into a same shared channel. More specifically, in section 7.1 is described the rationale of the proposed scheme and an overview of the device which implements it. In section 7.2 a model of the proposed device is derived which can be used to set the design parameters. Finally, in section 7.3 is verified that the proposed device works as expected through simulations.

¹The work presented in this chapter was published in [16] ©2013 and reprinted with permission from Elsevier.

7.1 Rationale and overview of the device

In a communications network the medium access control (MAC) is the technique used to regulate the placement of data frame onto a shared medium. The approach here proposed, is inspired by the MAC protocol used when a number of transmitting stations share the communications medium (i.e. bus, ring) to coordinate their transmissions so that they do not interfere with each other. Networks with this type of topologies, typically apply a protocol called Carrier Sense Multiple Access (CSMA) to detect if the media is carrying a signal before to transmit. In CSMA before transmitting, a node senses the medium to detect if this is already occupied by another transmitting node. If a carrier signal from another connected device is detected, the device attempting to transmit identifies the medium as busy; accordingly it will wait and try again sensing the channel after a random time interval. If no carrier signal is detected, the device can transmit its data. This mechanism avoids data collisions on the medium.

In microfluidic networks the carrier signal is a droplet and the shared channel is the ring that connects the microfluidic elements μfE_i to each other and to the microfluidic router. When a microfluidic element completes the needed set of operation on a droplet, this processed droplet will flow through the output channel of the element μfE_i again on the ring to move toward another element (e.g. a common detection point to analyze the droplet content, the microfluidic router or another microfluidic element). So, when an element has to transmit a droplet over the ring, a mechanism is necessary to manage the medium access because a collision can occur if another droplet is in the proximity of the junction between the output channel of the element μfE_i

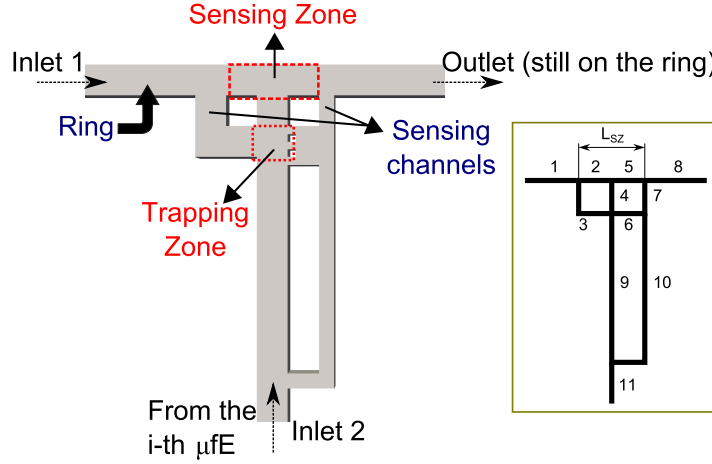


Figure 7.1: Device implementing Medium Access Control for droplets [16].

and the shared channel. In analogy with the CSMA mechanism, the element μfE_i that has a droplet to send must listen the channel before transmitting it. If the device detects a droplet on the ring that comes from a previous element, μfE_j , where $j = 1, \dots, i - 1$, near its output junction, it must wait and slows down or stops its output droplet as long as the area close to the junction is not busy. When there is no other droplet detected on the ring, the device releases it one.

In Fig. 7.1 is shown the proposed device for executing the medium access control functionalities and its scheme is sketched in the inset. The output of the microfluidic element μfE_i , flows into a shared channel (i.e. a segment of the ring) in which travel a train of droplets coming from other microfluidic elements. To ensure that no collisions occur between the droplet that has to be inserted into the shared channel and the other droplets that flow through it, two "sensing channels" are exploited upstream and downstream of a junction, respectively. The part of the shared channel between the two *sensing* channels is

referred to as "sensing zone"; the part of the output channel of the microfluidic element between the two sensing channels is called "trapping zone". If a droplet that travels along the shared channel is in the *sensing* zone and another droplet simultaneously is in the *trapping* zone, the latter will be slowed down or stopped until the *sensing* zone is empty of other droplets. The length of the *sensing* zone is such that the droplet is inserted not too close to other droplets to avoid interaction and coalescence between them.

The basic idea is exploit the increase in resistance due to the presence of droplets in the *sensing* zone to affect the pressure field and modify the flow fields around the droplet that is in the *trapping* zone so as to stop it. In fact, an increase in resistance in the *sensing* zone results in increase of flow rate in the *sensing* channels and that causes a pressure field hindering the droplet motion in the trapping zone.

7.2 Design of the device

To design the device, it was modeled as the equivalent Ohmic circuit shown in Fig. 7.2. The trapped droplet is represented as two fluidic resistors (R_{D_1} , R_{D_2}) for the two branches of the circuit that it directly affects. A static model is considered in which the droplet is in the *trapping* zone in order to find the conditions for which this droplet is trapped or not. The channel resistances are calculated by using eq. (2.12). Assuming R_D as the resistance of a droplet it follows that $R_{D_1} = R_{D_2} = R_D$.

Using this model, the channels dimensions are set that would result in the desired behavior. To simplify the circuit some assumptions

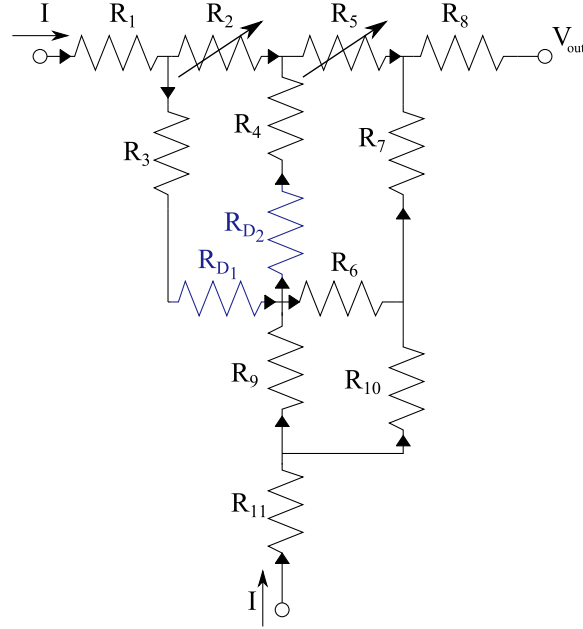


Figure 7.2: Electrical equivalent circuit of the device for MAC [16].

can be made. The flow rate at the inlet 1 and 2 are assumed equal. This can be achieved by configuring the flow paths to provide uniform resistances to fluid flow. The droplet moving in the *sensing* zone is considered as an additive resistance and take it into account by representing R_2 and R_5 as two variable resistors. The following four situations are analyzed which can be met in the *sensing* zone:

Case 1 no droplets are available in the *sensing* zone.

Case 2 there is a droplet in branch 2: the resistance of branch 2 is set to $R'_2 = R_2 + R_D$.

Case 3 there is a droplet in the branch 5: the resistance of branch 5 is set to $R'_5 = R_5 + R_D$.

Case 4 there is a droplet in branch 2 and another in branch 5: the resistances of branches 2 and 5 are set to $R'_2 = R_2 + R_D$ and $R'_5 = R_5 + R_D$.

The system must be designed in such a way that a droplet in the trapping zone enters the shared channel only in Case 1. The droplet, once in the trapping zone, can take two pathways: along the branch 4 or along the branch 6. The latter is designed with pillars at one end to prevent droplet from entering it.

The circuit was resolved using the Symbolic Math ToolboxTM to evaluate the voltage drops across R_{D_1} and R_{D_2} that represent the differential pressures across the droplet when this is in the *trapping* zone. By studying the sign of the difference between these two voltage drops $\epsilon = \Delta V_{R_{D_1}} - \Delta V_{R_{D_2}}$ the conditions for the trapping can be found. In fact, if $\epsilon > 0$ the droplet is trapped because it is forced to take the branch 6 but it is blocked because this branch is designed in such a way that droplets cannot enter it; if $\epsilon < 0$ the droplet goes along branch 4 and enters the shared channel.

From this study the desired behavior is obtained for the the values of resistances listed in table 7.1, for which:

Case 1 $\epsilon < 0 \forall R_D$

Case 2 $\epsilon > 0$ for $R_D > 1.19\alpha$

Case 3 $\epsilon > 0$ for $R_D > 3.9\alpha$

Case 4 $\epsilon > 0$ for $R_D > 0.97\alpha$

Parameter	$\frac{L_1}{w}$	$\frac{L_2}{w}$	$\frac{L_3}{w}$	$\frac{L_4}{w}$	$\frac{L_5}{w}$	$\frac{L_6}{w}$	$\frac{L_7}{w}$	$\frac{L_8}{w}$	$\frac{L_9}{w}$	$\frac{L_{10}}{w}$	$\frac{L_{11}}{w}$
Value	5	1	2	1	1	0.8	2	5	6.5	15	5

Table 7.1: Parameters characterizing the geometry illustrated in Figure 7.1 [16].

Therefore, when choosing $R_D > 3.9\alpha$, all the four cases can be satisfied. In fact, although it is difficult to exactly predict the droplet resistance, a suitable rule of thumb is that each droplet will increase the resistance of the segment of the channel it occupies by about 2-5 times [87].

7.3 MAC functionalities validation

To test the theoretical results a set of numerical simulations have been performed by setting the viscosities of the dispersed and continuous phases to $\mu_d = 1 \text{ mPa} \cdot \text{s}$, $\mu_c = 1.3 \text{ mPa} \cdot \text{s}$ and densities to $\rho_d = 1000 \text{ kg/m}^3$, $\rho_c = 1820 \text{ kg/m}^3$ with the interfacial tension between the two phases given as $\gamma = 12 \text{ mN/m}$. By using the values given in Table 7.1 the proper functioning of the device has been verified. Figure 7.3 shows the snapshots of the simulation output representing:

- the case in which two droplets flow in the *sensing* zone and the droplet in the *trapping* zone is stopped and released only when the last droplet leaves the *sensing* zone;

- the case in which no droplets flow in the *sensing* zone so the droplet is not trapped and flows into the shared channel. The insets in Fig. 7.3 show the system behavior in case the device implementing the Medium Access Control is not available. Notice that in Figs. 7.3(b) and 7.3(d) the insets show droplets collisions which will be incurred if no MAC functionalities are implemented.

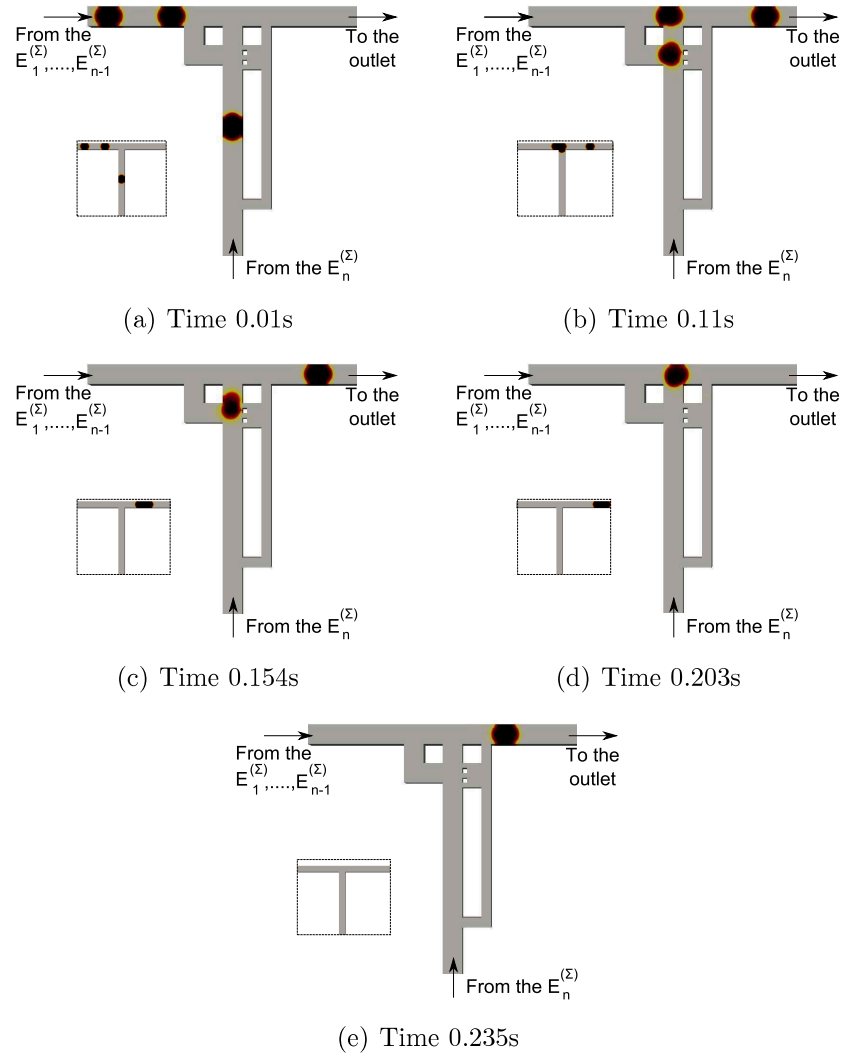


Figure 7.3: Simulation results that assess the correct MAC functioning [16].

CHAPTER
EIGHT

μ -NET: A MICROFLUIDIC COMMUNICATION
NETWORK

This chapter¹ introduces μ -NET which is a microfluidic communication network supporting the exchange of both information and chemical/biological samples carried by droplets among Lab-on-Chips within a single microfluidic device. More specifically, μ -NET is the first realization of the *Hydrodynamic Controlled microfluidic Networking* (HCN) paradigm discussed in chapter 5 to support the control of droplets movements inside a microfluidic device by exploiting hydrodynamic techniques only. The μ -NET integrates techniques to represent information by means of appropriate droplets patterns as well as switching and medium access control solutions presented in the previous chapters.

¹Part of the work presented in this chapter was published in [18] ©2015 IEEE.

8.1 μ -NET Overview and architecture

In the chapter 5, a networked LoC paradigm named *Hydrodynamic Controlled microfluidic Network* (HCN), has been introduced [132, 133, 15] with the purpose of extending classical communication concepts to the microfluidic domain by exploiting hydrodynamic microfluidic effects only. In particular, the HCN requirements and the resulting communication functional architecture have been introduced; also appropriate schemes for information encoding in the microfluidic domain have been analyzed.

Once the feasibility of the HCN paradigm has been demonstrated, this is time to approach the design of a complete microfluidic network, herein named μ -NET, which integrates all the functionalities previously defined for providing communication and networking facilities to a new generation of Programmable LoCs. In this chapter the detailed architecture of μ -NET is provided; design guidelines and feasible implementation of the minimum set of functionalities required by μ -NET are illustrated; a model is derived for the analysis of the μ -NET network performance; correctness of the operations performed by μ -NET is demonstrated through detailed OpenFOAM simulations.

In μ -NET two types of information can be distinguished:

- **Bio/chemical information:** this information is embodied in the characteristics of the physical matter composing the samples encapsulated into the droplets.
- **Digital information:** this information is encoded in the distance between droplets and is mainly used for signaling purposes in the μ -NET.

8.1.1 μ -NET interaction model

Let us consider a microfluidic system that includes a certain number N of LoCs, denoted as $\text{LoC}_1, \text{LoC}_2, \dots, \text{LoC}_N$, respectively, each of which executes a specific biochemical function and is identified by an address in the μ -NET network. Any microfluidic application requires a given sequence of functions to be performed by the networked LoCs.

Objective of μ -NET is to enable programmable, flexible, and dynamic setting of the sequence of LoCs that will be traversed by a sample carried by a droplet.

According to the HCN paradigm [15] (see chapter 5), μ -NET implements a channel associated signaling scheme and uses a request/response interaction model among the LoCs in which the *central entity* sends each sample to a specific LoC. The central entity is the *microfluidic router* (μ_R) that implements the manager role as discussed in chapter 5. When the corresponding operation is completed, the LoC will send the processed sample back to μ_R . In μ -NET the above interaction model is implemented over a double bus topology as shown in Figure 8.1 where a *Input bus* channel and a *Output bus* channel can be observed. More specifically, droplets containing samples to be processed flow through the *Input bus* towards the relevant LoC, whereas samples leaving LoCs flow through the *Output bus* towards the μ_R .

This device generates *microfluidic packets* consisting of a *payload* droplet which contains the sample to be processed, and a *header* droplet which is used for signaling purposes only. The address of the LoC to which the payload droplet should be delivered is represented by means of the distance between the header and payload droplets, as proposed in chapter 6.

Each LoC is connected to the Input and Output buses by means of a *Microfluidic Network Interface (MNI)*. The MNIs connected to $\text{LoC}_1, \text{LoC}_2, \dots, \text{LoC}_N$ are denoted as $\text{MNI}_1, \text{MNI}_2, \dots, \text{MNI}_N$, respectively. The MNI is responsible for the operations needed to detect the destination address encoded in the microfluidic packets flowing through the Input bus, and for switching the payload droplets accordingly.

Observe that, after payload droplets enter the addressed LoC, *orphan* header droplets continue to flow in the Input bus as shown in Fig. 8.1. Furthermore, the MNI is responsible for inserting the droplets leaving the LoC in the Output bus avoiding collisions with other droplets already flowing in it. In other words the MNI integrates *switching* and *medium access control (MAC)* functionalities.

Note that the double bus topology here proposed guarantees no interactions between the incoming packets and the processed payload droplets. If a single bus is used, the insertion of processed payload droplets in the same bus of the incoming packets could generate errors in the operations performed by the switches as they interpret distances between droplets as addressing information.

In the following, the integration problems related to the design of an MNI will be discussed, starting from the individual switch and MAC functionalities elaborated in the chapters 6 and 7 respectively. In fact, as already discussed, the condition for MAC functioning is that the input flow rates in the two inlets of the device must be the same. Referring to Figure 7.1, this means that the pressure field created by the droplet in the sensing zone can stop the droplet in the trapping

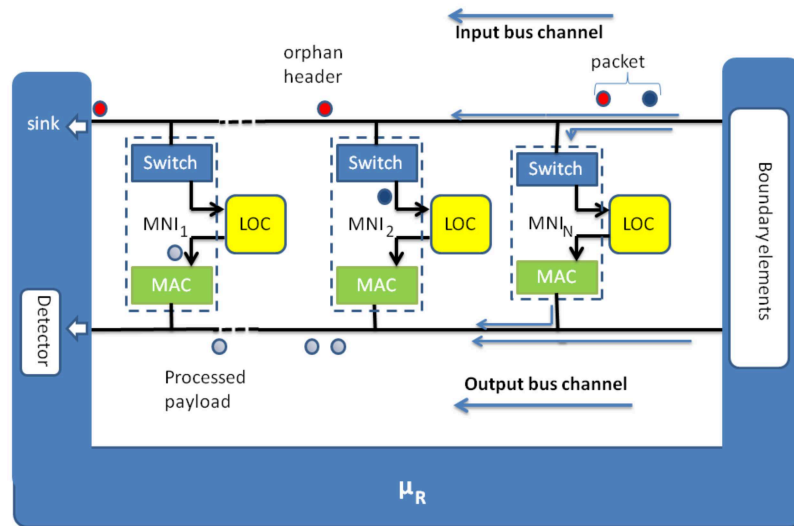


Figure 8.1: μ -NET architecture.

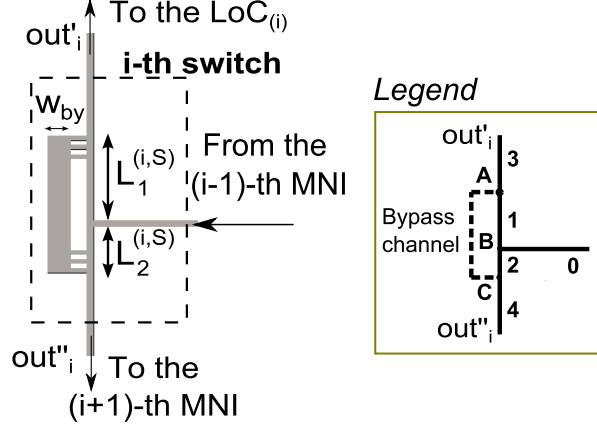


Figure 8.2: Distance-based switching [17, 15].

zone if the following condition is satisfied [16]:

$$Q_{11}^{(i,M)} \cong Q_1^{(i,M)} \quad \forall i \leq N \quad (8.1)$$

where Q is the flow rate, i denotes the i -th MNI and M specifies that the flow rate is related to the MAC device.

In order to guarantee the above condition in μ -NET a refinement of the MAC design is needed as presented in the next section.

For sake of simplicity the switch and the device for MAC with their notations are reported in Figs.8.2 and 8.3, respectively

8.2 Microfluidic Networking Interface

In this section the MNI design in detail is described. This requires some notation to be introduced. Accordingly, section 8.2.1 provides some notation that will be used throughout the rest of this chapter,

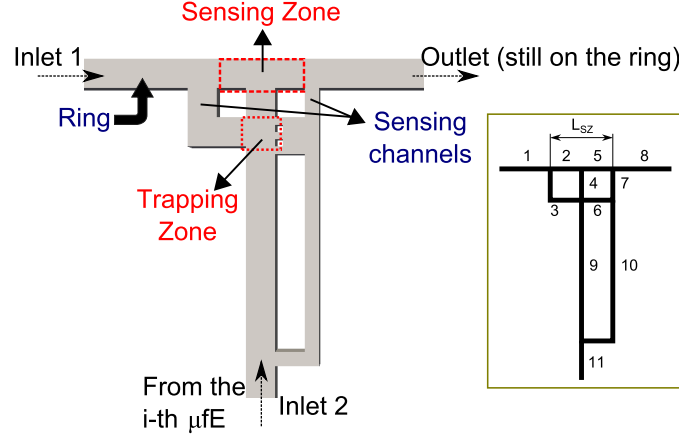


Figure 8.3: Device implementing medium access control of droplets [16].

whereas section 8.2.2 describes how to design a complete MNI integrating both switching and MAC functionalities discussed individually in the previous chapters.

8.2.1 Notation and electrical analogy

The Pipe j of the element implementing the function ϕ in the i -th MNI is denoted as $\text{Pipe}_j^{(i,\phi)}$. As already said, in μ -NET the MNIs implement two functions only, that is switching (in which case $\phi = S$) and MAC (in which case $\phi = M$). Furthermore, the hydrodynamic resistance of $\text{Pipe}_j^{(i,\phi)}$ is denoted as $R_j^{(i,\phi)}$ and the flow rate in $\text{Pipe}_j^{(i,\phi)}$ as $Q_j^{(i,\phi)}$. Note that the resistance $R_j^{(i,\phi)}$ depends on the geometry of $\text{Pipe}_j^{(i,\phi)}$; more specifically if the section of such pipe is rectangular, then it is:

$$R_j^{(i,\phi)} = \alpha \cdot \frac{L_j^{(i,\phi)}}{w_j^{(i,\phi)}} \quad (8.2)$$

where α is a constant defined in eq. (2.13), while $L_j^{(i,\phi)}$ and $w_j^{(i,\phi)}$ are the length and the width of Pipe $_j^{(i,\phi)}$, respectively. The difference of pressure at the edges of Pipe $_j^{(i,\phi)}$, denoted as $\Delta P_j^{(i,\phi)}$, is related to the hydrodynamic resistance of Pipe $_j^{(i,\phi)}$ and the flow inside such pipe by the Hagen-Poiseuille law (see Sec. 2.3), i.e.,

$$\Delta P_j^{(i,\phi)} = R_j^{(i,\phi)} \cdot Q_j^{(i,\phi)} \quad (8.3)$$

8.2.2 Design

The MNI cannot be realized by merely integrating the switching scheme discussed in chapter 6 and the MAC scheme proposed in chapter 7, because the interrelation between the microfluidic channels in the switch and MAC schemes would impact the overall resistance seen by the fluid flows. In the following, first the major criticality to be faced in the design of a complete MNI will be explained and then a solution to such problem will be presented.

The MAC scheme proposed in [16] requires the relationship in eq. (8.1) to hold as discussed in chapter 7. Such relationship cannot be satisfied in the μ -NET network (depicted in Figure 8.1), unless a new element is introduced. In fact, note that in Figure 8.1 the flow rate decreases as it moves along the Input bus, whereas it increases as it moves along the Output bus. Moreover, the flow rate entering the MAC, $Q_{11}^{(i,M)}$, is the same entering the switch of the same MNI and therefore it is a fraction of the flow on the Input bus before the i -th MNI. So, while $Q_1^{(i,M)}$ increases as i increases, $Q_{11}^{(i,M)}$ decreases as i increases. For this reason eq. (8.1) cannot hold for all values of i simultaneously.

In order to satisfy eq. (8.1) for any value of i , the introduction of a microfluidic flow equalizer is needed as discussed below.

The flow equalizer envisioned in μ -NET balances the flow rates entering from Pipes 1 and 11 of the MAC equivalent electric circuit. Given that in most practical cases the flow in the Output bus is usually much larger than the flow coming from the LoCs (i.e. $Q_{11}^{(i,M)} < Q_1^{(i,M)}$), objective of the flow equalizer is to convey a portion of the flow coming from the Output bus towards the input of the MAC circuit arriving from the LoC. The assumption $Q_{11}^{(i,M)} < Q_1^{(i,M)}$ is always true for two reasons:

1. the flow $Q_{11}^{(i,M)}$ is divided at each switch, therefore it decreases along the Input bus;
2. the continuous phase flow injected by the pump in the Output bus $Q_1^{(1,M)}$ can be set independently from the flow $Q_{11}^{(1,M)}$ and in particular $Q_1^{(1,M)} > Q_{11}^{(1,M)}$; moreover it will never decrease as it moves along the Output bus.

In μ -NET the flow equalizer is implemented as shown in Figure 8.4(a) and is completely defined through the parameters L_{conn} , w_{conn} , L'_{bal} , and w'_{bal} . Appropriate values of such parameters can be determined through the analysis of the resulting whole microfluidic circuit.

For this purpose, the electrical equivalent of the microfluidic network shown in Figure 8.4(b) is considered. In the electrical equivalent circuit, the flow equalizer has been replaced with the resistance R_{bal} . By applying delta-star transformations the electrical circuit shown in Figure 8.4(b) can be reduced to the circuit shown in Figure 8.4(c),

where the resistances R_x , R_y and R_z can be obtained as:

$$\begin{cases} R_x^{(i,M)} = R_{11}^{(i,M)} + R_G^{(i,M)} + R_A^{(i,M)} \\ R_y^{(i,M)} = R_1^{(i,M)} + R_I^{(i,M)} + R_D^{(i,M)} \\ R_z^{(i,M)} = R_8^{(i,M)} + R_H^{(i,M)} \end{cases} \quad (8.4)$$

which require the values of the resistances given in Table 8.1

$R_A^{(i,M)} = \frac{R_9^{(i,M)} R_{10}^{(i,M)}}{R_6^{(i,M)} + R_9^{(i,M)} + R_{10}^{(i,M)}}$	$R_B^{(i,M)} = \frac{R_6^{(i,M)} R_9^{(i,M)}}{R_6^{(i,M)} + R_9^{(i,M)} + R_{10}^{(i,M)}}$	$R_C^{(i,M)} = \frac{R_6^{(i,M)} R_{10}^{(i,M)}}{R_6^{(i,M)} + R_9^{(i,M)} + R_{10}^{(i,M)}}$
$R_D^{(i,M)} = \frac{R_3^{(i,M)} R_2^{(i,M)}}{R_3^{(i,M)} + R_4^{(i,M)} + R_2^{(i,M)}}$	$R_E^{(i,M)} = \frac{R_4^{(i,M)} R_2^{(i,M)}}{R_3^{(i,M)} + R_4^{(i,M)} + R_2^{(i,M)}}$	$R_F^{(i,M)} = \frac{R_3^{(i,M)} R_4^{(i,M)}}{R_3^{(i,M)} + R_4^{(i,M)} + R_2^{(i,M)}}$
$R_G^{(i,M)} = \frac{(R_7^{(i,M)} + R_C^{(i,M)})(R_F^{(i,M)} + R_B^{(i,M)})}{R_7^{(i,M)} + R_C^{(i,M)} + R_F^{(i,M)} + R_B^{(i,M)} + R_5^{(i,M)} + R_E^{(i,M)}}$		
$R_H^{(i,M)} = \frac{(R_5^{(i,M)} + R_E^{(i,M)})(R_7^{(i,M)} + R_C^{(i,M)})}{(R_5^{(i,M)} + R_E^{(i,M)} + R_F^{(i,M)} + R_B^{(i,M)} + R_7^{(i,M)} + R_C^{(i,M)})}$		
$R_I^{(i,M)} = \frac{(R_5^{(i,M)} + R_E^{(i,M)})(R_F^{(i,M)} + R_B^{(i,M)})}{R_5^{(i,M)} + R_E^{(i,M)} + R_F^{(i,M)} + R_B^{(i,M)} + R_7^{(i,M)} + R_C^{(i,M)}}$		

Table 8.1: Resistances of the electrical equivalent circuit of the device for MAC (see Figure 5(c)) reduced by using star-delta transformations, required in eq. (8.4).

The MAC device operates correctly if the relationship in eq. (8.1) is satisfied; thus, in the electrical equivalent shown in Figure 8.4(b), parameters must be set in such a way that

$$i_{11}^{(i,M)} \cong i_1^{(i,M)} \quad \forall i \leq N \quad (8.5)$$

where $i_j^{(i,\phi)}$ denotes the current flowing in the resistance $R_j^{(i,\phi)}$. Therefore, relationship in eq. (8.5) is satisfied if the resistance R_{bal} is such that the current $i_0^{(i,M)}$ is split into two (approximately) equal parts. This occurs if the following relationship holds:

$$R_y^{(i,M)} = R_x^{(i,M)} + R_{bal} \rightarrow R_{bal} = R_y^{(i,M)} - R_x^{(i,M)} \quad (8.6)$$

Notice that R_{bal} is the electrical equivalent of the hydrodynamic resistance introduced by the flow equalizer and is given by the sum of the contributions related to the three segments shown in Figure 8.4(a), that is:

$$R_{bal} = \alpha \left(2 \frac{L_{conn}}{w_{conn}} + \frac{L'_{bal}}{w'_{bal}} \right) \quad (8.7)$$

It follows that the parameters L_{conn} , w_{conn} , L'_{bal} , and w'_{bal} characterizing the flow equalizer must be set in such a way that the hydrodynamic resistance R_{bal} calculated in eq. (8.7) satisfies eq. (8.6). To validate the functioning of the flow equalizer, in Figure 8.5 is plotted the streamline pattern of the flows obtained through OpenFOAM simulations.

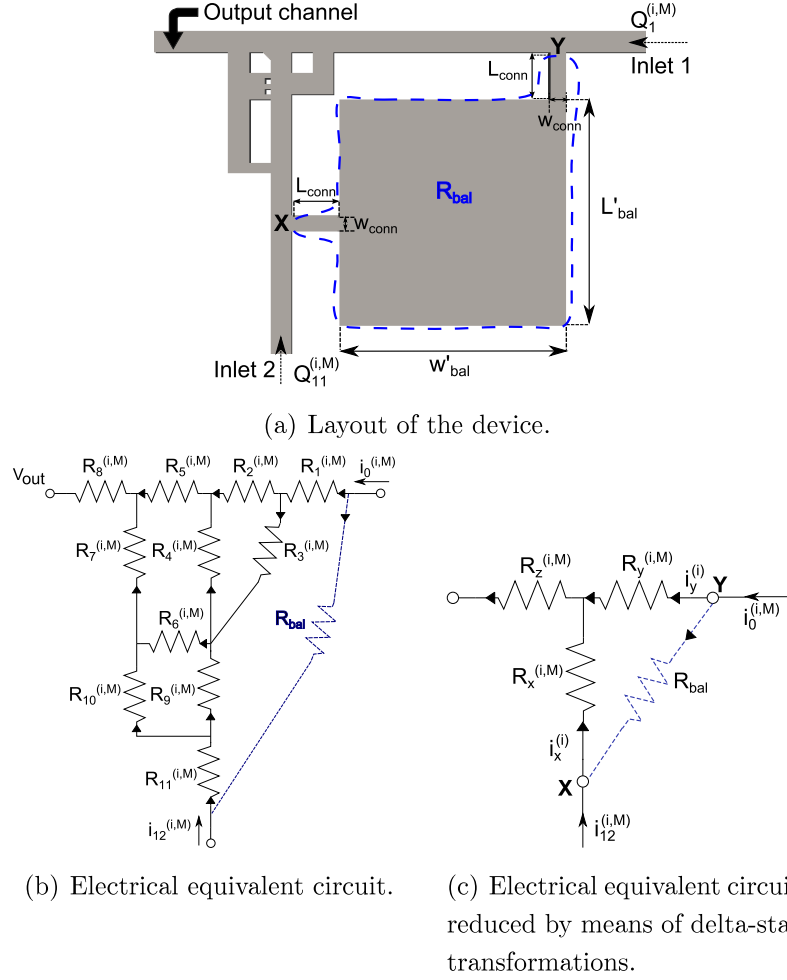


Figure 8.4: Representations of the equalized MAC proposed for μ -NET [18].

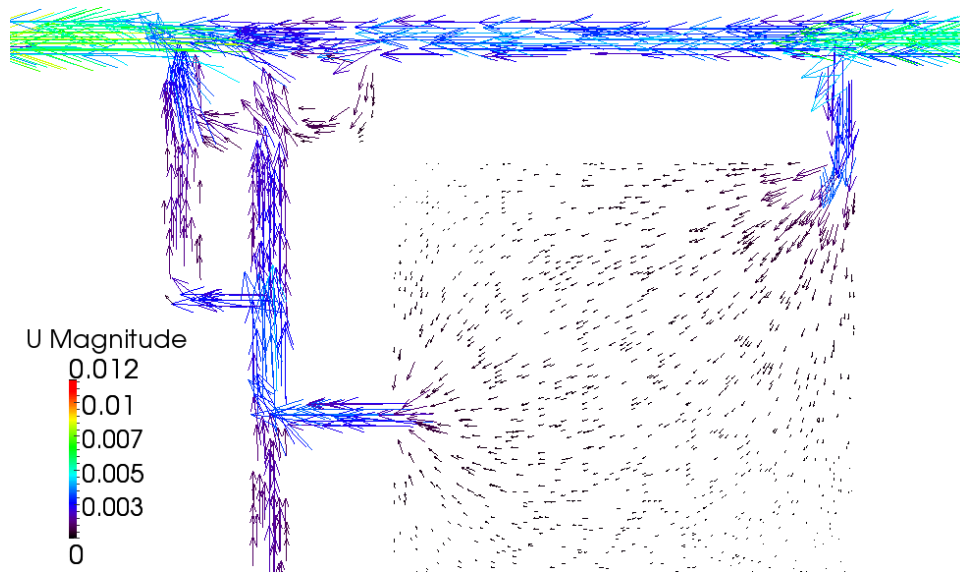


Figure 8.5: Simulation results of streamline pattern in the flow equalizer channel.

8.3 μ -NET Analysis: design tips

The previous section has discussed the integration problems related to the design of an MNI starting from the individual switch and MAC functionalities elaborated in [16], respectively. In this section, it is analyzed how droplets propagate along μ -NET pipes in order to achieve two objectives:

- Identify how the microfluidic router μ_R must set the distance between the header and payload droplets, D_{HP} , in such a way that the payload droplet will enter the intended LoC. In other words, the aim is to identify the *addressing* rules;
- Evaluate the *throughput* of the μ -NET defined as the expected number of successfully delivered microfluidic packets in a second. For this reason, it is needed to identify a lower bound on the distance, D_{PH} , between two consecutive microfluidic packets flowing through the Input bus. Note in fact that the distance D_{PH} is proportional to the minimum time interval between the generations of two packets, and therefore, is reciprocal to the throughput of the μ -NET.

To achieve the above objectives an analytical framework for evaluating the velocity of the droplets in any pipe of the μ -NET will be first derived in section 8.3.1. In particular, referring to the Input bus, as discussed in section 6.2, the flow decreases at any MNI because in the related switch it is split in the flow entering the LoC, and the one continuing along the Input bus towards the next switch. Referring to Figure 8.6, where the μ -NET microfluidic network is shown as a whole, this is the case of $Q_0^{(i-1,S)}$ which is split in $Q_3^{(i,S)}$ and $Q_0^{(i,S)}$

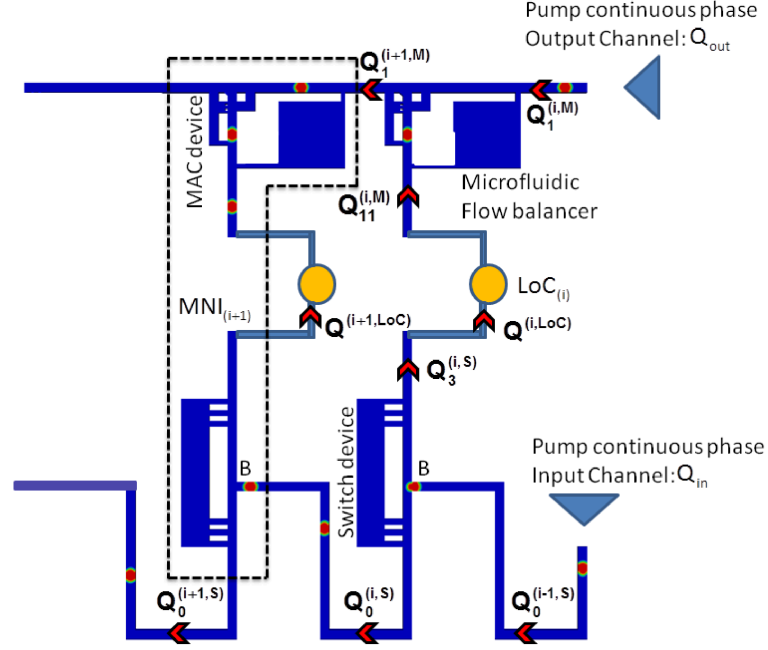


Figure 8.6: μ -NET network scheme [18].

at the switching point B. So, velocity of droplets along the Input bus changes from pipe to pipe. These differences in velocity result in modifications of the distance between droplets as they flow through the μ -NET: given that a distance encoding approach is used, such distance modifications must be considered to evaluate both D_{HP} and D_{PH} . This will be the focus of sections 8.3.2 and 8.3.3, respectively. Finally, in section 8.3.4 will be shown simulation results validating the μ -NET design.

8.3.1 Circuit analysis

The velocity of a droplet in a pipe can be calculated as the ratio between the flow rate and the section of the pipe. Accordingly, in the following a methodology to evaluate the flow rate in each pipe of the μ -NET is presented.

As already done in section 8.2, the microfluidic-electrical analogy is exploited. The electrical circuit equivalent to the μ -NET microfluidic network is quite complex; however, it can be reduced as shown in Figures 8.7. More specifically, Figure 8.7(a) shows the MNI electrical equivalent circuit; then Figure 8.7(b) shows the simplified electrical equivalent circuit. Figure 8.7(c) shows the network obtained as a series of delta-star transformations of the circuit shown in Figure 8.7(b) taking into account the corresponding segments of the Input and Output buses as well as the corresponding LoC. In Figure 8.7(c) the resistances R_{α_i} , R_{β_i} , and R_{γ_i} can be written as:

$$\begin{aligned} R_{\alpha_i} &= R_0^{(i+1,S)} + R_y^{(i,S)} + R_z^{(i+1,S)} \\ R_{\beta_i} &= R^{(i,LoC)} + R_x^{(i,S)} + \bar{R}_x^{(i,M)} \\ R_{\gamma_i} &= \bar{R}_y^{(i+1,M)} + \bar{R}_z^{(i,M)} \quad \text{for } i=1,2,\dots,N \end{aligned} \quad (8.8)$$

where N is the number of MNIs of the μ -NET. The values of resistances involved in Figure 8.7(b) are listed in Table 8.2.

The topology of the electrical equivalent circuit shown in Figure 8.7(c) is a *ladder network* and can be analyzed by iteration. In particular, each cell of the electrical equivalent circuit can be analyzed considering the equivalent downstream and upstream resistances, R_{down} and R_{up} , as depicted in Figure 8.8.

The equivalent downstream resistances seen after the i -th cell of

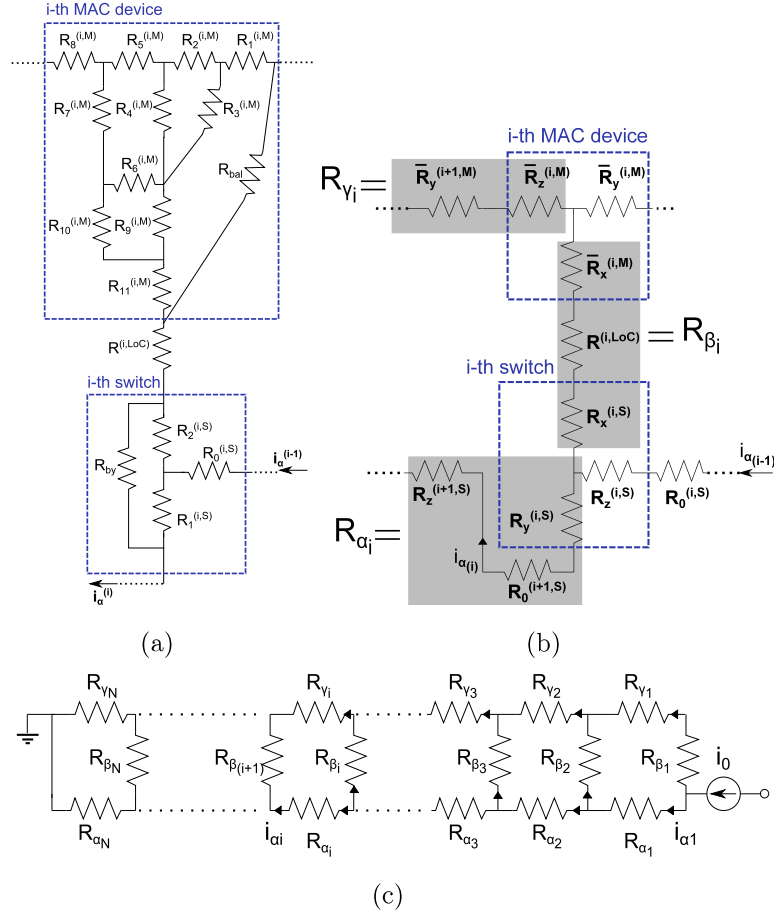


Figure 8.7: Electrical equivalent circuit of μ NET reduced by using delta-star transformations [18].

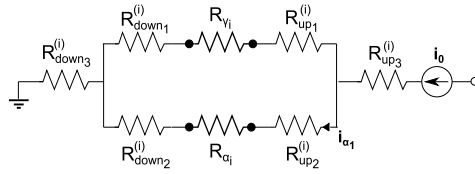


Figure 8.8: Cell i of the μ -NET electrical equivalent circuit [18].

Parameter	Description
$R_x^{(i,S)} = \frac{R_{by} R_1^{(i,S)}}{R_1^{(i,S)} + R_2^{(i,S)} + R_{by}}$	equivalent resistance of the branch 1 of the switch
$R_y^{(i,S)} = \frac{R_{by} R_2^{(i,S)}}{R_1^{(i,S)} + R_2^{(i,S)} + R_{by}}$	equivalent resistance of the branch 2 of the switch
$R_z^{(i,S)} = \frac{R_1^{(i,S)} R_2^{(i,S)}}{R_1^{(i,S)} + R_2^{(i,S)} + R_{by}}$	equivalent resistance of switch input
$\bar{R}_x^{(i,M)} = \frac{R_x^{(i,M)} R_{bal}}{R_x^{(i,M)} + R_y^{(i,M)} + R_{bal}}$	equivalent resistance of MAC input 2
$\bar{R}_y^{(i,M)} = \frac{R_y^{(i,M)} R_{bal}}{R_x^{(i,M)} + R_y^{(i,M)} + R_{bal}}$	equivalent resistance of MAC input 1
$\bar{R}_z^{(i,M)} = \frac{R_x^{(i,M)} R_y^{(i,M)}}{R_x^{(i,M)} + R_y^{(i,M)} + R_{bal}} + R_z$	equivalent resistance of MAC output
$R^{(i,LoC)}$	equivalent resistance of the i -th LoC
$R_0^{(i+1,S)}$	equivalent resistance of the channel that connects the i -th switch with the $(i+1)$ -th

Table 8.2: Equivalent resistances illustrated in Figure 8.7(b).

the electrical network can be recursively expressed as:

$$\begin{aligned}
 R_{down_1}^{(i)} &= \frac{(R_{\gamma(i+1)} + R_{down_1}^{(i+1)})R_{\beta(i+1)}}{R_{\gamma(i+1)} + R_{down_1}^{(i+1)} + R_{\beta(i+1)} + R_{\alpha(i+1)} + R_{down_1}^{(i+1)}}; \\
 R_{down_2}^{(i)} &= \frac{(R_{\alpha(i+1)} + R_{down_2}^{(i+1)})R_{\beta(i+1)}}{R_{\gamma(i+1)} + R_{down_1}^{(i+1)} + R_{\beta(i+1)} + R_{\alpha(i+1)} + R_{down_1}^{(i+1)}}; \\
 R_{down_3}^{(i)} &= \sum_{k=N}^i \frac{(R_{\alpha(i+1)} + R_{down_2}^{(i+1)})(R_{\gamma(i+1)} + R_{down_1}^{(i+1)})}{R_{\gamma(i+1)} + R_{down_1}^{(i+1)} + R_{\beta(i+1)} + R_{\alpha(i+1)} + R_{down_1}^{(i+1)}}, \\
 \text{for } i &= 1, 2, \dots, N-1
 \end{aligned} \tag{8.9}$$

where $R_{down_1}^{(N)} = R_{down_2}^{(N)} = 0$. Analogously, the equivalent upstream resistances seen before the i -th cell of the electrical network can be recursively expressed as:

$$\begin{aligned}
 R_{up_1}^{(i)} &= \frac{(R_{\gamma(i-1)} + R_{up_1}^{(i-1)})R_{\beta_i}}{R_{\gamma(i-1)} + R_{up_1}^{(i-1)} + R_{\beta_i} + R_{\alpha(i-1)} + R_{up_2}^{(i-1)}}; \\
 R_{up_2}^{(i)} &= \frac{(R_{\alpha(i-1)} + R_{up_2}^{(i-1)})R_{\beta_i}}{R_{\gamma(i-1)} + R_{up_1}^{(i-1)} + R_{\beta_i} + R_{\alpha(i-1)} + R_{up_2}^{(i-1)}}; \\
 R_{up_3}^{(i)} &= \sum_{k=1}^i \frac{(R_{\alpha(i-1)} + R_{up_2}^{(i-1)})(R_{\gamma(i-1)} + R_{up_1}^{(i-1)})}{R_{\gamma(i-1)} + R_{up_1}^{(i-1)} + R_{\beta_i} + R_{\alpha(i-1)} + R_{up_2}^{(i-1)}}, \\
 \text{for } i &= 2, 3, \dots, N.
 \end{aligned} \tag{8.10}$$

where, $R_{up_1}^{(1)} = R_{\beta_1}$ and $R_{up_2}^{(1)} = 0$.

By using these values into the *current divider rule*, the value of the current i_{α_i} is obtained in each of the pipes of the Input bus in Figure

8.7(c):

$$i_{\alpha_i} = i_0 \frac{R_{up_1}^{(i)} + R_{\gamma_i} + R_{down_1}^{(i)}}{R_{up_1}^{(i)} + R_{\gamma_i} + R_{down_1}^{(i)} + R_{up_2}^{(i)} + R_{\alpha_i} + R_{down_2}^{(i)}} \quad \text{for } i = 1, 2, \dots, N. \quad (8.11)$$

where, i_0 is the input current. Once the value of the currents i_{α_i} is estimated, thanks to the analogy between the electrical and microfluidic domains, the flow rate is estimated as well and the velocity v_{α_i} of a droplet at the outlet of the i -th MNI can be calculated as:

$$v_{\alpha_i} = \frac{Q_{\alpha_i}}{\Sigma} \quad (8.12)$$

where Q_{α_i} corresponds to i_{α_i} and Σ is the section of the channel.

8.3.2 Addressing

In this section it is evaluated how the distance between the header and payload droplets changes as they pass through the switches in the MNIs. Then the implications on the address encoding utilized in μ -NET will be discussed.

To find how the distance between droplets changes as they flow through the network, let the distance between two droplets entering the switch of the i -th MNI be denoted as $D_{HP}^{(i)}$ as in Figure 8.9(a). Furthermore, let $v_0^{(i,S)} = v_{\alpha_i}$ represent the velocity of the droplets in the pipe of resistance R_{α_i} leading to the i -th MNI and $v_2^{(i,S)}$ the velocity of the droplets in $\text{Pipe}_2^{(i,S)}$. Moreover in the designed μ -NET all microfluidic circuits implementing the switching and MAC functions are characterized by the same geometrical characteristics. Such choice reduces the number of parameters involved in the design process and therefore, if viable solutions exist, reduces the design complexity. As a result, in the following it is assumed that $L_2^{(i,S)} = L_2^{(S)}$, $L^{(i,S)} = L^{(S)}$ and $w^{(i,S)} = w^{(S)}$ for any $i \leq N$.

In Figures 8.9 is represented the position of the header and payload droplets in four relevant time instants:

- t_0 : the time instant when the header droplet arrives at the bifurcation point B (see Figure 8.9(a)).
- t_1 : the time instant when the header droplet arrives at point C (see Figure 8.9(b)).
- t_2 : the time instant when the payload droplet arrives at the bifurcation point B (see Figure 8.9(c)).

- t_3 : the time instant when the payload droplet arrives at point C (see Figure 8.9(d)).

Let us suppose a packet arrives at the switching point B of the i -th MNI as in Figure 8.9(a). Both header and payload droplets continue to flow in the Input bus towards the next MNIs if the header droplet has passed the point C when the payload droplet arrives at the point B , as in Figure 8.9(c). In order to guarantee the above conditions, let us consider the time $T_1 = (t_2 - t_0)$ that the payload droplet takes to move from the condition in Figure 8.9(a) to the condition in Figure 8.9(c), that is the time required to cover the distance $D_{HP}^{(i)}$ at the velocity v_{α_i} ; clearly $T_1 = D_{HP}^{(i)} / v_{\alpha_i}$. Analogously, when the header droplet is at point B it takes a time $T_2 = (t_1 - t_0) = L_2^S / v_2^{(i,S)}$ to arrive at the point C . So, if $T_1 > T_2$ then both the droplets will continue to flow along the Input bus towards the next MNI; on the contrary if $T_1 < T_2$ then the payload droplet will be switched towards the LoC in the i -th MNI. It is evident that in the latter case an orphan header droplet will flow into the Input bus. The condition $T_1 < T_2$ is denoted as the *switching condition*. Let us focusing on the case $T_1 > T_2$ and let us now calculate $D_{HP}^{(i+1)}$. The distance $D_{HP}^{(i+1)}$ can be calculated as the distance covered by the header droplet along the Pipe $_4^{(i,S)}$ in the time interval between t_1 and t_3 . In such a time interval the header droplet flows at the velocity $v_4^{(i,S)} = v_{\alpha_{i+1}}$. Therefore, $D_{HP}^{(i+1)}$ can be calculated as

$$D_{HP}^{(i+1)} = v_{\alpha_{i+1}}(t_3 - t_1) \quad (8.13)$$

The term $(t_3 - t_1)$ can be calculated as

$$t_3 - t_1 = (t_3 - t_2) + (t_2 - t_0) - (t_1 - t_0) \quad (8.14)$$

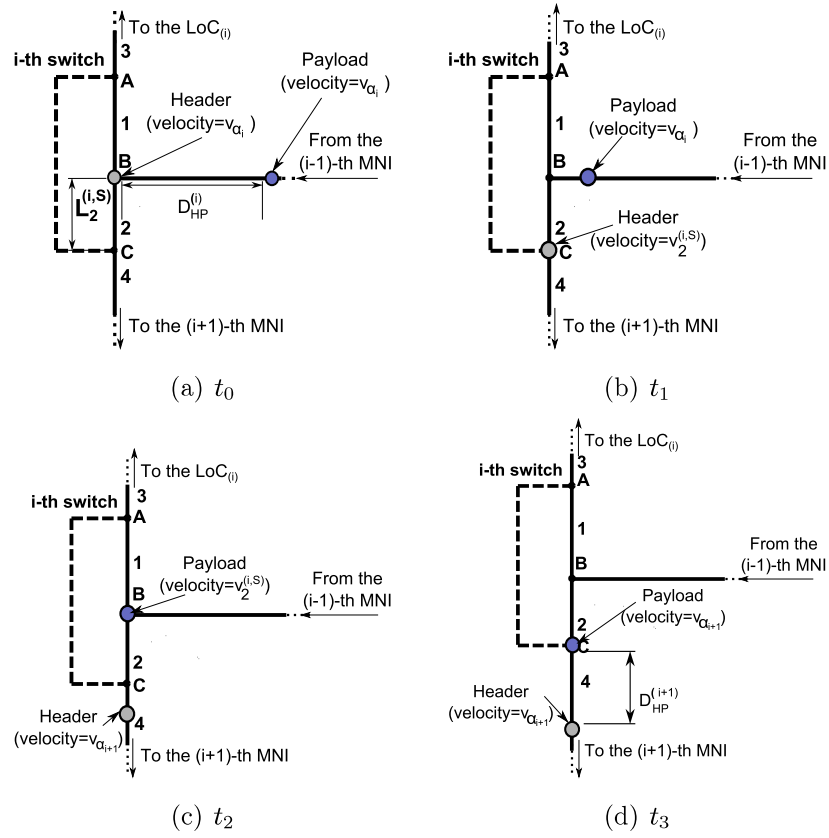


Figure 8.9: Droplets positions at different times [18].

where

$$t_3 - t_2 = L_2^{(S)}/v_2^{(i,S)}; \quad t_2 - t_0 = D_{HP}^{(i)}/v_{\alpha_i}; \quad t_1 - t_0 = L_2^{(S)}/v_2^{(i,S)} \quad (8.15)$$

By replacing eqs. (8.15) in eq. (8.14) $t_3 - t_1$ can be written as

$$t_3 - t_1 = D_{HP}^{(i)}/v_{\alpha_i} \quad (8.16)$$

and therefore

$$D_{HP}^{(i+1)} = \frac{v_{\alpha_{i+1}}}{v_{\alpha_i}} D_{HP}^{(i)} \quad (8.17)$$

By iterating the expression in eq. (8.17), the following equation is obtained

$$D_{HP}^{(i+1)} = \frac{v_{\alpha_{i+1}}}{v_{\alpha_1}} D_{HP}^{(1)} \quad (8.18)$$

where v_{α_1} and $D_{HP}^{(1)}$ are the velocity and the distance between the header and the payload droplets at the inlet of the first MNI in the μ -NET and are set by the microfluidic router μ_R .

Let us now calculate how the μ_R has to set the distance $D_{HP}^{(1)}$ to correctly address the i -th MNI. To this purpose the case where the *switching condition* holds at the i -th MNI is considered that is $T_1 < T_2$ as shown in Figure 8.10. In this figure, the distance $\bar{D}_{HP}^{(i+1)}$ will be equal to:

$$\bar{D}_{HP}^{(i+1)} = \frac{v_2^{(i,S)}}{v_{\alpha_i}} D_{HP}^{(i)} \quad (8.19)$$

In order to calculate the velocity $v_2^{(i,S)}$, let us note that:

$$v_2^{(i,S)} = \frac{R_1^{(S)}}{R_1^{(S)} + (R_2^{(S)} + R_{droplet})} \cdot v_{\alpha_i} \quad (8.20)$$

Note that in eq. (8.20) the additive resistance induced by the presence of the droplet in Pipe₂^(i,S) is considered; if the ratio between

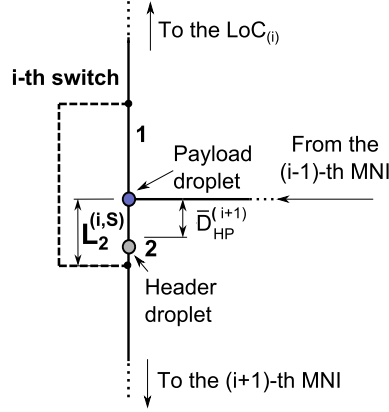


Figure 8.10: Distance between header and payload droplets when the i -th LoC is addressed [18].

the viscosities of the dispersed and continuous phases, μ_r , is higher than 1, i.e, $\mu_r > 1$, then the resistance ($R_2^{(S)} + R_{droplet}$) is given by (see eq. (3.10))[15]

$$R_2^{(S)} + R_{droplet} = \frac{\alpha}{w^{(S)}} [L_2^{(S)} + L_{droplet}(\mu_d - \mu_c)] \quad (8.21)$$

where μ_d and μ_c represent the viscosities of the dispersed and continuous phases, respectively, and $L_{droplet}$ is the droplet length.

By plugging eq. (8.20) in eq. (8.19), recalling eq. (8.2) it follows that

$$\bar{D}_{HP}^{(i+1)} = D_{HP}^{(i)} \frac{L_1^{(S)}}{L_1^{(S)} + L_2^{(S)} + L_{droplet}(\mu_c - \mu_d)} \quad (8.22)$$

Given that the case $T_1 < T_2$ is considered, then

$$\bar{D}_{HP}^{(i+1)} < L_2^{(S)} \quad (8.23)$$

Accordingly, replacing eq. (8.18) in eq. (8.23) it follows that

$$D_{HP}^{(1)} \frac{v_{\alpha_i}}{v_{\alpha_1}} \frac{L_1^{(S)}}{L_1^{(S)} + L_2^{(S)} + L_{droplet}(\mu_c - \mu_d)} < L_2^{(S)} \quad (8.24)$$

that, yields to

$$D_{HP}^{(1)} < \frac{v_{\alpha_1}}{v_{\alpha_i}} \frac{L_2^{(S)}(L_1^{(S)} + L_2^{(S)} + L_{droplet}(\mu_c - \mu_d))}{L_1^{(S)}} \quad (8.25)$$

It follows that in order to guarantee that the payload droplet

- goes towards i -th LoC, and
- passes through the $(i - 1)$ -th MNI without being switched towards the $(i - 1)$ -th LoC

the microfluidic router must set the distance between the header and payload droplets so that the following relationship is satisfied:

$$\begin{aligned} \frac{v_{\alpha_1}}{v_{\alpha_{(i)}}} \frac{L_2^{(S)}(L_1^{(S)} + L_2^{(S)} + L_{droplet}(\mu_c - \mu_d))}{L_1^{(S)}} &< D_{HP}^{(1)} < \\ &< \frac{v_{\alpha_1}}{v_{\alpha_{i+1}}} \frac{L_2^{(S)}(L_1^{(S)} + L_2^{(S)} + L_{droplet}(\mu_c - \mu_d))}{L_1^{(S)}} \end{aligned} \quad (8.26)$$

Note that the values of the velocities required in eq. (8.26) can be calculated by replacing the currents with the related flow rates in eq. (8.11) and eq. (8.12). As an example, in Table 8.3 a valid addressing scheme is reported for a μ -NET connecting up to eight LoCs in the case $R_{\beta_i} = R_{\beta_{(i-1)}} = 34.15\alpha$, $R_{\alpha_i} = R_{\alpha_{(i-1)}} + 2i\alpha$, $R_{\gamma_i} = R_{\gamma_{(i-1)}} + 2i\alpha$, with $R_{\alpha_N} = 78.7\alpha$, $R_{\gamma_N} = 9.8\alpha$. The address of each MNI is chosen as the average value $D_{HP}^{*(i)}$ of the respective addressing interval in eq. (8.26). Therefore, this equation can be rewritten as

$$D_{HP}^{(i)} = D_{HP}^{*(i)} \pm \delta_{margin} \quad (8.27)$$

where δ_{margin} is a confident margin to absorb the fluctuations in the actual value of $D_{HP}^{*(i)}$ at the receiving MNI which could cause errors in the delivery of payload droplets. The expression for δ_{margin} is the following:

$$\delta_{margin} = \frac{v_{\alpha_i} - v_{\alpha_{(i+1)}}}{2(v_{\alpha_i} + v_{\alpha_{(i+1)}})} \quad (8.28)$$

Figure 8.11 shows the variation of δ_{margin} , as percentage of $D_{HP}^{*(i)}$, for the seven μ -NET configurations in Table 8.3. The plot shows that for small a μ -NET, connecting up to four LoCs, the addressing is robust against possible fluctuations in $D_{HP}^{*(i)}$.

Number of connected LoCs	Address of 1st LoC	Address of 2nd LoC	Address of 3rd LoC	Address of 4th LoC	Address of 5th LoC	Address of 6th LoC	Address of 7th LoC	Address of 8th LoC
2	0.0014	0.0022	0	0	0	0	0	0
3	0.0014	0.0022	0.0038	0	0	0	0	0
4	0.0014	0.0022	0.0037	0.0050	0	0	0	0
5	0.0014	0.0022	0.0035	0.0046	0.0055	0	0	0
6	0.0014	0.0021	0.0034	0.0042	0.0049	0.0056	0	0
7	0.0014	0.0021	0.0032	0.0039	0.0044	0.0050	0.0056	0
8	0.0014	0.0021	0.0031	0.0036	0.0040	0.0044	0.0050	0.0057

Table 8.3: Example of a valid addressing (that is, $D_{HP}^{*(i)}$ values) for seven μ -NETs connecting up to eight LoCs (the distances are expressed in millimeters).

8.3.3 Throughput analysis

In this section the throughput of the μ -NET is evaluated defined as the expected number of successfully delivered microfluidic packets in a second. Accordingly, the throughput can be calculated as the ratio

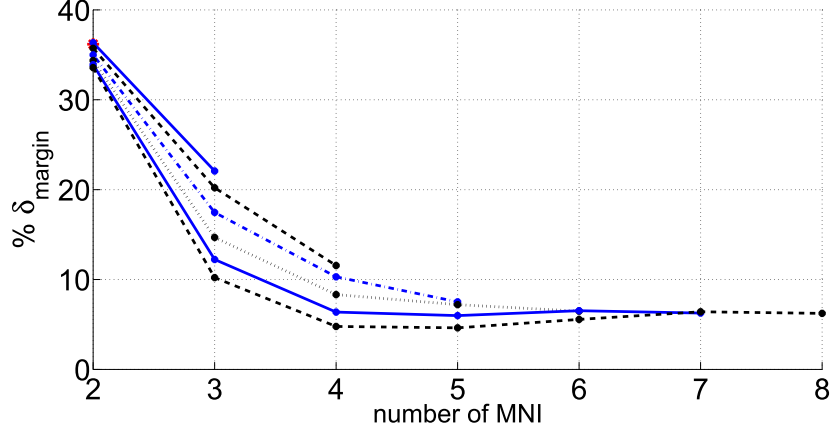


Figure 8.11: Variation of δ_{margin} , as percentage of $D_{HP}^{*(i)}$, for seven μ -NET configurations connecting up to eight LoCs.

between the velocity of the droplets as they enter the Input bus, v_{α_1} , and the distance $D_{PH}^{(1)}$ between two consecutive microfluidic packets set by the microfluidic router μ_R . The velocity of the droplets when they enter the Input bus is proportional to the input flow rate $Q_0^{(1,S)}$. Moreover, it is evident that the flow rate at the μ -NET input cannot be higher than a given threshold to avoid the breakup of droplets at the switches bifurcation as experimentally observed as explained in section 3.4.3. This threshold value depends on the properties of the fluid phases (see eq. (3.8)); for example for the performed simulations is $Q_0^{(1,S)} = 4 \times 10^{-12} \text{ m}^3/\text{s}$. The throughput analysis was carried out by implementing the presented theoretical model in Mathworks MATLAB environment by using the fluid properties and channel dimensions reported in Table IV to calculate the channel resistances

according to the eq. (3.10).

As far as the addressing scheme is concerned, let us stress that the i -th MNI switches any droplet with a distance from the previous one that satisfies the eq. (8.26); so, referring to Figure 8.12, in order to prevent any decoding error, it must be guaranteed at all MNIs of the μ -NET that:

1. the distance between consecutive header droplets, $D_{HH}^{(i)}$, is higher than $L_2^{(S)}$

$$D_{HH}^{(i)} > L_2^{(S)} \quad \forall i \leq N \quad (8.29)$$

2. the distance between consecutive microfluidic frames, $D_{PH}^{(i)}$, is higher than $L_2^{(S)}$

$$D_{PH}^{(i)} > L_2^{(S)} \quad \forall i \leq N \quad (8.30)$$

To understand the reasons for this constraints, let us first suppose that the relationship in (8.29) between two header droplets does not hold for a given i^* , and that the payload droplet of the first packet has left the Input bus before reaching the i^* -th MNI, that is, the first header droplet is *orphan* at the i^* -th MNI. Under the above assumptions, the two header droplets will be interpreted by the switch of the i^* -th MNI as a unique packet in which the second droplet is the payload and will be forwarded towards the i^* -th LoC in order to satisfy the relationship in eq. (8.23). Let us now consider the condition 2), assuming that there are two sets of header-payload, i.e. two consecutive microfluidic packets. If the relationship given in (8.29) holds, when a header droplet reaches the bifurcation point of the i -MNI the payload of the previous packet has left the i -MNI, this guarantees that

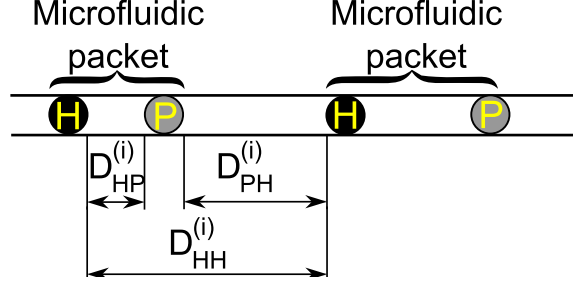


Figure 8.12: Distances between droplets [18].

a payload-header sequence is not interpreted incorrectly by a MNI as a header-payload sequence. However, the condition on D_{HH} is contained in the condition on D_{PH} since $D_{HH} > D_{HP} + D_{PH}$ (see Figure 8.12) hence, in the following only the condition in eq. (8.30) will be taken into account. In order to satisfy this relationship at any MNI, it must be consider that the distance between two consecutive microfluidic packets decreases as they traverse the Input bus, analogously to what is said about $D_{HP}^{(i)}$. Therefore, $D_{PH}^{(1)}$ must be set in such a way that eq. (8.26) is never satisfied, that is, $D_{PH}^{(1)}$ must not match any valid $D_{HP}^{(1)}$. The above requirements can be satisfied by imposing a lower-bound on $D_{PH}^{(1)}$, which is denoted as $D_{PH}^{(\min)}$, given as follows:

$$D_{PH}^{(1)} > D_{PH}^{(\min)} = \frac{Q_{\alpha_1}}{Q_{\alpha_{(N-1)}}} \frac{L_2^{(S)}(L_1^{(S)} + L_2^{(S)} + L_{droplet}(\mu_c - \mu_d))}{L_1^{(S)}}. \quad (8.31)$$

Therefore, the maximum achievable throughput is given by $v_{\alpha_1}/D_{PH}^{(\min)}$. In Figure 8.13 is shown the throughput calculated when the eq. (8.31) is satisfied. As expected, in Figure 8.13(a) the throughput decreases as the number of MNIs, N , increases. In fact, as N

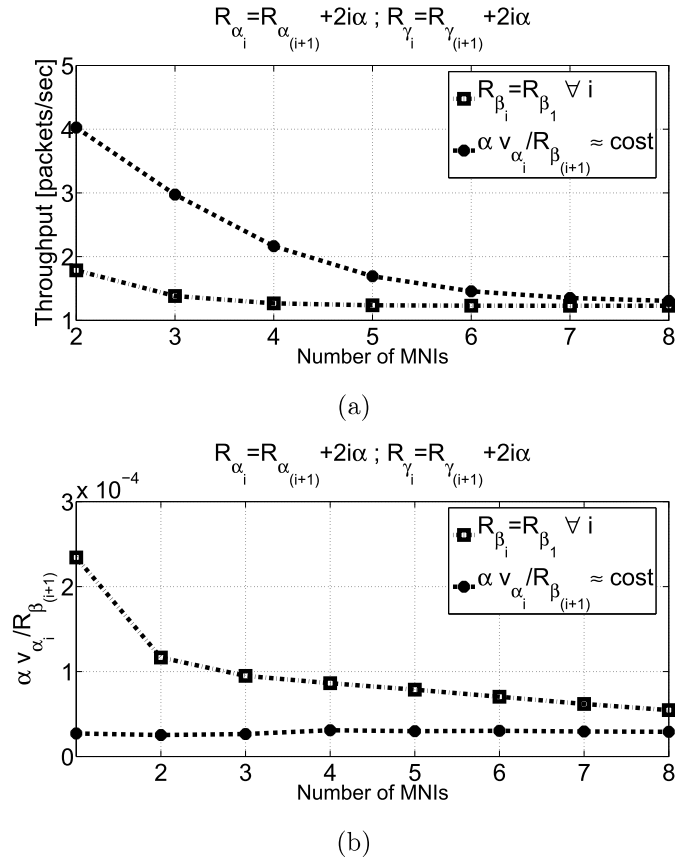


Figure 8.13: Throughput of μ -NET vs. the number of MNIs, N , obtained in two different settings [18].

increases, $D_{PH}^{(\min)}$ increases and, thus, throughput decreases. Also, note that two curves are plotted in Figure 8.13(a). One refers to the case in which the equivalent resistance R_{β_i} is the same at all MNIs, whereas the other refers to the case in which the resistances R_{β_i} are set proportionally to the flow rate Q_{α_i} . Figure 8.13(b) shows the ratio $(\alpha v_{\alpha_i})/R_{\beta_{i+1}}$ in the two above settings. Comparing the corresponding curves shown in Figure 8.13(a), observe that the second setting provides a significant improvement (more than 200% improvement) in throughput. This performance improvement is due to the fact that the second setting guarantees lower decrease in the flow rate along the Input bus and, therefore, lower decrease in the distance between consecutive droplets. In particular, eq. (8.17) states that the reduction in the distance between consecutive droplets occurring when a packet flows through the i -th MNI is due to the difference between v_{α_i} e $v_{\alpha_{i+1}}$ before and after the MNI; this one of course is related to the flow velocity before the MNI, v_{α_i} and the hydrodynamic resistance of the branch towards the LoC in the MNI, $R_{\beta_{i+1}}$. Thus, the higher $R_{\beta_{i+1}}$, the lower the flow entering the MNI and, therefore, the higher the flow velocity $v_{\alpha_{i+1}}$ which results in lower valid values for $D_{PH}^{(1)}$ and thus, higher achievable throughput.

In Figures 8.14(a) and 8.14(b) are plotted the throughput vs. the input flow velocity, v_{α_1} , and the sum of the two switch pipes length, $L_1^{(S)}$ and $L_2^{(S)}$ respectively, in case the μ -NET consists of eight MNIs. As expected, the throughput increases with the input flow velocity and decreases with $L_1^{(S)} + L_2^{(S)}$; this is because an increase in $L_2^{(S)}$ results in an increase in $D_{PH}^{(\min)}$ as in eq. (8.31).

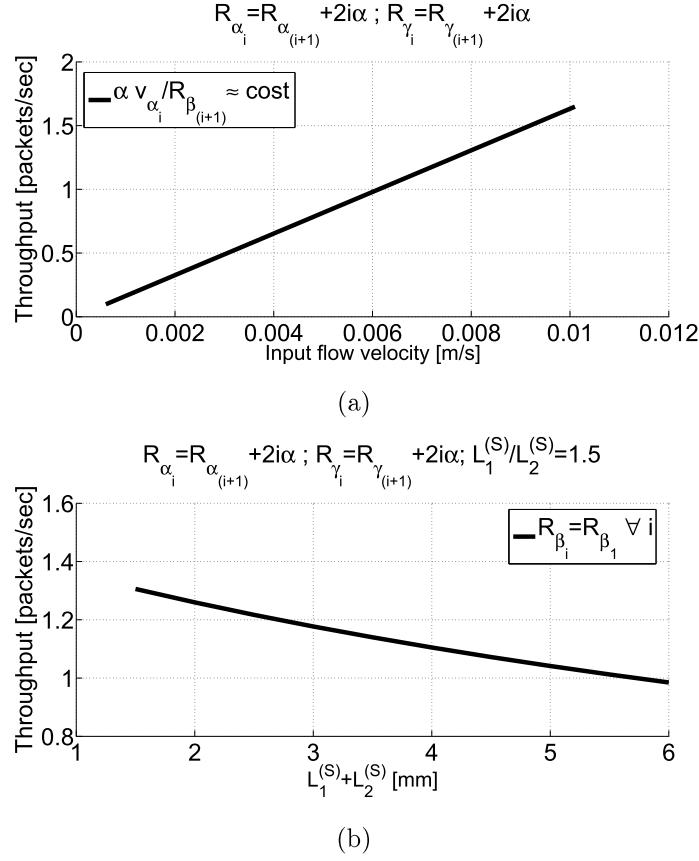


Figure 8.14: Throughput of a μ -NET with $N = 8$ vs. (a) the input flow velocity; (b) the sum of the length of the Pipe 1, $L_1^{(S)}$, and the Pipe 2, $L_2^{(S)}$, of the switch [18].

8.3.4 Simulation results

To validate the model a simulation campaign has been performed using a OpenFOAM software[122]. Simulations allowed to study the propagation of droplets along the microfluidic network as well as the operations executed by the μ -NET. In simulations oil droplets (PFD, $\mu_d = 5$ mPa·s, $\rho_d = 1941$ kg/m³) dispersed in water ($\mu_c = 1$ mPa·s, $\rho_c = 1000$ kg/m³) are considered. A no-slip boundary condition at the channel walls and a static contact angle of 140 are imposed. Moreover, the values of the parameters characterizing the geometry of the microfluidic circuits performing switching and MAC functions in each MNI are given in Table 8.4². Note that the values in Table 8.4 satisfy all the design conditions required for the properly switch operations discussed in chapter 6. In particular, for the considered fluid parameters $\mu_r = 5$, therefore to design the switch device the relationship in eq. (6.3) has been used.

In Figure 8.15 is shown:

- how the value of the distance $D_{HP}^{(i)}$ between the header and payload droplets changes along the Input bus in case the μ -NET network consists of three MNIs, i.e., $N = 3$.

²For the sake of completeness observe that in the flow equalizer, the condition for microfluidic channels is still valid. In fact, the Reynolds number $Re = \frac{\rho v D_H}{\mu_c}$ where ρ is the density of the continuous phase, μ_c is its dynamic viscosity, v is the fluid velocity which in the presented setting is $v \in [0.0006; 0.01]$ and $D_H = (2hw)/((h+w))$ is the hydraulic diameter of the microchannel which in the design is equal to $D_H = 96.12\mu\text{m}$ being h the height of the expansion area equal to $50\mu\text{m}$ and $w'_{bal} = 1250\mu\text{m}$ the weight of the expansion area - is required to be lower than 2100; in this settings it is $Re \approx 1$.

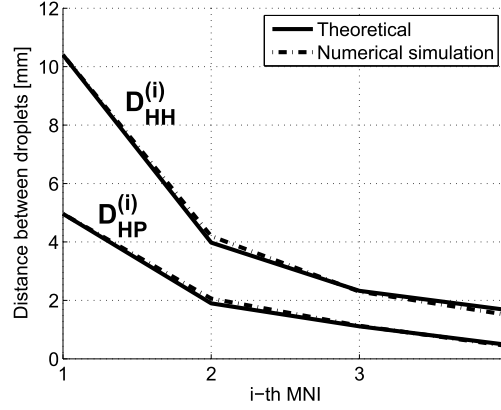


Figure 8.15: Values of the distances $D_{HP}^{(i)}$ and $D_{HH}^{(i)}$ for different values of i [18].

- how the value of the distance $D_{HH}^{(i)}$ between two header droplets (the first of which is *orphan*) changes along the Input bus in case the μ -NET network consists of three MNIs, i.e., $N = 3$.

For each of the above cases two curves are plotted: one has been obtained analytically, the other has been obtained through simulations. Results shown in Figure 8.15 confirm the accuracy of the derived model.

To validate the correctness of the operations performed by the μ -NET as a whole, Figure 8.16 shows five snapshots of the simulation output representing that:

- no collision occurs between the droplet **a** and the droplet **b** (Figure 8.16(a)-8.16(d));
- the distance D_{HP} between the header droplet **c** and the payload droplet **d** is such that the payload droplet **d** is forwarded to

Switch	Parameter	$\frac{L_{by}^{(i,S)}}{w_{by}^{(i,S)}}$	$\frac{L_1^{(i,S)}}{w_1^{(i,S)}}$	$\frac{L_2^{(i,S)}}{w_2^{(i,S)}}$	h	L_d	
	Value	3 μm	9 μm	6 μm	50 μm	150 μm	
MAC	Parameter	$\frac{L_1^{(i,M)}}{w_1^{(i,M)}}$	$\frac{L_2^{(i,M)}}{w_2^{(i,M)}}$	$\frac{L_3^{(i,M)}}{w_3^{(i,M)}}$	$\frac{L_4^{(i,M)}}{w_4^{(i,M)}}$	$\frac{L_5^{(i,M)}}{w_5^{(i,M)}}$	
	Value	9.35 μm	1 μm	3 μm	1 μm	1 μm	
	Parameter	$\frac{L_6^{(i,M)}}{w_6^{(i,M)}}$	$\frac{L_7^{(i,M)}}{w_7^{(i,M)}}$	$\frac{L_8^{(i,M)}}{w_8^{(i,M)}}$	$\frac{L_9^{(i,M)}}{w_9^{(i,M)}}$	$\frac{L_{10}^{(i,M)}}{w_{10}^{(i,M)}}$	$\frac{L_{11}^{(i,M)}}{w_{11}^{(i,M)}}$
	Value	0.8 μm	1 μm	7.25 μm	3 μm	7 μm	2 μm

Table 8.4: Parameters characterizing the MNIs geometry integrated in the μ -NET illustrated in Figure 8.16.

the LoC (this is modeled as the resistance of a straight channel) (Figures 8.16(a)-8.16(d));

- the distance D_{HH} between two consecutive orphan header droplets **e** and **f** is such that they do not address a LoC but continue to flow towards the sink (Figure 8.16(a) and Figure 8.16(e)).

Moreover, notice that the payload-header sequences are correctly interpreted by each MNI, that is no header is switched towards any molecular processor.

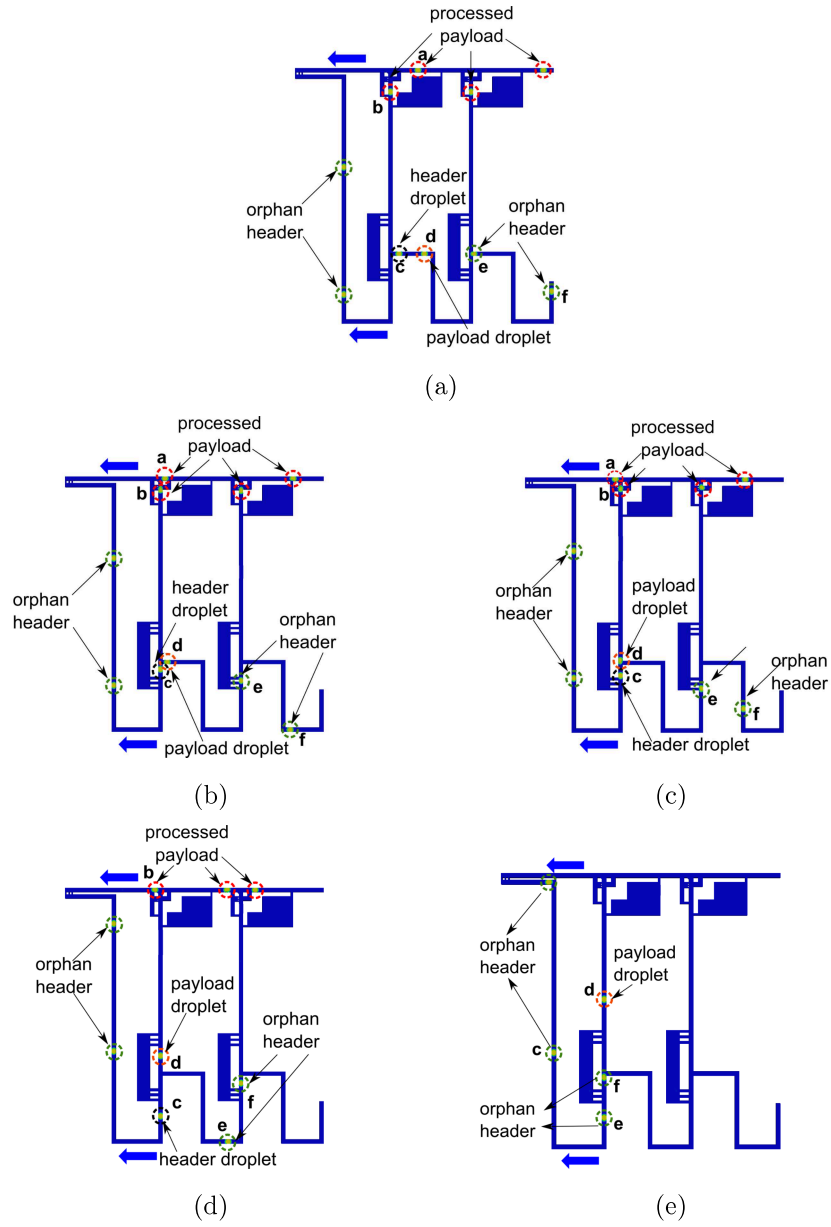


Figure 8.16: Simulation results that demonstrate the μ -NET functioning [18].

CONCLUSIONS AND SUGGESTIONS FOR FURTHER WORKS

The current challenge of droplet-based microfluidics is the improvement of the LoC technology through the development of a programmable versatile platform integrating multiple processing protocols. To this goal, one of the most crucial issues is the realization of a communication network of cooperating LoCs that enables the possibility of combining specialized functions through a flexible and modular microfluidic communication network.

This work focused on the design of addressing, switching and medium access control functions as the pillars of the microfluidic networking paradigm, and shows how these conventional networking functions can be implemented in a microfluidic technological domain to foster the realization of programmable microfluidic systems.

Accordingly, the traditional communication and networking

paradigms were redefined by introducing networking functionalities which rely on the use of a passive, simple, and low cost microfluidic technology, i.e. the hydrodynamic manipulation of droplets through microchannel geometries without any active on-chip actuator. Therefore, a microfluidic communication network paradigm, namely *Hydrodynamic Controlled Microfluidic Network*(HCN), was proposed.

To support information exchange among the connected entities in HCN, appropriate schemes for encoding the addressing information have to be introduced. Several approaches to information encoding were analyzed in this work while investigating the use of signaling in microfluidic communication networks. For each different encoding methodology, some compatible switch devices were identified from literature or introduced to correctly address the microfluidic elements connected into a microfluidic communication network.

Among these encoding schemes, the distance between consecutive droplets was chosen for address encoding in the HCN. In particular, the information in HCN is organized in *microfluidic packets* which consist of two droplets: a *header* droplet and a *payload* droplet. The *payload droplet* contains the bio/chemical information (e.g. a sample) which will be processed by the LoCs, whereas the *header* droplet is used for signaling purposes, in fact, the address of the recipient LoC is encoded in the distance between these two droplets.

Starting from the above addressing scheme, a passive microfluidic switch was presented and assessed through numerical simulations. In this switch, the distance between *header* and *payload* droplets determines the path that the *payload* droplet will take at a bifurcation. Moreover, a prototype of the microfluidic switch was realized and its

experimental testing was presented and compared with results obtained from numerical simulations.

Later on, a hydrodynamic circuit which implements the *Medium Access Control* (MAC) function was reported. It is intended to avoid undesired droplets collisions which would disturb the microfluidic processing. Also this device was assessed showing the results through numerical simulations.

Once the feasibility of the HCN paradigm was demonstrated through the implementation of networking elements, the design of a complete microfluidic network was presented, herein named μ -NET, which integrates all the functionalities previously defined for providing communication and networking facilities to a new generation of programmable LoCs. In fact, in μ -NET (i) the address of the microfluidic device (i.e. LoC) to which a droplet should be sent is appropriately encoded into droplets distance; (ii) the switching is executed to steer the droplets inside the addresses microfluidic device; (iii) the medium access control is applied to avoid collisions between droplets.

In particular, the detailed architecture of μ -NET with a double bus topology is provided, this guarantees no interactions between the incoming packets and the processed payload droplets. Furthermore, the design of a complete networking element, denoted as *Microfluidic Network Interface* (MNI) was illustrated. The MNI integrates switching and MAC functionalities.

Finally, a model is derived for the analysis of the μ -NET network considering the analogy between the Hagen-Poiseuille law and the Ohm law. Detailed numerical simulation results were reported to both verify the model correctness and the overall operations performed by μ -NET.

The numerical simulations presented in this thesis to assess the functioning of each designed device were carried out through the OpenFOAM software. The not so straightforward settings of this platform were also detailed in this thesis.

The models and devices presented in this dissertation could have broad application in passive droplet-based microfluidic devices. In fact, the use of droplets allows to encapsulate and manipulate a large variety of micro-scale materials including live cells, single molecules (e.g. DNA and proteins) and other biological and chemical species. As a result, possible applications of the HCN range from molecular detection to diagnostics. However, microfluidic communications is still in its infancy and there are many possible research opportunities.

This thesis is only the first step towards a possible introduction of networking solutions in the microfluidic domain. The main idea behind this work was to prove the true feasibility of this new approach, through the design of a complete microfluidic communication network, even if further studies can be carried out to improve and enhance its capabilities. For example a microfluidic chip of the μ -NET could be fabricated providing an experimental setup to accurately verify the networking functionalities and performance, by using fluids with different physical parameters. Moreover, this thesis presented the implementation of a bus topology network but the HCN paradigm may be extended to more complex network topologies, such as rings. Indeed, a new implementation of the switch device is actually in the testing phase. This has been designed to enhance the capabilities of the HCN network, minimize the overhead and implement more powerful and performing network topologies. This switch, named as *multi-droplets switch*, is able to direct a series of equally spaced payload droplets, i.e.

generated at a constant frequency, towards the addressed microfluidic element requiring only a header droplet.

Another potential subject to further studies is the implementation of a real biochemical application to prove the effectiveness of the proposed model. For example, it could be useful to create a multi-purpose chip employed for different types of experiments allowing to select the serial set of basic operations to perform, such as bacterial cultures, determination of anti-biograms, and chemostat. Furthermore, the microfluidic communication network could allow to execute in parallel, biochemical analyses and syntheses that require different reaction or incubation times, such as measurements of enzymatic kinetics, protein crystallization, and determination of blood clotting time.

9.1 Results of the research activity: publications

The results of the research activity presented in this dissertation were published in the following papers:

Journals

- De Leo, E.; Donvito, L.; Galluccio, L.; Lombardo, A.; Morabito, G.; Zanolì, L.M., "Communications and Switching in Microfluidic Systems: Pure Hydrodynamic Control for Networking Labs-on-a-Chip," in *Communications, IEEE Transactions on*, vol.61, no.11, pp.4663-4677, 2013.
- Donvito, L.; Galluccio, L.; Lombardo, A.; Morabito, G.", Mi-

crofluidic networks: Design and simulation of pure hydrodynamic switching and medium access control”, *Nano Communication Networks*, vol.4, no.4, pp.164-171, 2013.

- Donvito, L., Galluccio, L., Lombardo, A., Morabito, G., Nicolosi, A., Reno, M. ”Experimental validation of a simple, low-cost, T-junction droplet generator fabricated through 3D printing” *Journal of Micromechanics and Microengineering*, vol.25, no.3, 2015.
- De Leo, E.; Donvito, L.; Galluccio, L.; Lombardo, A.; Morabito, G.; Zanolì, L.M., ”Communications and Switching in Microfluidic Systems: Pure Hydrodynamic Control for Networking Labs-on-a-Chip,” in *Communications, IEEE Transactions on* , vol.61, no.11, pp.4663-4677, 2013.
- Donvito, L.; Galluccio, L.; Lombardo, A.; Morabito, G., ” μ -NET: A Network for Molecular Biology Applications in Microfluidic Chips,” in *Networking, IEEE/ACM Transactions on*, 2015, to appear, doi:10.1109/TNET.2015.2472564

Conference Proceedings

- De Leo, E.; Donvito, L.; Galluccio, L.; Lombardo, A.; Morabito, G.; Zanolì, L.M., ”Design and assessment of a pure hydrodynamic microfluidic switch,” in *Communications (ICC), 2013 IEEE International Conference on* , pp.3165-3169, 2013.
- De Leo, E.; Donvito, L.; Galluccio, L.; Lombardo, A.; Morabito, G., ”Microfluidic networks: design and test of a pure hy-

drodynamic switching function,” in *Communications Workshops (ICC), 2013 IEEE International Conference on*, pp.787-791, 2013.

- De Leo, E.; Donvito, L.; Galluccio, L.; Lombardo, A.; Morabito, G.; Zanolì, L.M., ”Networked Lab-on-a-Chip: Enhancing LoCs through Microfluidic Communications and Networking”, *Student Poster Session-IEEE INFOCOM*, 2013.
- Donvito, L.; Galluccio, L.; Lombardo, A.; Morabito, G., ”On the assessment of microfluidic switching capabilities in NLoC networks”, in *Proceedings of ACM The First Annual International Conference on Nanoscale Computing and Communication (NANOCOM’ 14)*, pp.19:1-19:7, 2014.

BIBLIOGRAPHY

- [1] E. Lauga, M. P. Brenner, and H. A. Stone, *Microfluidics: The no-slip boundary condition*. Springer Berlin Heidelberg, 2007.
- [2] A. San-Miguel and L. Hang, “Microfluidics as a tool for *C. elegans* research,” *The C. elegans Research Community*, 2013. [Online]. Available: <http://www.wormbook.org>
- [3] L. Donvito, L. Galluccio, A. Lombardo, G. Morabito, A. Nicolosi, and M. Reno, “Experimental validation of a simple, low-cost, t-junction droplet generator fabricated through 3d printing,” *Journal of Micromechanics and Microengineering*, vol. 25, no. 3, p. 035013, 2015. [Online]. Available: <http://stacks.iop.org/0960-1317/25/i=3/a=035013>
- [4] A. M. Pit, M. H. G. Duits, and F. Mugele, “Droplet manipulations in two phase flow microfluidics,” *Micromachines*, vol. 6, no. 11, p. 1455, 2015.
- [5] S. K. Cho, H. Moon, and C.-J. Kim, “Creating, transporting, cutting, and merging liquid droplets by electrowetting-based ac-

- uation for digital microfluidic circuits,” *Microelectromechanical Systems, Journal of*, vol. 12, no. 1, pp. 70–80, 2003.
- [6] K. Ahn, J. Agresti, H. Chong, M. Marquez, and D. Weitz, “Electrocoalescence of drops synchronized by size-dependent flow in microfluidic channels,” *Applied Physics Letters*, vol. 88, no. 26, p. 264105, 2006.
- [7] J. D. Tice, H. Song, A. D. Lyon, and R. F. Ismagilov, “Formation of droplets and mixing in multiphase microfluidics at low values of the reynolds and the capillary numbers,” *Langmuir*, vol. 19, no. 22, pp. 9127–9133, 2003.
- [8] H. Song, M. R. Bringer, J. D. Tice, C. J. Gerdt, and R. F. Ismagilov, “Experimental test of scaling of mixing by chaotic advection in droplets moving through microfluidic channels,” *Applied Physics Letters*, vol. 83, no. 22, pp. 4664–4666, 2003.
- [9] M. Prakash, “Microfluidic logic: Chemistry and computation,” Ph.D. dissertation, Massachusetts Institute of Technology, 2007.
- [10] M. Prakash and N. Gershenfeld, “Microfluidic bubble logic,” *Science*, vol. 315, no. 5813, 2007.
- [11] M. J. Fuerstman, P. Garstecki, and G. M. Whitesides, “Coding/decoding and reversibility of droplet trains in microfluidic networks,” *Science*, vol. 315, no. 5813, 2007.
- [12] B. Kintses, L. D. van Vliet, S. R. Devenish, and F. Hollfelder, “Microfluidic droplets: new integrated workflows for biological

- experiments,” *Current Opinion in Chemical Biology*, vol. 14, no. 5, pp. 548–555, 2010.
- [13] M. Lee, J. W. Collins, D. M. Aubrecht, R. A. Sperling, L. Solomon, J.-W. Ha, G.-R. Yi, D. A. Weitz, and V. N. Manoharan, “Synchronized reinjection and coalescence of droplets in microfluidics,” *Lab on a Chip*, vol. 14, no. 3, pp. 509–513, 2014.
- [14] L. Donvito, L. Galluccio, A. Lombardo, and G. Morabito, “On the assessment of microfluidic switching capabilities in nloc networks,” in *Proceedings of ACM The First Annual International Conference on Nanoscale Computing and Communication*, ser. NANOCOM’ 14. New York, NY, USA: ACM, 2014, pp. 19:1–19:7. [Online]. Available: <http://doi.acm.org/10.1145/2619955.2619976>
- [15] E. De Leo, L. Donvito, L. Galluccio, A. Lombardo, G. Morabito, and L. Zanolì, “Communications and switching in microfluidic systems: Pure hydrodynamic control for networking labs-on-a-chip,” *Communications, IEEE Transactions on*, vol. 61, no. 11, pp. 4663–4677, November 2013.
- [16] L. Donvito, L. Galluccio, A. Lombardo, and G. Morabito, “Microfluidic networks: Design and simulation of pure hydrodynamic switching and medium access control,” *Nano Communication Networks*, vol. 4, no. 4, pp. 164 – 171, 2013. [Online]. Available: <http://www.sciencedirect.com/science/article/pii/S187877891300046X>

- [17] E. De Leo, L. Galluccio, A. Lombardo, and G. Morabito, "On the feasibility of using microfluidic technologies for communications in labs-on-a-chip," in *Proc. of IEEE ICC 2012*, Jun. 2012.
- [18] L. Donvito, L. Galluccio, A. Lombardo, and G. Morabito, " μ -net: A network for molecular biology applications in microfluidic chips," *Networking, IEEE/ACM Transactions on*, vol. PP, no. 99, pp. 1–1, 2015.
- [19] W.-L. Chou, P.-Y. Lee, C.-L. Yang, W.-Y. Huang, and Y.-S. Lin, "Recent advances in applications of droplet microfluidics," *Micromachines*, vol. 6, no. 9, pp. 1249–1271, 2015.
- [20] S.-Y. Teh, R. Lin, L.-H. Hung, and A. P. Lee, "Droplet microfluidics," *Lab Chip*, vol. 8, no. 2, January 2008.
- [21] T. Hasegawa, K. Nakashima, F. Omatsu, and K. Ikuta, "Multi-directional micro-switching valve chip with rotary mechanism," *Elsevier Sensors and Actuators A: Physical*, vol. 143, no. 2, May 2008.
- [22] K. Ikuta, A. Takahashi, K. Ikeda, and S. Maruo, "Fully integrated micro biochemical laboratory using biochemical ic chips," in *Proc. of IEEE MEMS 2003*, January 2003.
- [23] A. M. Amin, M. Thottethodi, T. N. Vijaykumar, S. Wereley, and S. C. Jacobson, "Aquacore: a programmable architecture for microfluidics," in *Proc. of ISCA '07*, June 2007.

- [24] J. P. Urbanski, W. Thies, C. Rhodes, S. Amarasinghe, and T. Thorsen, “Digital microfluidics using soft lithography,” *Lab Chip*, vol. 6, no. 1, January 2006.
- [25] L. M. Fidalgo and S. J. Maerkl, “A software-programmable microfluidic device for automated biology,” *Lab Chip*, vol. 11, no. 9, May 2011.
- [26] T. Thorsen, S. J. Maerkl, and S. R. Quake, “Microfluidic large-scale integration,” *Science*, vol. 298, no. 5593, 2002.
- [27] E. C. Jensen, A. M. Stockton, T. N. Chiesl, J. Kim, A. Bera, and R. A. Mathies, “Digitally programmable microfluidic automaton for multiscale combinatorial mixing and sample processing,” *Lab Chip*, 2013.
- [28] W. H. Grover and R. A. Mathies, “An integrated microfluidic processor for single nucleotide polymorphism-based dna computing,” *Lab Chip*, vol. 5, no. 10, 2005.
- [29] E. C. Jensen, B. P. Bhat, and R. A. Mathies, “A digital microfluidic platform for the automation of quantitative biomolecular assays,” *Lab Chip*, vol. 10, no. 6, 2010.
- [30] P. K. Yuen, “Smartbuild-a truly plug-n-play modular microfluidic system,” *Lab Chip*, vol. 8, no. 8, pp. 1374–1378, 2008.
- [31] C.-G. Yang, Z.-R. Xu, and J.-H. Wang, “Manipulation of droplets in microfluidic systems,” *TrAC Trends in Analytical Chemistry*, vol. 29, no. 2, February 2010.

- [32] D. Mark, S. Haeberle, G. Roth, F. von Stetten, and R. Zengerle, "Microfluidic lab-on-a-chip platforms: requirements, characteristics and applications," *Chem. Soc. Rev.*, vol. 39, no. 3, March 2010.
- [33] R. Fair, "Digital microfluidics: is a true lab-on-a-chip possible?" *Microfluidics and Nanofluidics*, vol. 3, no. 3, 2007.
- [34] F. Jousse, R. Farr, D. R. Link, M. J. Fuerstman, and P. Garstecki, "Bifurcation of droplet flows within capillaries," *Physical Review E*, vol. 74, no. 3, September 2006.
- [35] D. A. Sessoms, A. Amon, L. Courbin, and P. Panizza, "Complex dynamics of droplet traffic in a bifurcating microfluidic channel: Periodicity, multistability, and selection rules," *Phys. Rev. Lett.*, vol. 105, no. 15, p. 154501, Oct 2010.
- [36] O. Cybulski and P. Garstecki, "Dynamic memory in a microfluidic system of droplets traveling through a simple network of microchannels," *Lab Chip*, vol. 10, no. 4, February 2010.
- [37] T. Glawdel, C. Elbuken, and C. Ren, "Passive droplet trafficking at microfluidic junctions under geometric and flow asymmetries," *Lab Chip*, vol. 11, Jan. 2011.
- [38] H. Bruus, *Theoretical Microfluidics*, ser. Oxford Master In Condensed Matter Physics. Oxford University Press, 2007.
- [39] P. Joseph and P. Tabeling, "Direct measurement of the apparent slip length," *Phys. Rev. E*, vol. 71, p. 035303, Mar 2005.

- [40] H. Stone, A. Stroock, , and A. Ajdari, “Engineering flows in small devices,” *Annual Review of Fluid Mechanics*, vol. 36, no. 1, pp. 381–411, 2004.
- [41] D. C. Tretheway and C. D. Meinhart, “A generating mechanism for apparent fluid slip in hydrophobic microchannels,” *Physics of Fluids*, vol. 16, no. 5, pp. 1509–1515, 2004.
- [42] J. Harting, C. Kunert, and J. Hyvluoma, “Lattice boltzmann simulations in microfluidics: probing the no-slip boundary condition in hydrophobic, rough, and surface nanobubble laden microchannels,” *Microfluidics and Nanofluidics*, vol. 8, no. 1, pp. 1–10, 2010.
- [43] M. Cieplak, J. Koplik, and J. R. Banavar, “Boundary conditions at a fluid-solid interface,” *Phys. Rev. Lett.*, vol. 86, pp. 803–806, 2001.
- [44] C. L. M. H. Navier, “Mémoire sur les lois du mouvement des fluids,” *Mem. Acad. Sci. Inst. Fr.*, vol. 6, pp. 389–416, 1823.
- [45] R. Bashir, “Biomems: state-of-the-art in detection, opportunities and prospects,” *Advanced drug delivery reviews*, vol. 56, no. 11, pp. 1565–1586, 2004.
- [46] J. C. McDonald and G. M. Whitesides, “Poly (dimethylsiloxane) as a material for fabricating microfluidic devices,” *Accounts of chemical research*, vol. 35, no. 7, pp. 491–499, 2002.

- [47] R. Dangla, F. Gallaire, and C. Baroud, "Microchannel deformations due to solvent-induced pdms swelling," *Lab Chip*, vol. 10, 2010.
- [48] E. Sollier, C. Murray, P. Maoddi, and D. Di Carlo, "Rapid prototyping polymers for microfluidic devices and high pressure injections," *Lab Chip*, vol. 11, pp. 3752–3765, 2011.
- [49] P. M. van Midwoud, A. Janse, M. T. Merema, G. M. M. Groothuis, and E. Verpoorte, "Comparison of biocompatibility and adsorption properties of different plastics for advanced microfluidic cell and tissue culture models," *Analytical Chemistry*, vol. 84, no. 9, pp. 3938–3944, 2012.
- [50] J. N. Lee, C. Park, and G. M. Whitesides, "Solvent compatibility of poly(dimethylsiloxane)-based microfluidic devices," *Analytical Chemistry*, vol. 75, no. 23, pp. 6544–6554, 2003.
- [51] K. J. Regehr, M. Domenech, J. T. Koepsel, K. C. Carver, S. J. Ellison-Zelski, W. L. Murphy, L. A. Schuler, E. T. Alarid, and D. J. Beebe, "Biological implications of polydimethylsiloxane-based microfluidic cell culture," *Lab Chip*, vol. 9, pp. 2132–2139, 2009.
- [52] P. Kim, K. W. Kwon, M. C. Park, S. H. Lee, S. M. Kim, and K. Y. Suh, "Soft lithography for microfluidics: a review," *Biochip Journal*, vol. 2, no. 1, pp. 1–11, 2008.
- [53] P. J. Kitson, M. H. Rosnes, V. Sans, V. Dragone, and L. Cronin, "Configurable 3d-printed millifluidic and microfluidic 'lab on a

- chip' reactionware devices," *Lab Chip*, vol. 12, pp. 3267–3271, 2012.
- [54] A. I. Shallan, P. Smejkal, M. Corban, R. M. Guijt, and M. C. Breadmore, "Cost-effective three-dimensional printing of visibly transparent microchips within minutes," *Analytical Chemistry*, vol. 86, no. 6, pp. 3124–3130, 2014.
- [55] G. Comina, A. Suska, and D. Filippini, "Low cost lab-on-a-chip prototyping with a consumer grade 3d printer," *Lab Chip*, pp. –, 2014.
- [56] J. O'Connor, J. Punch, N. Jeffers, and J. Stafford, "A dimensional comparison between embedded 3d-printed and silicon microchannels," *Journal of Physics: Conference Series*, vol. 525, no. 1, p. 012009, 2014.
- [57] A. Vitale, M. Quaglio, S. Turri, M. Cocuzza, and R. Bongiovanni, "Siloxane photopolymer to replace polydimethylsiloxane in microfluidic devices for polymerase chain reaction," *Polymers for Advanced Technologies*, vol. 24, no. 12, pp. 1068–1074, 2013.
- [58] N. Md Yunus and N. Green, "Fabrication of microfluidic device channel using a photopolymer for colloidal particle separation," *Microsystem Technologies*, vol. 16, no. 12, pp. 2099–2107, 2010.
- [59] C. Khoury, G. A. Mensing, and D. J. Beebe, "Ultra rapid prototyping of microfluidic systems using liquid phase photopolymerization," *Lab Chip*, vol. 2, pp. 50–55, 2002.

- [60] A. Taberham, M. Kraft, M. Mowlem, and H. Morgan, “The fabrication of lab-on-chip devices from fluoropolymers,” *Journal of Micromechanics and Microengineering*, vol. 18, no. 6, p. 064011, 2008.
- [61] J. Alvankarian and B. Y. Majlis, “A new uv-curing elastomeric substrate for rapid prototyping of microfluidic devices,” *Journal of Micromechanics and Microengineering*, vol. 22, no. 3, p. 035006, 2012.
- [62] T. Cubaud, U. Ulmanella, and C.-M. Ho, “Two-phase flow in microchannels with surface modifications,” *Fluid Dynamics Research*, vol. 38, no. 11, pp. 772–786, 2006.
- [63] B. Scheid, J. Delacotte, B. Dollet, E. Rio, F. Restagno, E. Van Nierop, I. Cantat, D. Langevin, and H. A. Stone, “The role of surface rheology in liquid film formation,” *EPL (Europhysics Letters)*, vol. 90, no. 2, p. 24002, 2010.
- [64] T. Cubaud and T. G. Mason, “Capillary threads and viscous droplets in square microchannels,” *Physics of Fluids*, vol. 20, no. 5, pp. –, 2008.
- [65] Y. Hu, D. Pine, and L. G. Leal, “Drop deformation, breakup, and coalescence with compatibilizer,” *Physics of Fluids*, vol. 12, no. 3, pp. 484–489, 2000.
- [66] S. Takagi and Y. Matsumoto, “Surfactant effects on bubble motion and bubbly flows,” *Annual Review of Fluid Mechanics*, vol. 43, pp. 615–636, 2011.

- [67] J. Xu, S. Li, J. Tan, Y. Wang, and G. Luo, "Controllable preparation of monodisperse o/w and w/o emulsions in the same microfluidic device," *Langmuir*, vol. 22, no. 19, pp. 7943–7946, 2006.
- [68] R. Dreyfus, P. Tabeling, and H. Willaime, "Ordered and disordered patterns in two-phase flows in microchannels," *Physical review letters*, vol. 90, no. 14, p. 144505, 2003.
- [69] Y. Zhang and L. Wang, *Microfluidics: fabrication, droplets, bubbles and nanofluids synthesis*. Springer, 2011.
- [70] E. Y. Tafti, K. Law, and R. Kumar, "Effect of surfactants on droplet formation in microchannels," in *Proc. of ECTC*, 2008.
- [71] J. Xu, S. Li, J. Tan, Y. Wang, and G. Luo, "Preparation of highly monodisperse droplet in a t-junction microfluidic device," *AIChE journal*, vol. 52, no. 9, pp. 3005–3010, 2006.
- [72] H. Gu, M. H. Duits, and F. Mugele, "Droplets formation and merging in two-phase flow microfluidics," *International journal of molecular sciences*, vol. 12, no. 4, pp. 2572–2597, 2011.
- [73] C. Cramer, P. Fischer, and E. J. Windhab, "Drop formation in a co-flowing ambient fluid," *Chemical Engineering Science*, vol. 59, no. 15, pp. 3045–3058, 2004.
- [74] P. Guillot, A. Colin, A. S. Utada, and A. Ajdari, "Stability of a jet in confined pressure-driven biphasic flows at low reynolds numbers," *Physical review letters*, vol. 99, no. 10, p. 104502, 2007.

- [75] P. Umbanhowar, V. Prasad, and D. Weitz, "Monodisperse emulsion generation via drop break off in a coflowing stream," *Langmuir*, vol. 16, no. 2, pp. 347–351, 2000.
- [76] S. L. Anna, N. Bontoux, and H. A. Stone, "Formation of dispersions using flow focusing in microchannels," *Applied physics letters*, vol. 82, no. 3, pp. 364–366, 2003.
- [77] Z. Nie, M. Seo, S. Xu, P. C. Lewis, M. Mok, E. Kumacheva, G. M. Whitesides, P. Garstecki, and H. A. Stone, "Emulsification in a microfluidic flow-focusing device: effect of the viscosities of the liquids," *Microfluidics and Nanofluidics*, vol. 5, no. 5, pp. 585–594, 2008.
- [78] P. Garstecki, M. J. Fuerstman, H. A. Stone, and G. M. Whitesides, "Formation of droplets and bubbles in a microfluidic t-junction: scaling and mechanism of break-up," *Lab on a Chip*, vol. 6, no. 3, pp. 437–446, 2006.
- [79] M. De Menech, P. Garstecki, F. Jousse, and H. Stone, "Transition from squeezing to dripping in a microfluidic t-shaped junction," *journal of fluid mechanics*, vol. 595, pp. 141–161, 2008.
- [80] J. Sivasamy, T.-N. Wong, N.-T. Nguyen, and L. T.-H. Kao, "An investigation on the mechanism of droplet formation in a microfluidic t-junction," *Microfluidics and nanofluidics*, vol. 11, no. 1, pp. 1–10, 2011.
- [81] J. Xu, S. Li, J. Tan, and G. Luo, "Correlations of droplet formation in t-junction microfluidic devices: from squeezing to drip-

- ping,” *Microfluidics and Nanofluidics*, vol. 5, no. 6, pp. 711–717, 2008.
- [82] M. Steegmans, C. Schron, and R. Boom, “Generalised insights in droplet formation at t-junctions through statistical analysis,” *Chemical Engineering Science*, vol. 64, no. 13, pp. 3042 – 3050, 2009.
- [83] V. van Steijn, C. R. Kleijn, and M. T. Kreutzer, “Predictive model for the size of bubbles and droplets created in microfluidic t-junctions,” *Lab Chip*, vol. 10, pp. 2513–2518, 2010.
- [84] T. Glawdel, C. Elbuen, and C. L. Ren, “Droplet formation in microfluidic t-junction generators operating in the transitional regime. I. experimental observations,” *Phys. Rev. E*, vol. 85, p. 016322, Jan 2012.
- [85] —, “Droplet formation in microfluidic t-junction generators operating in the transitional regime. II. modeling,” *Phys. Rev. E*, vol. 85, p. 016323, Jan 2012.
- [86] G. F. Christopher, N. N. Noharuddin, J. A. Taylor, and S. L. Anna, “Experimental observations of the squeezing-to-dripping transition in t-shaped microfluidic junctions,” *Phys. Rev. E*, vol. 78, p. 036317, Sep 2008.
- [87] T. Glawdel and C. Ren, “Global network design for robust operation of microfluidic droplet generators with pressure-driven flow,” *Microfluidics and Nanofluidics*, vol. 13, no. 3, pp. 469–480, 2012.

- [88] H. Gu, C. U. Murade, M. H. G. Duits, and F. Mugele, “A microfluidic platform for on-demand formation and merging of microdroplets using electric control,” *Biomicrofluidics*, vol. 5, no. 1, p. 011101, 2011.
- [89] M. G. Pollack, A. D. Shenderov, and R. B. Fair, “Electrowetting-based actuation of droplets for integrated microfluidics,” *Lab Chip*, vol. 2, pp. 96–101, 2002.
- [90] D. J. Collins, T. Alan, K. Helmerson, and A. Neild, “Surface acoustic waves for on-demand production of picoliter droplets and particle encapsulation,” *Lab Chip*, vol. 13, pp. 3225–3231, 2013.
- [91] S. Zeng, B. Li, X. Su, J. Qin, and B. Lin, “Microvalve-actuated precise control of individual droplets in microfluidic devices,” *Lab Chip*, vol. 9, no. 10, pp. 1340–1343, 2009.
- [92] R. Lin, J. S. Fisher, M. G. Simon, and A. P. Lee, “Novel on-demand droplet generation for selective fluid sample extraction,” *Biomicrofluidics*, vol. 6, no. 2, p. 024103, 2012.
- [93] B.-C. Lin and Y.-C. Su, “On-demand liquid-in-liquid droplet metering and fusion utilizing pneumatically actuated membrane valves,” *Journal of Micromechanics and Microengineering*, vol. 18, no. 11, p. 115005, 2008.
- [94] S.-Y. Park, T.-H. Wu, Y. Chen, M. A. Teitell, and P.-Y. Chiou, “High-speed droplet generation on demand driven by pulse laser-induced cavitation,” *Lab on a Chip*, vol. 11, no. 6, pp. 1010–1012, 2011.

- [95] S. Jambovane, D. J. Kim, E. C. Duin, S.-K. Kim, and J. W. Hong, "Creation of stepwise concentration gradient in picoliter droplets for parallel reactions of matrix metalloproteinase ii and ix," *Analytical chemistry*, vol. 83, no. 9, pp. 3358–3364, 2011.
- [96] Dolomite microfluidics.
- [97] M. A. Unger, H.-P. Chou, T. Thorsen, A. Scherer, and S. R. Quake, "Monolithic microfabricated valves and pumps by multi-layer soft lithography," *Science*, vol. 288, no. 5463, pp. 113–116, 2000.
- [98] C. N. Baroud, M. Robert de Saint Vincent, and J.-P. Delville, "An optical toolbox for total control of droplet microfluidics," *Lab Chip*, vol. 7, no. 8, 2007.
- [99] R. Seemann, M. Brinkmann, T. Pfohl, and S. Herminghaus, "Droplet based microfluidics," *Reports on Progress in Physics*, vol. 75, no. 1, January 2012.
- [100] Y.-C. Tan, J. S. Fisher, A. I. Lee, V. Cristini, and A. P. Lee, "Design of microfluidic channel geometries for the control of droplet volume, chemical concentration, and sorting," *Lab Chip*, vol. 4, no. 4, 2004.
- [101] D. R. Link, S. L. Anna, D. A. Weitz, and H. A. Stone, "Geometrically mediated breakup of drops in microfluidic devices," *Phys. Rev. Lett.*, vol. 92, no. 5, February 2004.
- [102] M.-C. Jullien, M.-J. T. M. Ching, C. Cohen, L. Menetrier, and P. Tabeling, "Droplet breakup in microfluidic t-junctions

- at small capillary numbers,” *Physics of Fluids (1994-present)*, vol. 21, no. 7, p. 072001, 2009.
- [103] D. N. Adamson, D. Mustafi, J. X. J. Zhang, B. Zheng, and R. F. Ismagilov, “Production of arrays of chemically distinct nanolitre plugs via repeated splitting in microfluidic devices,” *Lab Chip*, vol. 6, pp. 1178–1186, 2006.
- [104] M. G. Simon and A. P. Lee, “Microfluidic droplet manipulations and their applications,” in *Microdroplet Technology*. Springer, 2012, pp. 23–50.
- [105] D. R. Link, E. Grasland-Mongrain, A. Duri, F. Sarrazin, Z. Cheng, G. Cristobal, M. Marquez, and D. A. Weitz, “Electric control of droplets in microfluidic devices,” *Angewandte Chemie International Edition*, vol. 45, no. 16, April 2006.
- [106] P. R. Gascoyne, J. V. Vykoukal, J. A. Schwartz, T. J. Anderson, D. M. Vykoukal, K. W. Current, C. McConaghy, F. F. Becker, and C. Andrews, “Dielectrophoresis-based programmable fluidic processors,” *Lab on a Chip*, vol. 4, no. 4, pp. 299–309, 2004.
- [107] M. Herrmann, J. Lopez, P. Brady, and M. Raessi, “Thermocapillary motion of deformable drops and bubbles,” in *Proceedings of the Summer Program*, 2008, p. 155.
- [108] J. Köhler, T. Henkel, A. Grodrian, T. Kirner, M. Roth, K. Martin, and J. Metze, “Digital reaction technology by micro segmented flowcomponents, concepts and applications,” *Chemical Engineering Journal*, vol. 101, no. 1, pp. 201–216, 2004.

- [109] K. Handique and M. A. Burns, “Mathematical modeling of drop mixing in a slit-type microchannel,” *Journal of Micromechanics and Microengineering*, vol. 11, no. 5, p. 548, 2001.
- [110] H. Song, J. D. Tice, and R. F. Ismagilov, “A microfluidic system for controlling reaction networks in time,” *Angewandte Chemie*, vol. 115, no. 7, pp. 792–796, 2003.
- [111] P. Paik, V. K. Pamula, and R. B. Fair, “Rapid droplet mixers for digital microfluidic systems,” *Lab on a Chip*, vol. 3, no. 4, pp. 253–259, 2003.
- [112] G. Cristobal, J.-P. Benoit, M. Joanicot, and A. Ajdari, “Microfluidic bypass for efficient passive regulation of droplet traffic at a junction,” *Applied Physics Letters*, vol. 89, no. 3, July 2006.
- [113] L. F. Cheow, L. Yobas, and D.-L. Kwong, “Digital microfluidics: Droplet based logic gates,” *Applied Physics Letters*, vol. 90, no. 5, January 2007.
- [114] G. Katsikis, J. S. Cybulski, and M. Prakash, “Synchronous universal droplet logic and control,” *Nature Physics*, 2015.
- [115] K. Song, G. Hu, X. Hu, R. Zhong, X. Wang, and B. Lin, “Encoding and controlling of two droplet trains in a microfluidic network with the loop-like structure,” *Microfluidics and Nanofluidics*, pp. 1–13, 2015.
- [116] H. Wong, C. J. Radke, and S. Morris, “The motion of long bubbles in polygonal capillaries. part 2. drag, fluid pressure and

- fluid flow,” *Journal of Fluid Mechanics*, vol. 292, pp. 95–110, June 1995.
- [117] C. N. Baroud, F. Gallaire, and R. Dangla, “Dynamics of microfluidic droplets,” *Lab Chip*, vol. 10, no. 16, June 2010.
- [118] S. A. Vanapalli, A. G. Banpurkar, D. van den Ende, M. H. G. Duits, and F. Mugele, “Hydrodynamic resistance of single confined moving drops in rectangular microchannels,” *Lab Chip*, vol. 9, no. 7, 2009.
- [119] S. R. Hodges, O. Jensen, and J. M. Rallison, “The motion of a viscous drop through cylindrical tube,” *Journal of fluid mechanics*, vol. 501, February 2004.
- [120] F. Jousse, G. Lian, R. Janes, and J. Melrose, “Compact model for multi-phase liquid-liquid flows in micro-fluidic devices,” *Lab Chip*, vol. 5, no. 6, March 2005.
- [121] P. Parthiban and S. A. Khan, “Filtering microfluidic bubble trains at a symmetric junction,” *Lab Chip*, vol. 12, no. 3, February 2012.
- [122] OpenFOAM software, <http://www.openfoam.com/>.
- [123] V. Cristini and Y.-C. Tan, “Theory and numerical simulation of droplet dynamics in complex flows-a review,” *Lab Chip*, vol. 4, no. 4, pp. 257–264, 2004.
- [124] A. Faghri and Y. Zhang, *Transport phenomena in multiphase systems*. Academic Press, 2006.

- [125] J. Liu and N. Trung Nguyen, "Numerical simulation of droplet-based microfluidics-a review," *Micro and Nanosystems*, vol. 2, no. 3, pp. 193–201, 2010.
- [126] L. Amaya-Bower and T. Lee, "Lattice boltzmann simulations of bubble formation in a microfluidic t-junction," *Philosophical Transactions of the Royal Society of London A: Mathematical, Physical and Engineering Sciences*, vol. 369, no. 1945, pp. 2405–2413, 2011.
- [127] S. Chen and G. D. Doolen, "Lattice boltzmann method for fluid flows," *Annual review of fluid mechanics*, vol. 30, no. 1, pp. 329–364, 1998.
- [128] C. W. Hirt and B. D. Nichols, "Volume of fluid (vof) method for the dynamics of free boundaries," *Journal of computational physics*, vol. 39, no. 1, pp. 201–225, 1981.
- [129] H. Rusche, "Computational fluid dynamics of dispersed two-phase flows at high phase fractions," Ph.D. dissertation, Imperial College of Science, Technology, and Medicine-London, 2002.
- [130] Salome software, <http://www.salome-platform.org/>.
- [131] P.-H. Yuh, C.-L. Yang, and Y.-W. Chang, "Bioroute: A network-flow-based routing algorithm for the synthesis of digital microfluidic biochips," *Computer-Aided Design of Integrated Circuits and Systems, IEEE Transactions on*, vol. 27, no. 11, November 2008.

- [132] E. De Leo, L. Donvito, L. Galluccio, A. Lombardo, G. Morabito, and L. Zanolì, “Design and assessment of a pure hydrodynamic microfluidic switch,” in *Communications (ICC), 2013 IEEE International Conference on*, June 2013, pp. 3165–3169.
- [133] E. De Leo, L. Donvito, L. Galluccio, A. Lombardo, and G. Morabito, “Microfluidic networks: design and test of a pure hydrodynamic switching function,” in *Communications Workshops (ICC), 2013 IEEE International Conference on*, June 2013, pp. 787–791.
- [134] S. Wirdatmadja, D. Moltchanov, P. Bolcos, J. Väliäho, J. Kreutzer, P. Kallio, and Y. Koucheryavy, “Data rate performance of droplet microfluidic communication system,” in *Proceedings of the Second Annual International Conference on Nanoscale Computing and Communication*, ser. NANOCOM’15, 2015, pp. 5:1–5:6.
- [135] A. Biral and A. Zanella, “Introducing purely hydrodynamic networking functionalities into microfluidic systems,” *Nano Communication Networks*, vol. 4, no. 4, pp. 205 – 215, 2013.
- [136] B. El Debs, R. Utharala, I. V. Balyasnikova, A. D. Griffiths, and C. A. Merten, “Functional single-cell hybridoma screening using droplet-based microfluidics,” *Proceedings of the National Academy of Sciences*, vol. 109, no. 29, pp. 11 570–11 575, 2012.
- [137] D. Pekin, Y. Skhiri, J.-C. Baret, D. Le Corre, L. Mazutis, C. Ben Salem, F. Millot, A. El Harrak, J. B. Hutchison, J. W. Larson, D. R. Link, P. Laurent-Puig, A. D. Griffiths, and

- V. Taly, "Quantitative and sensitive detection of rare mutations using droplet-based microfluidics," *Lab Chip*, vol. 11, pp. 2156–2166, 2011.
- [138] W. Choi, M. Hashimoto, A. K. Ellerbee, X. Chen, K. J. M. Bishop, P. Garstecki, H. A. Stone, and G. M. Whitesides, "Bubbles navigating through networks of microchannels," *Lab Chip*, vol. 11, 2011.
- [139] A. Zanella and A. Biral, "Introducing purely hydrodynamic networking mechanisms in microfluidic systems," in *Proc. of IEEE MoNaCom 2013*, June 2013.
- [140] A. Biral and A. Zanella, "Bringing purely hydrodynamic networking functionalities in microfluidic systems," *To appear in Nano Communication Networks*, 2013.
- [141] J.-C. Baret, O. J. Miller, V. Taly, M. Ryckelynck, A. El-Harrak, L. Frenz, C. Rick, M. L. Samuels, J. B. Hutchison, J. J. Agresti, D. R. Link, D. A. Weitz, and A. D. Griffiths, "Fluorescence-activated droplet sorting (fads): efficient microfluidic cell sorting based on enzymatic activity," *Lab Chip*, vol. 9, pp. 1850–1858, 2009.
- [142] Y. Harada, D. H. Yoon, T. Sekiguchi, and S. Shoji, "Size-oriented passive droplet sorting by using surface free energy with micro guide groove," in *Micro Electro Mechanical Systems (MEMS), 2012 IEEE International Conference on*, 2012, pp. 1105–1108.

- [143] A. Zanella and A. Biral, “Design and analysis of a microfluidic bus network with bypass channels,” in *Communications (ICC), 2014 IEEE International Conference on*, June 2014, pp. 3993–3998.
- [144] N.-T. Nguyen, S. Lassemone, and F. A. Chollet, “Optical detection for droplet size control in microfluidic droplet-based analysis systems,” *Sensors and Actuators B: Chemical*, vol. 117, no. 2, 2006.
- [145] T. Thorsen, R. W. Roberts, F. H. Arnold, and S. R. Quake, “Dynamic pattern formation in a vesicle-generating microfluidic device,” *Phys. Rev. Lett.*, vol. 86, no. 18, Apr. 2001.
- [146] A. Biral, D. Zordan, and A. Zanella, “Transmitting information with microfluidic systems,” in *Communications (ICC), 2015 IEEE International Conference on*, 2015, pp. 1103–1108.
- [147] 3D Systems, <http://www.3dsystems.com/>.
- [148] A. R. Abate, J. J. Agresti, and D. A. Weitz, “Microfluidic sorting with high-speed single-layer membrane valves,” *Applied Physics Letters*, vol. 96, no. 20, p. 203509, 2010.
- [149] J. J. Agresti, E. Antipov, A. R. Abate, K. Ahn, A. C. Rowat, J.-C. Baret, M. Marquez, A. M. Klibanov, A. D. Griffiths, and D. A. Weitz, “Ultrahigh-throughput screening in drop-based microfluidics for directed evolution.” *Proceedings of the National Academy of Sciences of the United States of America*, vol. 107, no. 9, pp. 4004–4009, 2010.

- [150] C. N. Baroud, J.-P. Delville, F. m. c. Gallaire, and R. Wunnenburger, "Thermocapillary valve for droplet production and sorting," *Phys. Rev. E*, vol. 75, no. 4, p. 046302, Apr 2007.
- [151] T. Franke, A. R. Abate, D. A. Weitz, and A. Wixforth, "Surface acoustic wave (SAW) directed droplet flow in microfluidics for PDMS devices," *Lab Chip*, vol. 9, no. 18, pp. 2625–2627, 2009.
- [152] D. A. Sessoms, M. Belloul, W. Engl, M. Roche, L. Courbin, and P. Panizza, "Droplet motion in microfluidic networks: hydrodynamic interactions and pressure drop measurements," *Physical Review*, vol. 80, Jul. 2009.
- [153] O. Cybulski and P. Garstecki, "Dynamic memory in a microfluidic system of droplets traveling through a simple network of microchannels," *Lab Chip*, vol. 10, no. 4, pp. 484–493, 2010.
- [154] Z. Han, W. Li, Y. Huang, and B. Zheng, "Measuring rapid enzymatic kinetics by electrochemical method in droplet-based microfluidic devices with pneumatic valves," *Analytical Chemistry*, vol. 81, no. 14, pp. 5840–5845, 2009.
- [155] H. Song, H.-W. Li, M. S. Munson, T. G. Van Ha, and R. F. Ismagilov, "On-chip titration of an anticoagulant argatroban and determination of the clotting time within whole blood or plasma using a plug-based microfluidic system," *Analytical Chemistry*, vol. 78, pp. 4839–4849, 2006.
- [156] W. Liu, H. J. Kim, E. M. Lucchetta, W. Du, and R. F. Ismagilov, "Isolation, incubation, and parallel functional testing

- and identification by fish of rare microbial single-copy cells from multi-species mixtures using the combination of chemistode and stochastic confinement,” *Lab Chip*, vol. 9, pp. 2153–2162, 2009.
- [157] E. De Leo, L. Galluccio, A. Lombardo, and G. Morabito, “Networked labs-on-a-chip (nloc): Introducing networking technologies in microfluidic systems,” *Nano Communication Networks*, vol. 3, no. 4, 2012.
- [158] W. Engl, M. Roche, A. Colin, P. Panizza, and A. Ajdari, “Droplet traffic at a simple junction at low capillary numbers,” *Phys. Rev. Lett.*, vol. 95, no. 20, Nov. 2005.
- [159] B. Zheng, J. D. Tice, and R. F. Ismagilov, “Formation of droplets of alternating composition in microfluidic channels and applications to indexing of concentrations in droplet-based assays,” *Analytical chemistry*, vol. 76, no. 17, pp. 4977–4982, 2004.
- [160] L. Zanolì, M. Licciardello, R. D’Agata, C. Lantano, A. Calabretta, R. Corradini, R. Marchelli, and G. Spoto, “Peptide nucleic acid molecular beacons for the detection of PCR amplicons in droplet-based microfluidic devices,” *Analytical and Bioanalytical Chemistry*, vol. 405, no. 2-3, January 2013.